FINAL
CONTRACT REPORT
VTRC 09-CR14

FIELD TESTING OF THE WOLF CREEK CURVED GIRDER BRIDGE: PART II: STRAIN MEASUREMENTS

JACQUELINE E. MILLER
Graduate Research Assistant

THOMAS T. BABER
Associate Professor

Department of Civil and Environmental Engineering
University of Virginia

http://www.virginiadot.org/vtrc/main/online_reports/pdf/09-cr12.pdf

Standard Title Page - Report on Federally Funded Project

1. Report No.: FHWA/VTRC 09-CR14	2. Government Accession No.:	3. Recipient's Catalog No.:
4. Title and Subtitle: Field Testing of the Wolf Creek Curved Girder Bridge: Part II: Strain Measurements		5. Report Date: June 2009
		6. Performing Organization Code:
7. Author(s): Jacqueline E. Miller and Thomas T. Baber		8. Performing Organization Report No.: VTRC 09-CR14
9. Performing Organization and Address: Virginia Transportation Research Council 530 Edgemont Road Charlottesville, VA 22903		10. Work Unit No. (TRAIS):
		11. Contract or Grant No.: 83146
12. Sponsoring Agencies' Name and Address: Virginia Department of Transportation 1401 E. Broad Street Richmond, VA 23219 Federal Highway Administration 400 North 8th Street, Room 750 Richmond, VA 23219-4825		13. Type of Report and Period Covered: Final Contract
		14. Sponsoring Agency Code:

15. Supplementary Notes:
This project (including both the Part I and Part II studies) was financed with federal Part II State Planning and Research (SPR) funds at an estimated cost of $155,147.

16. Abstract:

The Wolf Creek Bridge is a curved, multi-girder three span steel composite bridge located south of Narrows, Virginia, that was completed in 2006. A finite element (FE) model of the bridge revealed that pier flexibility may be important in modeling the bridge. In addition, questions have been raised as to the effectiveness of the C15x33 diaphragms in providing lateral transfer of loads between members.

This study was conducted as Phase II of a project for which the overall goal was to use field testing to obtain a better understanding of the behavior of multi-span curved girder bridges. The Phase I study was published separately (Turnage and Baber, 2009). During Phase II, an array of 49 strain gages was installed on the superstructure of the bridge: 34 gages were installed on the four girders at the mid-point of the center span, and 15 gages were installed on the three diaphragm members located closest to mid-span. The bridge was then subjected to static and dynamic applications of a loaded dump truck for which the axle loads were quite close to those of an HS-20 truck. The static strains were measured when the truck was located at 19 different locations on the inner and outer lanes. The dynamic strains were measured under the truck crossing the bridge at normal traffic speed for the structure.

The static loading was then replicated on the FE model. The measured static strains were compared with the strains computed from the FE model. Both measured and computed strains on the girders were used to estimate distribution factors, which were compared to evaluate the effectiveness of moment transfer between girders. The measured static and dynamic strains were also compared to estimate dynamic amplification factors. Finally, measured and computed diaphragm strains were compared to evaluate the FE model's diaphragm girder approximation.

The study found that the diaphragms transfer relatively little load from the loaded lane toward the unloaded lane but slightly more load transfers toward the outer girders than toward the inner girders. Further, the FE model predicts slightly greater transfer of load between girders than was measured in the field, suggesting that the model overestimates the stiffness of the diaphragm to girder connection. Finally, the measured strains and strains computed using the FE model predict different neutral axis locations.

Following additional numerical studies, it was concluded that the FE model predicted the neutral axis to be higher than it should be, based upon transformed section calculations. In addition, full composite action based upon transformed section calculations should result in a neutral axis location higher than was determined from field data measurements. This suggests that some slip might be occurring between the girders and the haunches.

17 Key Words: Curved steel girder bridges, field testing, finite element modeling, strain measurements	18. Distribution Statement: No restrictions. This document is available to the public through NTIS, Springfield, VA 22161.

19. Security Classif. (of this report): Unclassified	20. Security Classif. (of this page): Unclassified	21. No. of Pages: 77	22. Price:

Form DOT F 1700.7 (8-72) Reproduction of completed page authorized

FINAL CONTRACT REPORT

FIELD TESTING OF THE WOLF CREEK CURVED GIRDER BRIDGE: PART II: STRAIN MEASUREMENTS

Jacqueline E. Miller
Graduate Research Assistant

Thomas T. Baber
Associate Professor

Department of Civil and Environmental Engineering
University of Virginia

Project Manager
Jose P. Gomez, Ph.D., P.E., Virginia Transportation Research Council

Contract Research Sponsored by
the Virginia Transportation Research Council
(A partnership of the Virginia Department of Transportation
and the University of Virginia since 1948)

In Cooperation with the U.S. Department of Transportation
Federal Highway Administration

Charlottesville, Virginia

June 2009
VTRC 09-CR14

DISCLAIMER

The project that is the subject of this report was done under contract for the Virginia Department of Transportation, Virginia Transportation Research Council. The contents of this report reflect the views of the authors, who are responsible for the facts and the accuracy of the data presented herein. The contents do not necessarily reflect the official views or policies of the Virginia Department of Transportation, the Commonwealth Transportation Board, or the Federal Highway Administration. This report does not constitute a standard, specification, or regulation. Any inclusion of manufacturer names, trade names, or trademarks is for identification purposes only and is not to be considered an endorsement.

Each contract report is peer reviewed and accepted for publication by Research Council staff with expertise in related technical areas. Final editing and proofreading of the report are performed by the contractor.

ABSTRACT

The Wolf Creek Bridge is a curved, multi-girder three span steel composite bridge located south of Narrows, Virginia, that was completed in 2006. A finite element (FE) model of the bridge revealed that pier flexibility may be important in modeling the bridge. In addition, questions have been raised as to the effectiveness of the C15x33 diaphragms in providing lateral transfer of loads between members.

This study was conducted as Phase II of a project for which the overall goal was to use field testing to obtain a better understanding of the behavior of multi-span curved girder bridges. The Phase I study was published separately (Turnage and Baber, 2009). During Phase II, an array of 49 strain gages was installed on the superstructure of the bridge: 34 gages were installed on the four girders at the mid-point of the center span, and 15 gages were installed on the three diaphragm members located closest to mid-span. The bridge was then subjected to static and dynamic applications of a loaded dump truck for which the axle loads were quite close to those of an HS-20 truck. The static strains were measured when the truck was located at 19 different locations on the inner and outer lanes. The dynamic strains were measured under the truck crossing the bridge at normal traffic speed for the structure.

The static loading was then replicated on the FE model. The measured static strains were compared with the strains computed from the FE model. Both measured and computed strains on the girders were used to estimate distribution factors, which were compared to evaluate the effectiveness of moment transfer between girders. The measured static and dynamic strains were also compared to estimate dynamic amplification factors. Finally, measured and computed diaphragm strains were compared to evaluate the FE model's diaphragm girder approximation.

The study found that the diaphragms transfer relatively little load from the loaded lane toward the unloaded lane but slightly more load transfers toward the outer girders than toward the inner girders. Further, the FE model predicts slightly greater transfer of load between girders than was measured in the field, suggesting that the model overestimates the stiffness of the diaphragm to girder connection. Finally, the measured strains and strains computed using the FE model predict different neutral axis locations.

Following additional numerical studies, it was concluded that the FE model predicted the neutral axis to be higher than it should be, based upon transformed section calculations. In addition, full composite action based upon transformed section calculations should result in a neutral axis location higher than was determined from field data measurements. This suggests that some slip might be occurring between the girders and the haunches.

Implications of this study could have a significant effect on future health monitoring applications as they pertain to both curved and straight girder bridges. It is essential that FE models in such long-term applications be able to reproduce the "as-built" response characteristics of a bridge. The current study raised significant issues about the ability to model the behavior of curved girder bridges correctly. Thus it will be important to perform subsequent numerical research studies to develop models that will result in more precise predictions and to use these and other methods being developed in any health monitoring applications.

FINAL CONTRACT REPORT

FIELD TESTING OF THE WOLF CREEK CURVED GIRDER BRIDGE: PART II: STRAIN MEASUREMENTS

Jacqueline E. Miller
Graduate Research Assistant

Thomas T. Baber
Associate Professor

Department of Civil and Environmental Engineering
University of Virginia

INTRODUCTION

Curved girder bridges are currently an important focus of study within structural engineering. A significant number of curved girder bridges first began to appear in the early 1960s as part of the nascent National Highway System, when it was discovered that such structures provide significant benefits when curved alignments are needed. Since the 1960s, the use of curved girder bridges has steadily increased. Roughly one fourth of the new bridges built from the early 1990s through today have been curved, many incorporating composite curved concrete-steel girders (Linzell, 2004b). Both box girders and I girders have been used in curved alignments, with I girders being the most common. Multi-I girder bridges are familiar to most structural engineers, having been widely used in their straight alignment, with parallel girders, and with periodic cross-frames or diaphragms.

The behavior of curved I-girders differs from that of straight girders in significant ways, both in the non-composite stage, and in the composite stage under service loadings. Research studies have reported the following distinctive behavior:

- Flange buckling stresses differ on the inside and outside of the curved web.
- Local buckling on the inner half of the tension flange is possible.
- Unless they are loaded in pure shear, web plates begin to bend laterally at the onset of loading forming an “S” shape, reducing web efficiency somewhat, and leading to higher flange stresses than would be observed in a straight girder.
- Longitudinal stiffeners may be effective in both tension and compression zones of curved girders.
- Bending and twisting of curved girder bridges are coupled, so flange stresses under vertical loadings vary across the flange. This phenomenon is often referred to as lateral bending, since it does involve variations in bending stresses across the flange width that would not be seen in straight girders.
- Because of the tendency to twist, cross-frames or diaphragms become primary members. In curved girder bridges, curvature effects tend to cause an appreciable portion of live loads to be transferred to the girders on the outside of the curve

(Linzell, 2004a). This transfer must take place through the cross-frames or diaphragms.

- In the presence of intermediate piers, a complex interaction between the superstructure and the piers may occur. Pier flexibility may significantly influence the strains under dead load and under vehicular loadings.

The inherent twisting effects particular to curved beams result in bimoments, which are "self-equilibrating normal stress resultants" at the ends of the beam (Oden, 1967). The bi-moments are caused by the curved beam warping out of plane, similar to the warping effects of torsion, so the strain in a curved section can be said to have two components: that due to curvature, and that due to the twist of the shear axis (Dabrowski, 1968). The total shear stress in curved beams is a combination of bending and torsional shear.

Along with these primary effects, there are important secondary effects that cannot be neglected. Radial deflection causes the compression flanges to tend to bow out under normal bending loads, amplifying the curvature effect. This leads to an increase in lateral flange bending in the compression flange, resulting in unequal bending stresses in the flanges. The variation in bending stresses in the cross section induces a change in the curvature of the flanges, resulting in additional radial deflections and causing an amplification of lateral bending moments in the compression flange (Hall, 1996).

Because of the complexity of curved girder bridges, there has been a continuing interest in the behavior of such bridges, including dynamic response characteristics, dynamic amplification factors, cross-frame and diaphragm behavior, and distribution of live loads in particular. Further, it has been observed in numerical studies that at least certain types of piers may interact with curved girder superstructures (Lydzinski, 2006), and this has been verified through field vibration studies (Turnage, 2007).

The current report is part of a research project directed toward the field study of the Wolf Creek Bridge, a curved girder bridge located in Bland County, Virginia. This research was undertaken with the intent of enhancing the understanding of curved girder bridge behavior, of answering specific questions about the behavior of the Wolf Creek Bridge, and to provide insights that will improve modeling capabilities for such bridges.

Background

Because of the complexity of curved girders and curved girder bridges, extensive research has been conducted since the early 1960s. Several comprehensive literature reviews have been published (McManus et al., 1969; Zureick, 1994; Zureick and Naqib, 1999; Linzell, 1999; Hall et al., 1999). A literature survey conducted in conjunction with the current project located in excess of 300 relevant papers. Only papers and reports with some relevance to the current studies are discussed in this section.

Experimental Studies

A number of experimental studies have been conducted since the mid 1960s to provide needed information to design engineers and those involved in specification development. Both laboratory and field studies have been conducted, and these are discussed in turn:

Laboratory Model Studies

Christiano and Culver (1969) and Culver and Christiano (1969) constructed a plexiglass model of a two span curved girder bridge consisting of two girders connected by plexiglass girder diaphragms, plus a "composite" plexiglass slab. Their model had a centerline radius of 96 in and the two girders each subtended an angle of 28.05°. Culver and Christiano (1969) discussed static tests on the model, while Christiano and Culver (1969) conducted experimental studies of the effect of moving sprung mass models on the system, and provided numerical analyses for comparison. The dynamic studies reported a larger dynamic amplification of warping moments than of vertical bending moments. Because of the limited extent of the studies, no inference was suggested for other curved girder bridges.

In a recent study, the Federal Highway Administration (FHWA) conducted full-scale laboratory studies on two single span 90 foot, three girder bridges in the Turner-Fairbanks Laboratory. Much of the effort in that study was focused upon the lateral load transfer characteristics of the cross-frames, and the loadings applied to the models were primarily static. Limited dynamic data were also collected using an electrodynamic shaker, but no definitive conclusions were reached about the dynamic response characteristics, in part because of limitations imposed by the available magnitude of dynamic loadings. Linzell et al. (2004a) discussed the erection period studies on the first of the two Turner-Fairbanks curved girder bridge models. Because of the laboratory setting, it was possible to apply an extensive array of load cells, potentiometers, LVDTs, tiltmeters, and strain gages to the structure. Responses computed using an ABAQUS finite element (FE) model were in reasonably close agreement with the measured responses of this structure.

Field Studies on Bridges In Service

Armstrong (1972) studied the dynamic response of a four girder, single span curved girder bridge, with a centerline span of 95 ft-0 in, subtending an angle of 33.6° at a radius of 162 ft-0 in to a series of controlled truck loadings. The focus of his study was evaluating dynamic amplification factors for curved girder bridges. He observed that the bottom chords of the double angle X braced cross-frames perform an important function in forcing the individual I-girders to act together, and that the outer girders tended to have a higher dynamic response than the inner girders. Armstrong (1972) also cited 9 other curved girder bridge field studies that were conducted by other researchers between 1964 and 1971.

Galambos et al. (2000) carried out field studies on a two span, four girder bridge with skewed supports to measure the strains that develop in cross-frames and girders during the construction period because of girder twisting and cross-frame mismatch. They then compared the measured strains with strains predicted by curved girder bridge analysis software. In addition,

they conducted live load tests using measured trucks. Generally the experimental and computed results agreed reasonably well, except that the restrained warping of girders and some of the strains in cross-frames were not predicted very closely. Galambos et al. (2000) did not discuss pier flexibility effects. It is not mentioned in the paper whether the central pier was included in the computational model or not.

McElwain and Laman (2000) carried out field studies of three curved girder bridges to evaluate dynamic amplification factors and load distribution factors. Generally, their measured and computed load distribution factors agreed reasonably well. Womack et al. (2001) carried out field tests on a decommissioned three span steel I-girder bridge prior to demolition. The bridge had been designed as non-composite, although some composite action was observed during the experiments, especially near the mid-span instrumentation locations. Measured and calculated deflections generally agreed to within about 5%, and strains were within about 20%. The bridge deck had been designed as integral with the abutments, so the superstructure showed a considerable amount of rotational resistance at the abutments.

Domalik et al. (2005) monitored strains during construction of a two span curved plate girder bridge with unequal span lengths that was scheduled for completion in 2004. They were especially interested in measuring the global twisting effect caused by unequal span lengths, and the influence of girder rotation on the stresses developed in the flanges under vertical loads.

Analytical and Computational Studies

Local Plate Stability Studies

A number of analytical curved girder studies have focused upon local plate stability issues. The findings of some of these studies are relevant to the current field studies, and all of the studies are relevant to the design specifications under which the Wolf Creek Bridge was designed. Plate buckling considerations impose slenderness limits on both flanges and webs during the design of both straight and curved girders. Because of curvature, the buckling behavior of curved girder flanges and webs differ from that of straight girder flanges and webs, and these changes had to be properly incorporated in the design specifications thickness ratio limits. Such studies historically have involved extensive computation, as well as some experimental results.

Culver and Frampton (1970) studied the stability of elastic curved flange plates using the finite difference method. They found that the local flange buckling stresses are influenced in a complex manner by curvature, and by the rotational restraint provided by the web. When the web restraint was idealized as simply supported, the exterior flange plate buckling loads increased with curvature, but the interior flange plate buckling loads decreased. However, if the web restraint was idealized as fixed, the reverse occurred. They noted that the magnitude of this effect is relatively small within the range of curvatures typically used for curved girder bridges. Culver and Nasir (1972) extended the analysis to inelastic flange plates with residual stresses, and generalized the edge conditions at the web to include elastic restraints. They described this influence for several different flange to web thickness ratios, and provided design guidelines for curved girder flange plates.

Curvature has also been shown to have a strong influence on the stability behavior of I girder webs, even if the curvature is relatively small, since a curved web is no longer a plate, but a shallow shell. Culver, Dym and Brogan (1972) carried out early studies of curved web stability under edge stresses consistent with girder bending, and proposed web slenderness design limits. Abdel-Sayed (1973) extended this analysis to combined web bending and shear, using an eighth degree cylindrical shell model as a starting point. The work in these early studies provided the basis for web slenderness limits in the first edition of *Guide Specifications for Horizontally Curved Highway Bridges* (AASHTO, 1980). Davidson, Ballance, and Yoo (1999a, 1999b, 2000a, 2000b) performed more recent studies on web stability, considering bending, and combined bending and shear. They showed that curved web plates tend to begin out of surface deformation as soon as loading commences. The compression zone tends to bow outward, increasing the curvature, while the tension zone tends to move inward, reducing the curvature. Because of this behavior, longitudinal stiffeners have a beneficial effect in both compressive and tensile zones of curved girders. They also showed that classical buckling does occur under pure shear. For combined bending and shear a transition between the two types of behavior occurs. They also concluded that earlier guide specifications have highly conservative provisions for web slenderness.

Curved Girder Bridge Analysis

One important objective of the study is to compare measured stresses in the girders and diaphragms of the Wolf Creek Bridge with those predicted by a previously constructed FE model. Therefore, some discussion of available modeling alternatives is warranted. Multi-girder bridges can be analyzed using the FE method, and a variety of different approximations, and most of the approximations that have been used for straight alignment bridges can also be extended to curved girder bridges. For example, Wang et al. (2005) modeled a composite slab girder bridge using shell elements for the concrete deck and steel webs but frame elements for the girder flanges, and rigid links to simulate composite action. To simplify connection, they introduced “pseudo-elements” to permit cross-frames to be connected at locations other than the shell element nodes. Zhang and Aktan (1997) discussed a variety of different discretization techniques that may be used to model bridge superstructures. In a study associated with the Turner-Fairbanks curved girder studies, Tilley (2004) used shell elements to model both the deck and the girders of the second test bridge, and used rigid link elements to model composite action. Simons (2005) noticed that the rigid links appear to cause local flange distortion near the connection points in FE models, so he used shell elements to model the entire superstructure of the Wolf Creek Bridge. This approach was also used by Lydzinski (2006). To reduce the model size he idealized the hammerhead pier using a frame element approximation that was designed to reproduce the pier stiffness while overestimating the piers’ effective mass somewhat. He also conducted convergence studies to determine the minimal discretization level needed for reasonable response estimation. Lydzinski’s model, as modified by Turnage (2007) was used as the baseline FE model for comparison in the current studies.

The Wolf Creek Bridge

The Wolf Creek Bridge is a three-span, curved girder steel and concrete composite bridge located near Narrows, Virginia. The superstructure consists of four continuous plate girders running the length of the bridge, over two intermediate concrete hammerhead piers situated roughly 30% of the total span from each abutment, as shown in Figure 1. The piers' columns have a diameter of 5 ft0 in and extend 14 ft from the foundations to the bottom of the pier caps. The superstructure framing plan is shown in Figure 2. A series of C15x33.9 diaphragms support the girders laterally at various locations along the span. The diaphragms are fastened to the girders by bolted connections, as shown in Figure 3. The radius of curvature is 260 feet at the centerline, with the total span roughly 188 feet along the centerline curve subtending a total angle of 41°24 ft.

Figure 1. Wolf Creek Bridge, view from the South

The numbering scheme used in this report follows that of the construction plans. Girders and diaphragms are numbered consecutively from the outside of the curve inward, and the abutments and piers are denoted as "A" for the north end and "B" for the south end of the bridge. The end spans are accordingly referred to as spans A and B, and the main span is called the "center span."

PURPOSE AND SCOPE

The Wolf Creek Bridge, although apparently fairly simple in layout, has provided several challenges for accurate modeling. The bridge has the typical complications of a curved girder bridge. The web and flange plates are relatively thick, so local stability considerations are not of primary concern. However other aspects of the bridge's behavior have led to questions that can only be adequately addressed through field study. The modeling process undertaken by Lydzinski (2006) highlighted several specific points of concern:

- The dynamic response characteristics of the bridge as modeled using ANSYS appear to be significantly influenced by the inclusion, or exclusion of pier flexibility.
- The shell modeling process had difficulty handling the discrete bolted girder-diaphragm connections. The simplifying assumption was introduced that the connection was rigid. The adequacy of this assumption has not been verified, and the sufficiency of these diaphragms for lateral load transfer had been questioned during the design review process. At least some of the data provided by Turnage (2007)

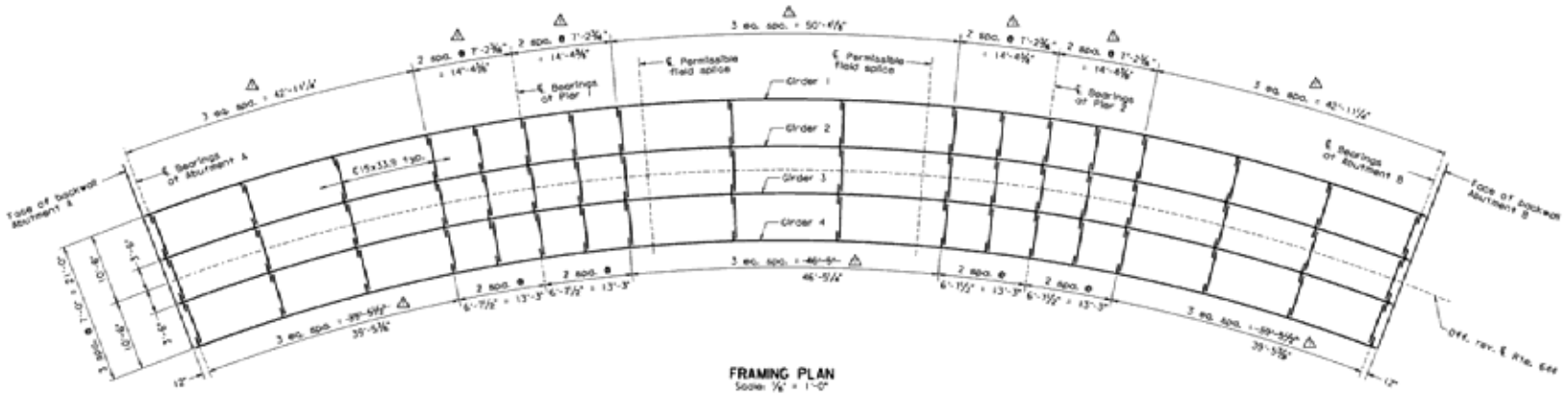

Figure 2. Framing Plan of the Wolf Creek Bridge

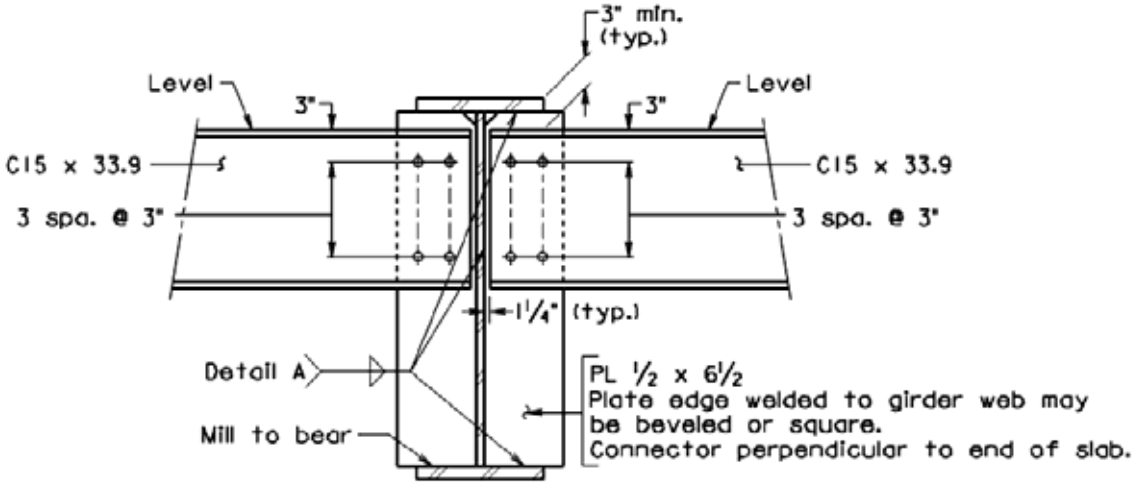

Figure 3. Diaphragm to Girder Connection Details

comparing field vibration data to the FE model suggests that the girder diaphragm connections may not be fully rigid.

- The interaction between the superstructure and the piers may significantly influence the distribution of moments between the girders, and between positive and negative regions.
- Turnage (2007) observed that the highway railing, tied into the superstructure at each end appears to significantly influence the free-vibration response characteristics, at least. Since the free-vibration studies were conducted using relatively small excitations, it is not clear that this effect on the boundary conditions will remain valid under larger vehicular loads.

These questions may be answered computationally with some confidence, once it has been shown that a computational model correctly predicts strains under vehicular loading for at least one cross-section of the bridge. Alternately, to the extent that the measured and computed strains differ, field data will provide information that can be used to subsequently improve the modeling process. Most importantly, insight gained by carrying out the studies will inform not only the modeling process, but also the design process for curved girder bridges as well. By comparing static and dynamic loadings, additional insight may be gained into the appropriate dynamic amplification factors for this structure. Therefore, the overall objective of the current studies is to obtain representative girder strain data from at least one cross-section of the Wolf Creek Bridge, plus diaphragm strain data, to compare the data with the previously developed computational model, and to address the key points introduced above in view of the comparison.

Phase I of this study was published separately (Turnage and Baber, 2009).

METHODS

Field Instrumentation Studies

Instrumentation Plan

An array of strain gages was installed on girders 1 through 4, at the middle of the center span. The instrumented cross-section of the bridge is illustrated in Figure 4. Each of the three inside girders, girders 2-4, was instrumented with eight weldable gages oriented parallel to the girder axis, while the outside girder, girder 1, was instrumented with ten weldable gages. The gage locations are illustrated in Figure 5. On both sides of each girder, gages were located at the outer edge of the top and bottom flanges, and at the top and bottom of the web near the web-flange connection. One gage was also located at mid-height of the web on each side of the girder 1. To ensure that the gages were properly identified during analysis, the gages on either side of the web were numbered consecutively beginning with the outer edge of the top flange, and ending with the outer edge of the bottom flange. To distinguish between the gages on either side of the web, gages located on the side of the girder away from the center of curvature of the bridge were designated as "outer" and those on the side of the girder toward the center of curvature were designated inner.

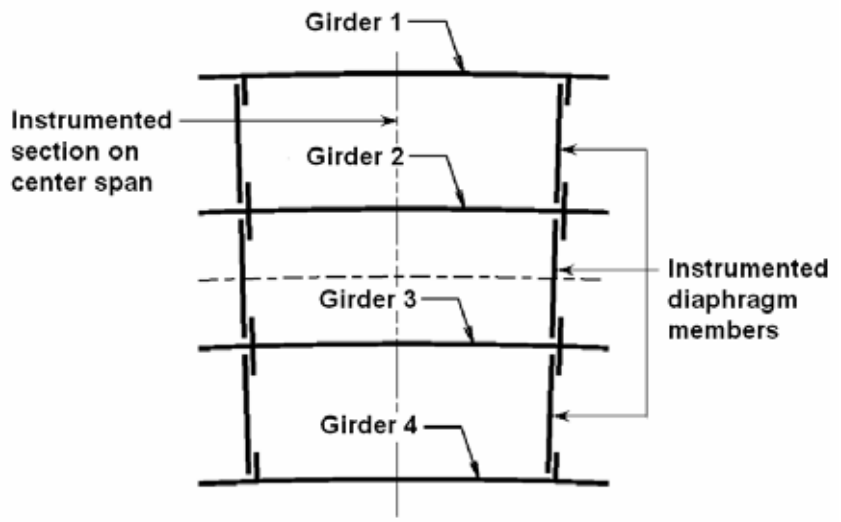

Figure 4. Mid-span of Center Section and Diaphragms

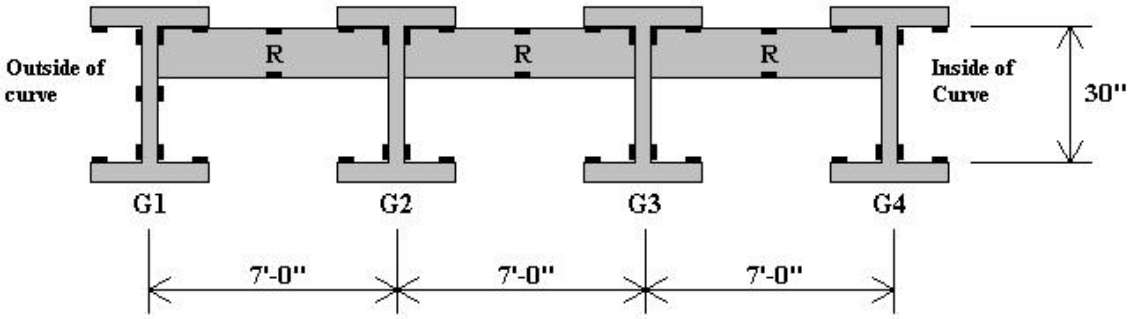

Figure 5. Gage Locations

The three diaphragms located nearest the middle of the center span, an average distance of 8.1 ft from middle, were each instrumented with two weldable gages and one rosette, as shown in Figures 4 and 5. In subsequent discussions, these diaphragms are referenced according to the girders at either end. For example, the diaphragm between girders 1 and 2 is referenced as diaphragm 1-2. The other two diaphragms are similarly referenced as diaphragms 2-3, and 3-4. Thus, diaphragm 1-2 is farthest from the center of curvature, while diaphragm 3-4 is closest to the center of curvature. All gages were installed on the side of the diaphragm channels toward the flanges, as shown in Figure 6. The weldable gages were installed at outer edges of the top and bottom flanges, and the rosette was located at mid-height of the web.

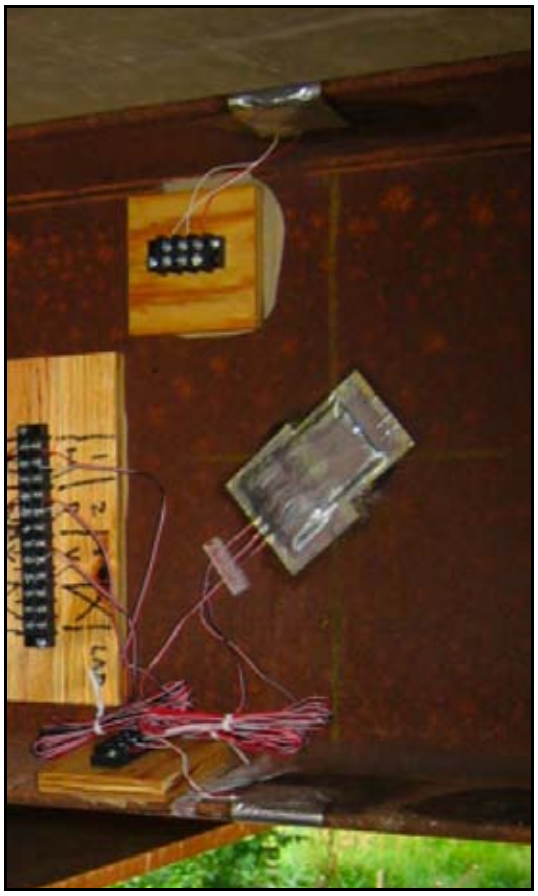

Figure 6. Gage Installation at Diaphragm

Gages

Vishay Micro-Measurements Strain Gages were used for this experiment. Because the Wolf Creek Bridge is constructed of weathering steel, a metal grinding wheel was used to strip away the rust in a small area surrounding the gage. The gages were installed first on girder 1, then girders 2-4 consecutively. Initially, some difficulty occurred during gage installation achieving a sufficiently smooth surface that the spot welder would not cause a spark. Because of this, one gage was damaged and was replaced. From this point on, surface preparation proceeded in two steps. First a grinding wheel was used to remove the layer of oxide on the bridge. Then a 120 grit flapper disk was used to further smooth the exposed metal surface. Once this surface preparation procedure was introduced no more gages were lost. The 120 grit flapper disk, applied by itself, was also capable of producing a sufficiently smooth surface, but using this

alternative procedure tended to produce excessive wear on the flapper disk. Following grinding, the surfaces were cleaned using established procedures for strain gages before the strain gages were applied. The exterior girder surfaces were painted, even though the steel is weathering steel, and it was found that an initial cleaning step using denatured alcohol was beneficial for these surfaces.

Two types of gages were used, a weldable single gage and a bondable, three element rosette. All gages used had 350 ohm resistance, which is compatible with the bridge completion modules in the data acquisition system. The weldable gages are of type W250B. A spot welder was used in accordance with techniques given by Vishay Micro-Measurements to ensure satisfactory attachment of the gage. The weldable gages have a resistance of 350.0 +/-0.4% Ω, a nominal gage factor of 2.03 +/-1.0% at 24°C, and a transverse sensitivity of -4.5 +/-0.2%. These gages were used on all instrumented members and constitute the majority of gages installed.

The bondable rosette used on the diaphragms is of type 250LR. An EPY-150 room temperature curing epoxy was applied to each gage, and a magnet was used to apply pressure to secure the gage in position during the curing period. Each 250LR rosette contains three separate strain gages, one oriented in each of three directions: horizontal, 45°, and vertical. The bondable gages have a resistance of 350.0 +/-0.6% Ω, a nominal gage factor of 2.08 +/-1.0% at 24°C, and a transverse sensitivity of +0.3 +/-0.2%. Three rosettes were installed, one on each of the three diaphragms closest to mid-span.

Following installation, each of the weldable and bondable gages was weatherproofed using the Micromeasurements M-Coat F kit. Each gage was first covered with a thin layer of Teflon tape. Then a layer of butyl rubber protection, a layer of aluminum foil tape, and an edge sealant of nitrile rubber were applied, to ensure proper gage functioning would be retained through the instrumentation period. Although several weeks elapsed between the gage installation and the measurements, no problems were observed with the function of any of the gages, and all channels yielded reasonable data.

Setup

After each of the gages was installed and waterproofed, the lead wires from each gage were connected to individual terminal strips, as shown in Figure 7. The terminal strips had previously been fastened to plywood blocks, which were painted with polyurethane for moisture protection and glued to the girders using construction adhesive. The intermediate terminal connections were used to decrease the possibility of a gage being damaged by an inadvertent pull on one of the leads. The terminal strip resistances were checked at this point to verify a good connection of each gage. A 22 gage, shielded 3 wire cable, which had been pre-labeled to ensure correct connection, was then attached to the opposing end of each terminal and run along the girder to Pier B, where it was connected to another terminal designated for each girder and diaphragm, as shown in Figure 8. The lead wires had been pre-cut, labeled, and bundled to minimize possibilities of errors during the connection procedure. Following connection of the lead wires and the shielded cable to the terminal strips, a layer of butyl rubber was applied to each terminal strip at the gages to retard moisture intrusion.

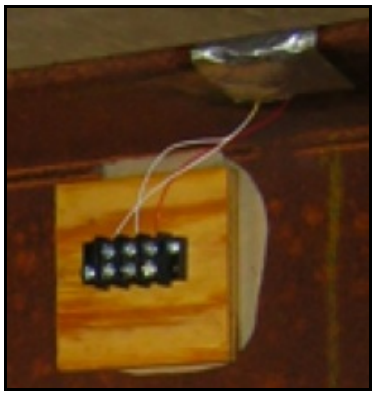

Figure 7. Terminal Strip and Gage

Figure 8. Terminal Strips at Pier B

The terminal strips at Pier B are largely protected from the weather by the bridge superstructure, and it was necessary to access the terminal strips during data collection, so they could not be waterproofed using butyl rubber. However, following the initial installation, the terminal strips at Pier B were covered with a sheet of landscaping fabric to provide some protection from the elements.

The final connection from the terminal strips at pier B to the data acquisition system (DAS) was achieved using a single composite cable. Twenty eight shielded lead wires were bundled together, organized into six smaller sub-groups and numbered to ensure each input channel could be associated with the correct gage for each run, since each test setup required connections to six terminal blocks at the pier.

The lead wires were connected to a 28 channel Megadac 3200 data acquisition system, running under the Optim supplied control software. The system has built-in bridge completion modules, which simplified hookup, software controllable gains, and excitation voltages. The system also features eight pole Butterworth filters with software programmable roll-off frequencies. The data acquisition system, with the lead wires connected is shown in Figure 9. Although the Optim DAS can run directly from battery power, the system used has been configured to run off 110 VAC, so power to the data acquisition system and the controlling computer was provided using a portable Honda generator.

Since the installation included 49 gages, all tests had to be run twice, first for girders 1 and 2, and diaphragms 1-2 and 2-3, and a second time for girders 3 and 4, and diaphragms 2-3 and 3-4. These sets of data are hereafter denoted as Setup 1 and Setup 2.

Data for Diaphragm 2-3 obtained from setups 1 and 2 was checked to evaluate consistency between setups.

Figure 9. Connection to Data Acquisition System

Troubleshooting

Before any data were collected for analysis, a day was dedicated to identify and correct any problems with the system and to choose the best parameters for the DAS. Several passes across the bridge were made using a work van with different parameter settings on the data acquisition system. Settings varied included voltage, channel gain, and filter frequency, in an attempt to obtain the best possible signal.

Since the expected strains were relatively small, a large excitation voltage was needed in order to achieve a sufficient voltage change across the gages for accurate readings. Thus it was decided to use the maximum available voltage of 10 volts. The gain was then set at the highest level that allowed all gages to remain within the range of the analog to digital converter. The most significant problem encountered was electrical noise interference, which after some analysis was identified as originating from the generator used to power the DAS. Grounding the generator and setting the filter roll off frequency at 25 Hz resolved this problem. Previous field accelerometer data and FE analysis had revealed that the bridge's response modes most likely to influence the response have natural frequencies below 25 Hz, so no significant strain information was lost with this setting.

Experimental Strain Studies

Test Vehicle

A 10-wheel Ford L9000 tandem axle dump truck with a full bed of gravel was selected to apply the loads. The measured weight of the loaded truck was 44,480 pounds, and information in the cab of the truck revealed the truck weight to be 16,405 pounds. The total weight is slightly larger than an HS 20 loading. Measurements of the truck bed, front and back axles, and distances

between the front, middle, and rear wheels were noted. The center of the load was located very near the middle axle, so this was used as the reference axle for positioning the static loads. Further information on the wheel load distribution is provided below, where the application of the vehicular load to the FE model is described.

Static Data Collection:

To gather static data, the bridge was divided into inner and outer lanes, and the truck was positioned such that the inner axle was located at nine locations that had been previously marked on both the inner and outer lanes of the bridge. These locations are shown on Figure 10. "0.4 A" denotes 40% of the far left span taken from the left abutment end, "0.4 B" denotes 40% of the far right span taken from the right abutment end, and so on. From left to right the measurements along the centerline are as follows: 22.4, 39.2, 56, 75, 94, 113, 132, 148.8, and 165.6 feet. The exact locations of these stations were marked, and load points on the inside and outside lanes were taken at the center of the respective lanes. Blank data were collected periodically by taking measurements with no load on the bridge to provide a zero shift baseline for the load data. Then, with the truck at the positions described above, data were gathered for approximately 30 seconds, and each reading was recorded into a separate file on the DAS for subsequent analysis. The length of the sample permitted averaging of strain values to eliminate any noise present in the measurements, and also allowed the level of noise to be estimated.

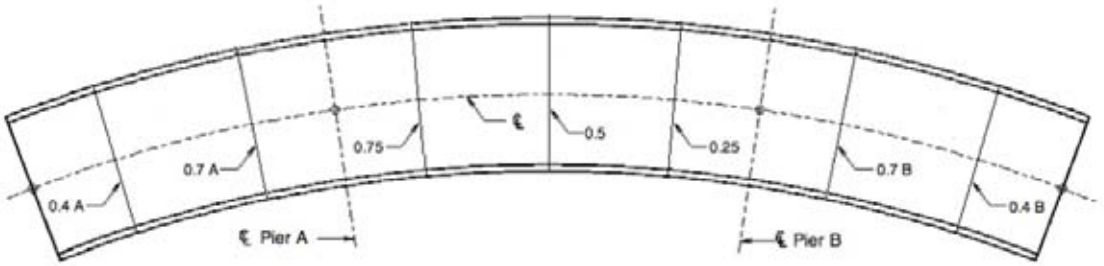

Figure 10. Center of Truckload Locations

Dynamic Data Collection

To generate dynamic data, the truck was driven across the bridge as rapidly as possible. Because of sharp entry and exit conditions, the small radius of curvature, relatively short span, and a stop sign located near one end of the bridge, 10-15 mph was the maximum speed that could be achieved. These constraints also prevented the truck from maintaining a constant speed as it crossed the bridge. However, because of the physical limits imposed by the bridge, the load data should be representative of the largest dynamic loads to which the bridge would actually be exposed on a regular basis. Some very heavy logging trucks occasionally use the bridge, but these vehicles have been observed to cross the bridge at a near crawl speed, so the dynamic amplification from the logging truck loads is probably small.

Two truck runs were made on both the inside and outside lanes, one for each of the DAS setups, setup 1 and setup 2. Each run was recorded separately with approximately 5 seconds of blank data taken both before the truck entered the bridge and after it exited the bridge, to permit an accurate baseline for the unloaded bridge to be established.

Data Processing

Static Data

The final static strain estimates were obtained by averaging the columns of data recorded from each strain gage over the number of collection points obtained during the 30 second sampling period. Each data point was then calibrated to the unloaded state by subtracting the average of the blank data for the current setup taken with no load on the bridge.

Dynamic Data

The baseline value for correcting the dynamic data was obtained by averaging the blank data collected during the short time period before the truck entered the bridge on each run. This average was subtracted from each data point recorded during the truck runs to establish a zero baseline. These corrected strain readings were plotted in μstrains versus time, which generated graphs to represent the strain changes at each gage location under a dynamic load.

Static/Dynamic Comparison

A comparison of the static and dynamic data was carried out to verify the validity and consistency of the results and provide information on dynamic amplification, as well as to locate any discrepancies. Establishing a direct correlation between static and dynamic data was not straightforward, since the static data were taken at specific stations measured along the bridge, while the dynamic data were taken over a period of time with no precise way of indicating when the truck passed each static load location. To further complicate matters, a constant velocity was not possible for the dynamic runs as mentioned above. An approximation was thus necessary to indicate when the truck passed each interval during the dynamic run, to allow the static data and the dynamic data to be directly compared. This was achieved by replotting the static data against a *nominal* time axis.

In order to match the static data to the dynamic data, it was assumed that there would be relatively little live load bending strain in the girders when the truck was located directly over the piers. The majority of the static data tended to validate this assumption. Therefore, the dynamic graphs were magnified and an estimate was made as to where the data changed signs. This was related to the static data at each pier, and the abutment. The same procedure was conducted at the maximum dynamic readings, shown in the static data to occur at the mid-span of the center span. Finally, the dynamic graphs were examined closely at the beginning of the truck passage to identify the point where the strain readings became nonzero. This was assumed to be when the truck entered the bridge. This point was a little more difficult to determine exactly, but a reasonable estimate was generally possible.

The time elapsed between each location was divided by the span length to calculate an approximate truck speed over each of the three spans. To identify the time at which the truck was located at each point, the distances between each of the remaining twelve locations were divided by the speed over the appropriate span. Then each static data point was assigned its corresponding time and graphed atop the dynamic data.

The load is distributed between three axles over a wheelbase of 19.3 feet, a distance of the same order of magnitude as the length of the bridge spans. Thus some of the approximations made of the pier locations and enter and exit conditions may not be very accurate. However, in the field the truck was visually observed to cross the bridge in about 13 seconds, which concurs with the time estimates obtained from the dynamic data in this comparison.

Second Setup Static Data Corrections

The static data curves obtained from the second setup were similar to those of the first setup, as well as those from all dynamic runs, but with a significant offset on the strain scale such as shown in Figure 11 for the outer gages on Girder 3. Such offsets were common for much of the strain data, but all channels obtained during setup 1 were adequately corrected to an unloaded baseline using the blank data fields obtained before and after loading. However, after several trials using the blank data assumed to be associated with setup 2, it was concluded that inadequate blank data sets were taken in the field for this setup. It was thus necessary to attempt to correct these strain readings using a different approach. Such a correction must be regarded as approximate, but it will allow comparison of static and dynamic data to a certain extent, and further will allow the static data to be interpreted reasonably.

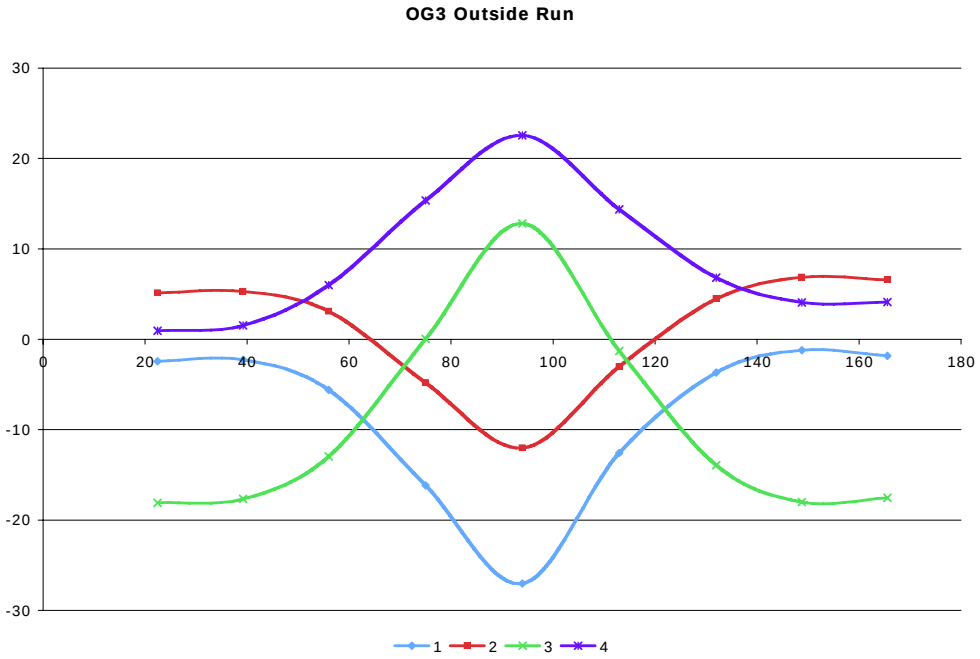

Figure 11. Example of Offset in Second Run Setup Data

Since the static and dynamic data were highly correlated in the first setup, and it was not possible to correct the static data from the second setup using a blank data set, it was assumed that the second setup's data should have a similar pattern. The strongest signal, indicated by the highest strain readings, was transmitted when the truck was located at mid-span of the center section. Thus these readings were taken to be the most accurate from the dynamic data and were used to correct the static data for setup 2. The difference between the dynamic and static readings at mid-span was used to calibrate each strain reading for the corresponding girder or diaphragm. The static corrections calculated in this manner are available in Miller (2008).

Since the dynamic data were oscillatory, an estimate had to be taken to identify the strain reading to be used to correct the static data. The setup 1 data indicated that the dynamic oscillations appear to be roughly equal above and below the static values, so the estimate used averaged the maximum and minimum values of the oscillations at the peak response. The shift may not be precise, but after the simple corrections were carried out the static and dynamic data lined up well over the entire span and appeared similar to the first setup results. Thus it can be assumed that the manual shift in data is reasonable.

Finite Element Analysis

Discussion of the Existing Model

In 2006, an FE model of the Wolf Creek Bridge was developed using the ANSYS program (Lydzinski, 2006). The model attempts to provide an accurate representation of the bridge superstructure in lengths, dimensions, and material properties. The model was formulated in cylindrical coordinates with over 30,000 elements. Nodes lie on radial lines, and concentric circles, thus facilitating analysis in terms of distance along the curve in radians (θ), and radius (r) and height (z) in inches. An isometric view of the model is shown in Figure 12.

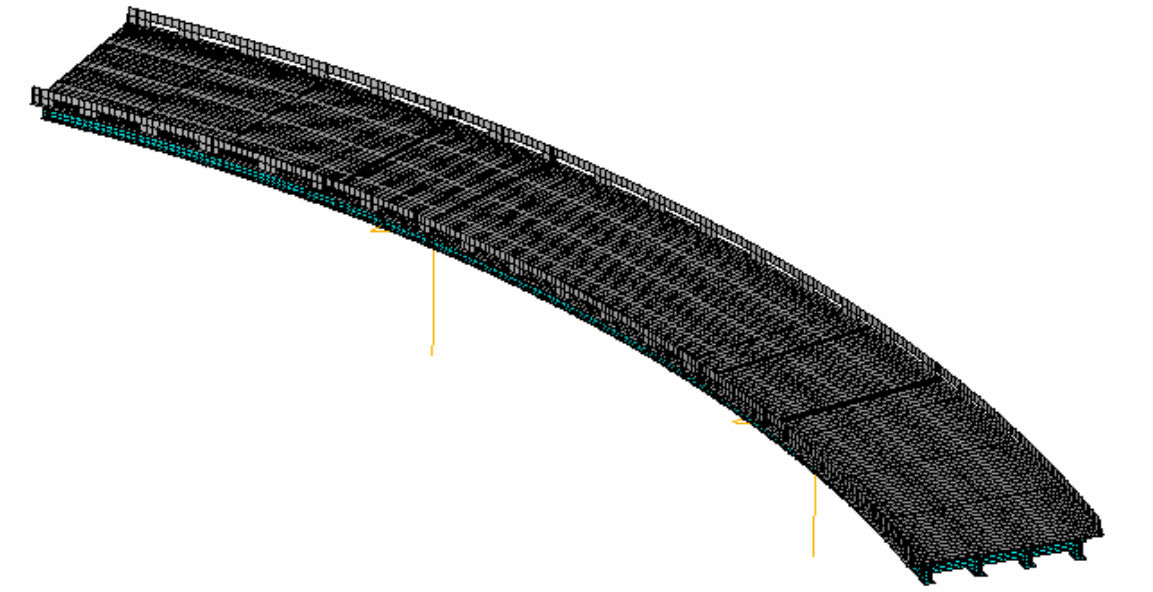

Figure 12. ANSYS Model of the Wolf Creek Bridge

The superstructure model was formulated entirely using shell elements, with the deck, girder, haunches, and railings all modeled with SHELL63, the discrete Kirchhoff element described by Batoz et al. (1980). The piers were modeled using frame elements, to reduce the total number of degrees of freedom in the overall model. The pier model was optimized to provide stiffness as close to that given by a three-dimensional solid model of the piers as possible. In Lydzinski's model, the slab was considered to be effective in both positive and negative bending regions of the structure, and no slip was permitted between the haunch and the girder top flanges. A number of convergence studies were conducted during the initial model

development to ensure that the model provides a reasonable representation of the bridge stiffness.

At the abutments, the model is constrained against translation in the *r* and *z* directions but free to deflect in the θ direction and rotate about all three axes. Following field vibration studies by Turnage (2007), during which it was discovered that the corrugated safety railings tied into the ends of the bridge were constraining longitudinal movement of the rails, additional translation constraints in the θ direction were applied at distinct nodes on the end of each of the four concrete railings to mimic the effect of the barrier railing present in the field. No attempt was made at that time to accurately model the steel safety barriers at either end, although a more recent study has attempted to model the stiffness of the end rails (Fuchs, 2008). Because Fuchs' work proceeded concurrently with the current study, her results have not been included in the current modeling effort. Steel and concrete material properties in accordance with the Wolf Creek Bridge construction plans were applied to the appropriate plate elements.

Although the FE model attempted to be as accurate as possible, it was necessary to introduce some approximations to control the size of the model. The expansion bearings at the abutments were, as discussed above, treated as ideal roller supports in the θ direction. The pinned supports at the piers were modeled by linking the degrees of freedom of the girders with the corresponding degrees of freedom of the piers, with no attempt to model the physical dimensions of the pins. The railings were modeled with shell elements, and certain details of the railings were simplified somewhat. Moreover, the as-built railing dimensions could only approximately be determined from the plans, so the final railing model was not exactly the same as the as-built railing.

Finally, modeling the diaphragm to girder bolted connections is a highly complex problem by itself, so a simplified diaphragm to girder connection had to be used in the model, in which the overlap region was treated as a single plate element of doubled thickness. This introduced two approximations: the connection was forced to be rigid, with no slip possible, and the lines of force transfer from the connection plates to the diaphragms' webs were changed slightly relative to the plane of the girder web.

Load Data

In the current study, the weight of the measured truck was applied statically at the nominal load points to replicate the bridge loadings. There is some inevitable approximation in this process, since the truck could not be *exactly* located transversely on the bridge during the load tests. Therefore, there may be a few inches of lateral positioning error inherent in the FE model, where the truck can, at least in principle, be precisely placed at an arbitrary lateral position. Dynamic loading of the FE model was not attempted, because of the imprecise manner in which it was necessary to apply the dynamic loading in the field. As discussed previously, precise velocities could not be obtained under field conditions, and in the absence of such information, attempting to prescribe a moving sprung mass model, or even a moving force model to the FE model would not yield very useful results. Therefore, the FE results discussed subsequently only consider static loading.

To obtain strain data from the FE model that could be compared to the strains measured in the field, the load data had to be carefully described. The total load is supported by ten tires, two on one axle in the front and eight on two axles in the rear; the rear tires support a majority of the load. The assumed load distribution between axles is shown Figure 13. Since the eight rear tires are situated in closely spaced pairs, the rear axle loads were separated into only four point loads to be located at the center of each pair, as shown in Figure 14. This approximation is valid given the limits of the ability to place the truck accurately in the radial direction in the field, and given the subsequent approximation necessary to apply the forces as nodal loads. Also, although the total weight of the truck is known, and the center of the load bed is approximately centered over the two rear axles, there is some approximation in the exact distribution of the loads between the axles that was used in the FE models.

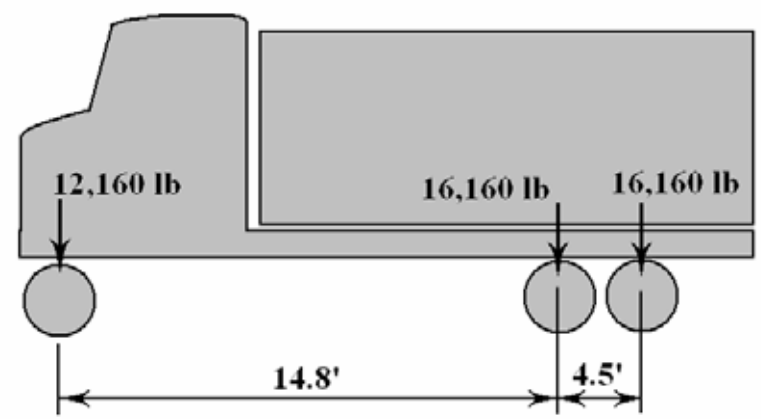

Figure 13. Idealized Test Vehicle Axle loads

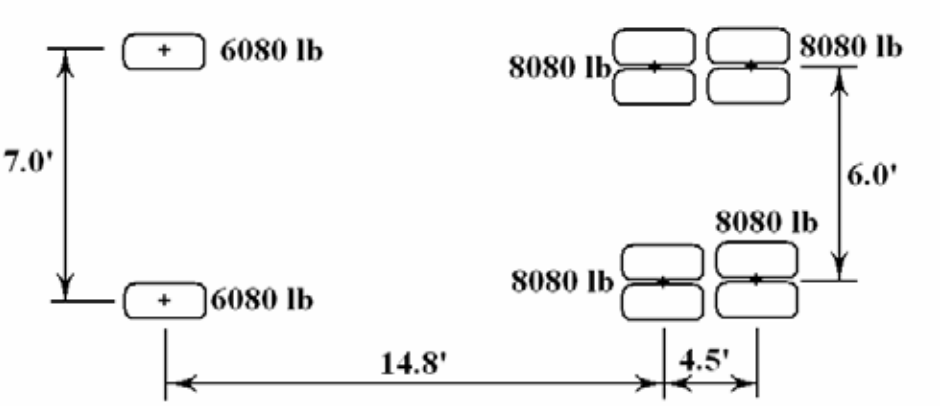

Figure 14. Point Load Model

In the FE software used in this analysis, point loads cannot be applied directly on elements and must instead be applied at individual nodes. As a result, it was necessary to distribute each point load to the four nodes at the corners of each appropriate element. With six point loads for each of eighteen loading locations, this distribution would have been tedious and time consuming to carry out by hand. Instead, an algorithm using *Matlab* was created to locate the elements on which point loads would need to be applied, and then apportion each point load to the corresponding nodes. The MATLAB m-file listings are provided in Appendix A.

The *r* and θ coordinates of a loading location were input into the algorithm, referenced to a particular point on the truck, and the 6 point loads were located on individual elements, according to their positions relative to the reference point, and the direction in which the truck was traveling. The point loads were then divided into components at the four nodes at the corners of the element using linear interpolation, and the node numbers and amount of load to be applied at each node was written into a text file. This text file was then directly input into *ANSYS*, leading to a load placement similar to that shown in Figure 15, and an analysis was run for that load position, from which the strain data could be read. This procedure was repeated for each of the locations corresponding to a static data set obtained in the field.

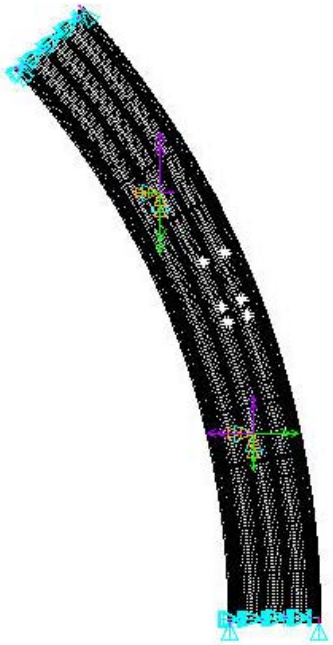

Figure 15. Point Loads Applied at Mid-span of the Outside Lane

Finite Element Output Manipulation

ANSYS has two output options from which strain data can be determined, element strains or nodal strains. The element data proved to be more difficult to interpret, as the sign convention and orientation of the elements was different for each element and no averaging of strains between adjacent elements occurs. Thus it was decided to utilize the nodal strains, which are provided in the active global coordinate system. The interesting directions for this study correspond to the radial (*r*), tangential (θ), and vertical (*z*) directions, so the global cylindrical coordinate system was made the active system.

In order to determine strain data from the FE model that compares to that gathered in the field, specific nodes had to be identified that correspond to the placement of the 49 strain gages in the field. For the girders this was done by identifying the row of nodes closest to the mid-span of the middle section. The nodes on the outside edges of each flange and the flange-web intersection were located for each girder, and at mid-height of the outside girder, as was instrumented in the field. Since the diaphragms on the south side of the bridge were

instrumented in the field, nodes at mid-length on the corresponding diaphragm elements in the FE model were located in accordance with field instrumentation.

Not all nodal locations corresponded exactly to the location of the strain gages installed in the field. This occurred at mid-height of each of the diaphragms, as well as at mid-height of girder 1 as shown in Figures 16 and 17. A method of averaging the values to compare to the field results was necessary for comparison. Graphing the strains from the FE model along the height of the girder and diaphragm webs showed a nearly linear relationship in each case. The height of the elements in both cases was small, as was the strain gradient between nodes. Thus a linear interpolation was considered acceptable to calculate the strains at mid-height of the web in both the diaphragms and girder 1. The strain data from each node were placed into tables and organized into graphs for subsequent comparison with the measured strains.

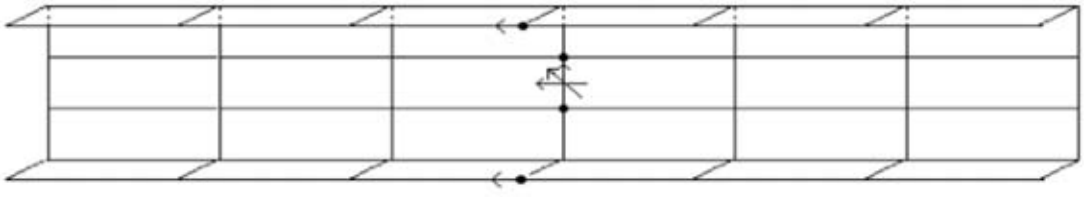

Figure 16. FE Model Diaphragm Elements and Strain Locations

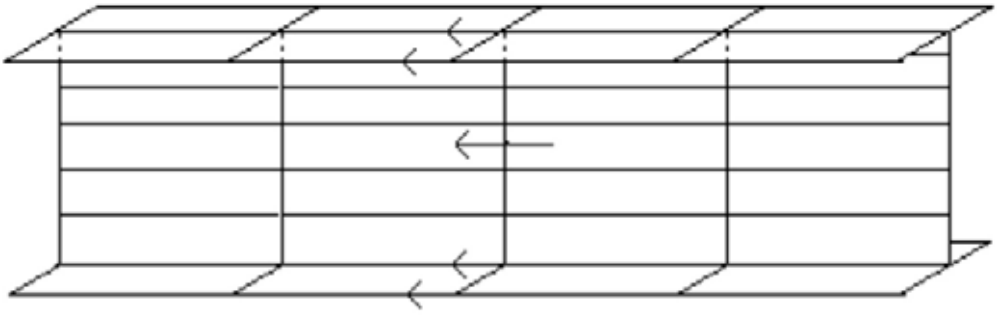

Figure 17. FE Model Girder Elements and Strain Locations

RESULTS

Field Data Analysis

Static Data

Strains at each of the 49 instrumented points were analyzed as a function of load position on the structure, using the technique described above. As an example of the static data, strain results obtained when the truck was located at the middle of the center span are shown in Figures 18 through 21. The truck is located in the outer lane in Figures 18 and 20, and in the inner lane in Figures 19 and 21. All values are given in μstrains. The strains shown on girders G1 and G2 and on diaphragms 1-2 and 2-3 were obtained from setup 1, while the strains shown on girders G3 and G4 and on diaphragm 3-4 were obtained from setup 2. As might be anticipated, the strains in girders G1 and G2 with the truck in the outer lane proved to be the largest strains of the

18 locations at which readings were taken. In the figures, negative strains represent compression and positive strains represent tension.

The measured static live load strain change in μstrain at each gage location was then plotted versus load position along the bridge. An example of the data for girder G1, obtained from the static loading, corrected for the baseline data, when the truck was located in the outer lane is shown in Figure 22. Complete static strain data are plotted in Appendix B.

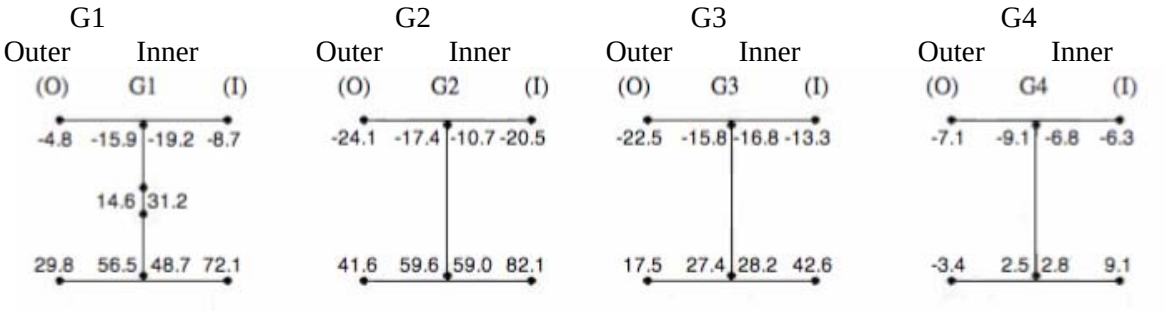

Figure 18. Girder Strains with Load at the Middle of the Main Span, Outside Run

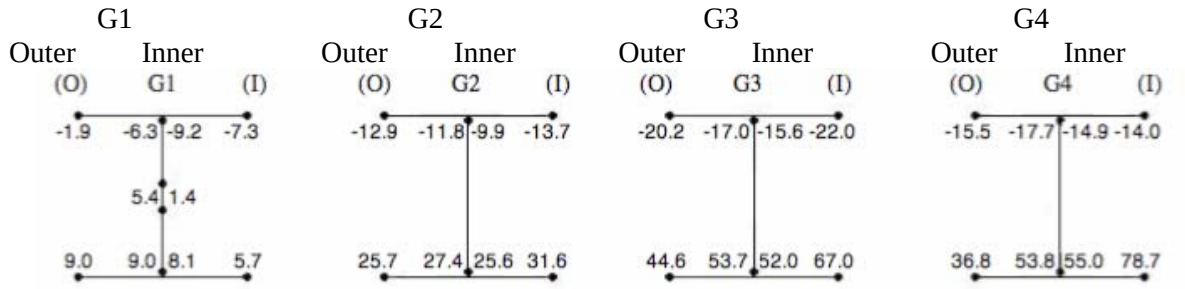

Figure 19. Girder Strains with Load at Mid-span, Inside Run

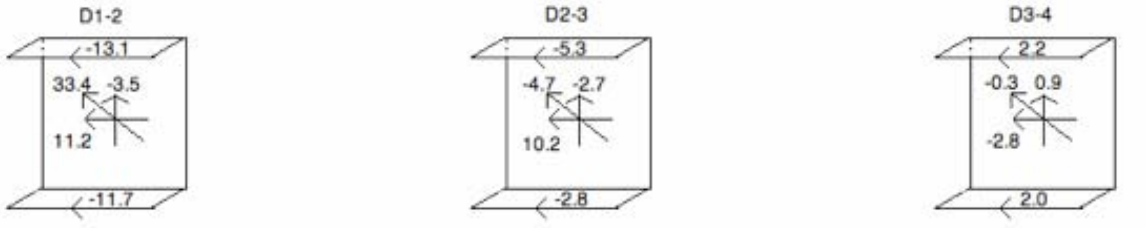

Figure 20. Diaphragm Strains with Load at Mid-span, Outside Run

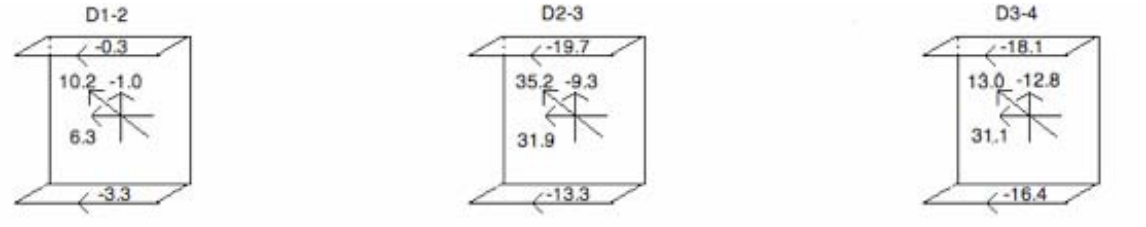

Figure 21. Diaphragm Strains with Load at Mid-span, Inside Run

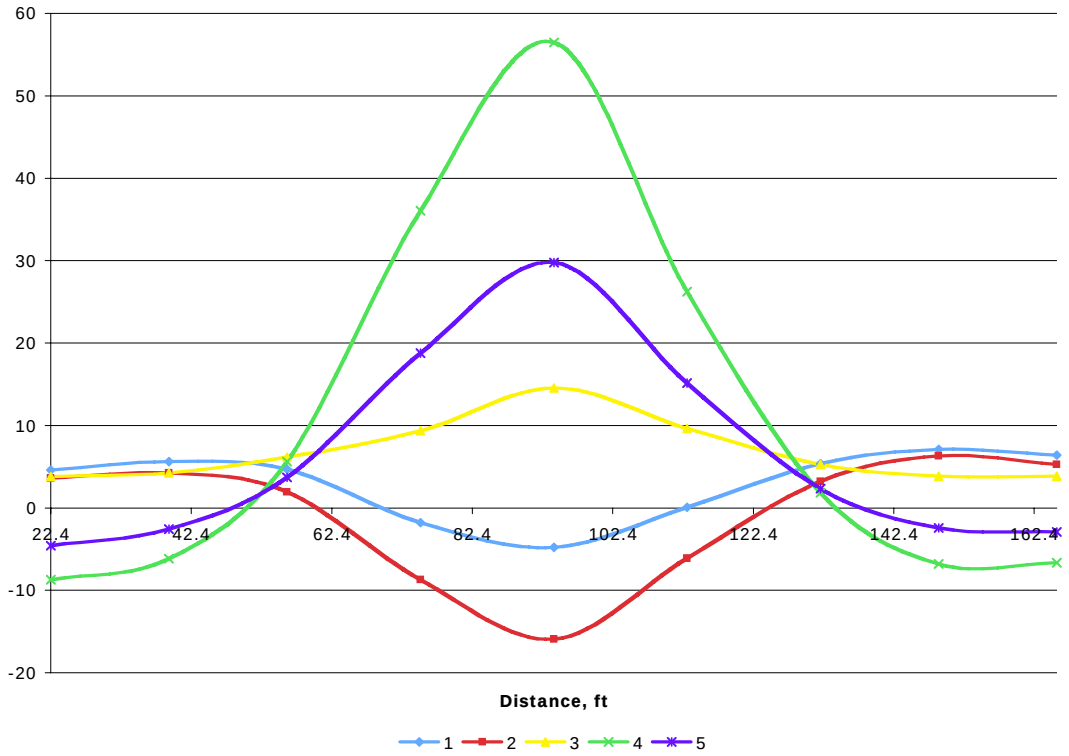

Figure 22. Static Load Data for Outside Girder 1, Outside Run

Dynamic Data

Driving the truck across the bridge generated a significant response in the lower natural frequencies in addition to the static response that had been measured previously. First bending-torsion mode response was particularly evident. This caused dynamic amplification of the data, relative to the static load data, which can clearly be seen when graphed. Together with the static load data, the dynamic data permits dynamic amplification factors to be estimated, after the static data has been shifted to the appropriate time ordinates as outlined above.

Static-Dynamic Comparison

The complete static and dynamic data comparison is shown graphically in Figures 23 through 44. Figures 23 through 33 show the measured strains when the truck is in the outer lane; and figures 34-44 show the measured strains when the truck is in the inner lane. The figures are arranged from the outside of the bridge to the inside of the bridge, with G1 data first, followed by D1-2, G2, D2-3, G3, D3-4, and G4 data in that order.

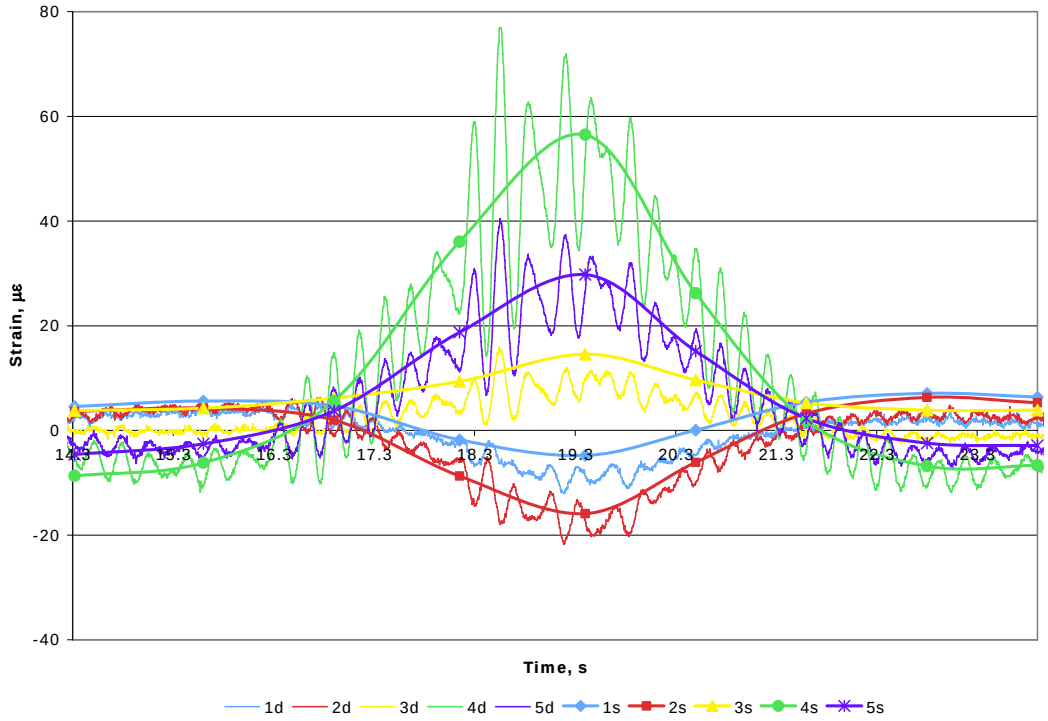

Figure 23. Static and Dynamic Strain Comparison, Outside of Girder 1, Outside Run

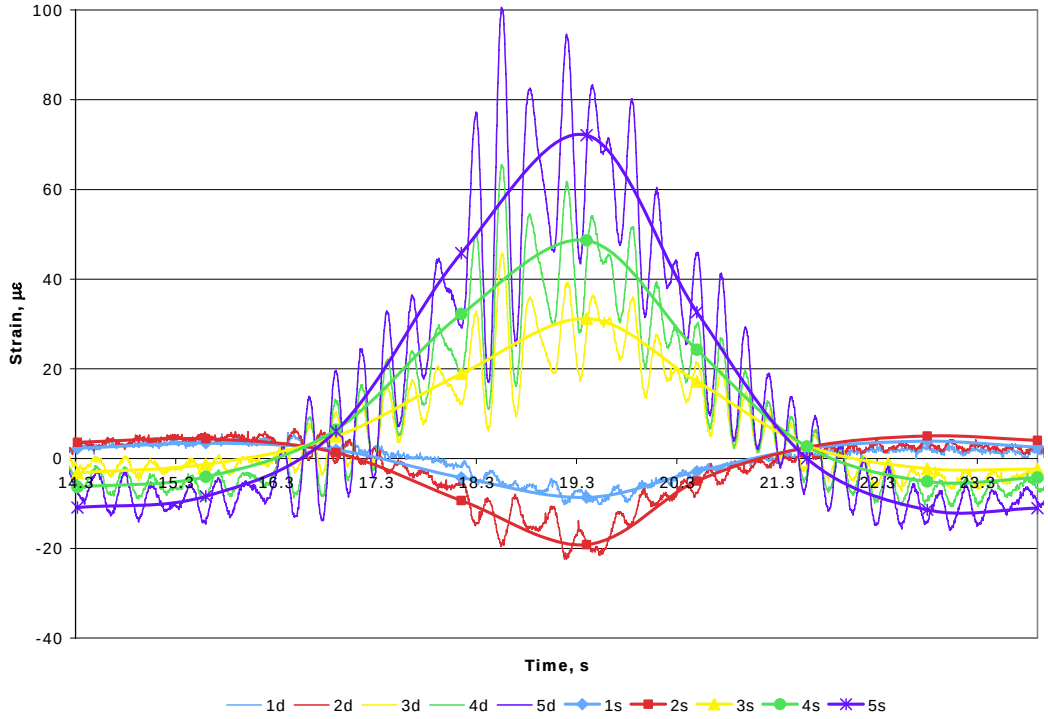

Figure 24. Static and Dynamic Strain Comparison, Inside of Girder 1, Outside Run

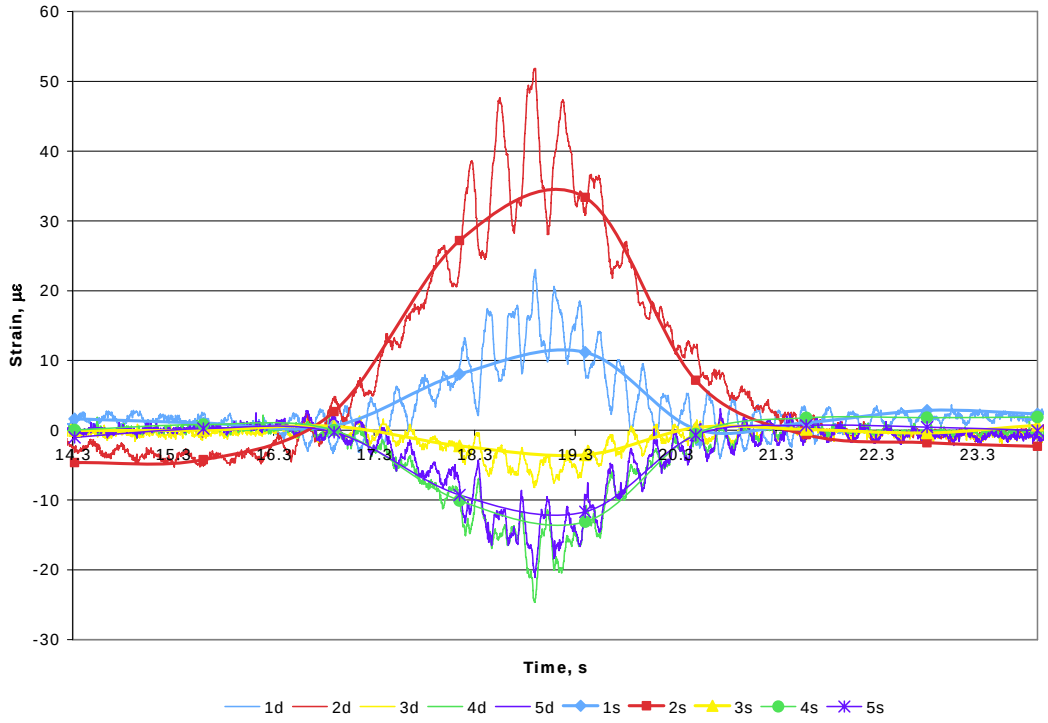

Figure 25. Static and Dynamic Strain Comparison, Diaphragm 1-2, Outside Run

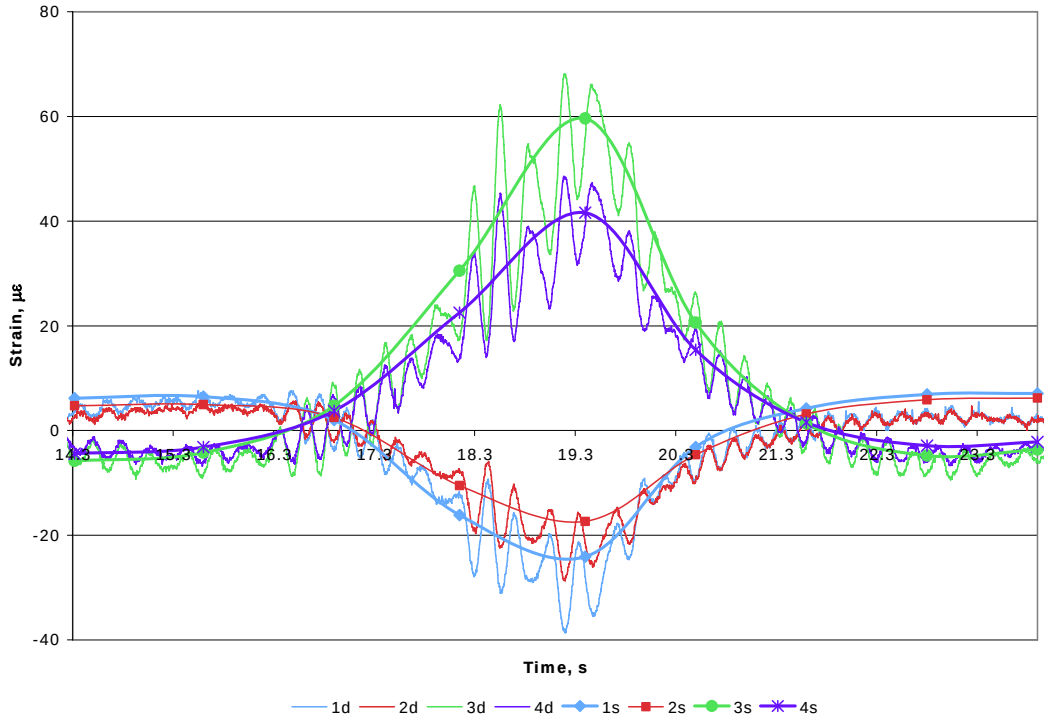

Figure 26. Static and Dynamic Strain Comparison, Outside of Girder 2, Outside Run

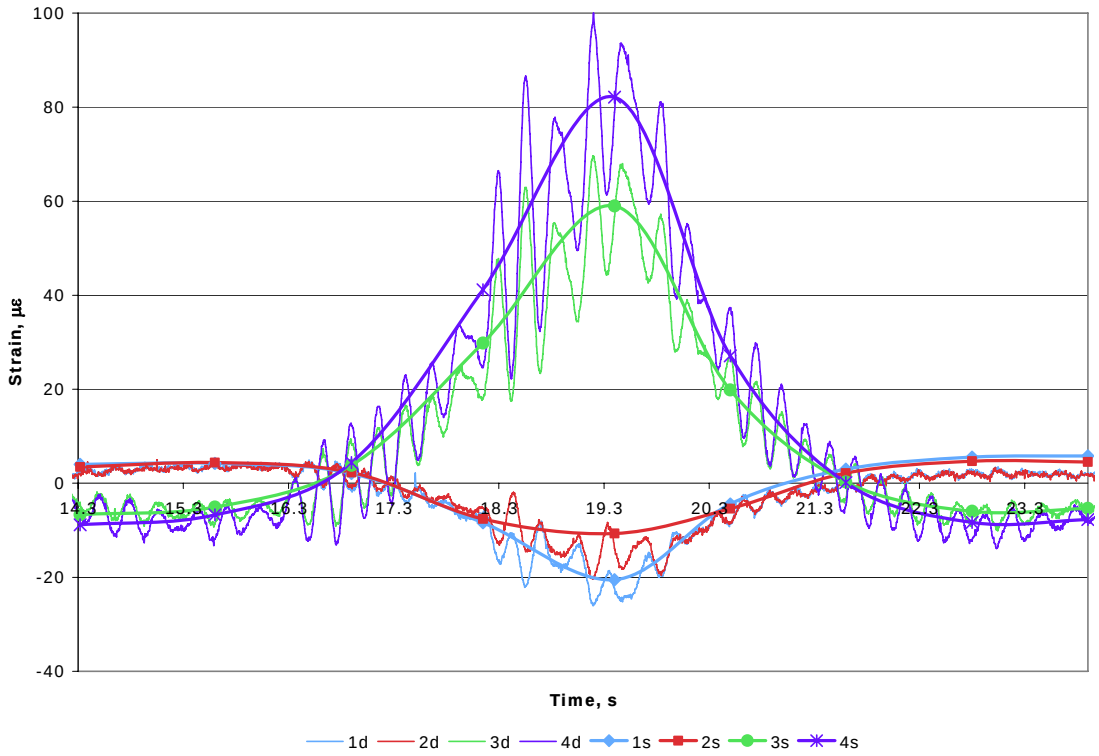

Figure 27. Static and Dynamic Strain Comparison, Inside of Girder 2, Outside Run

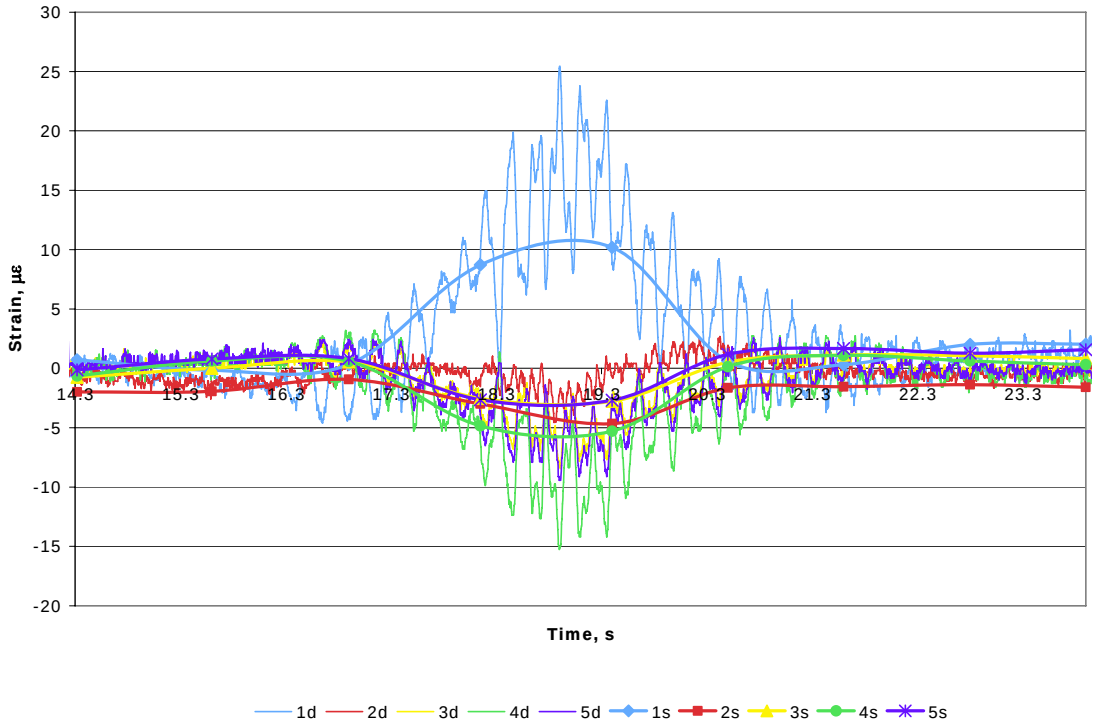

Figure 28. Static and Dynamic Strain Comparison, Diaphragm 2-3, Outside Run

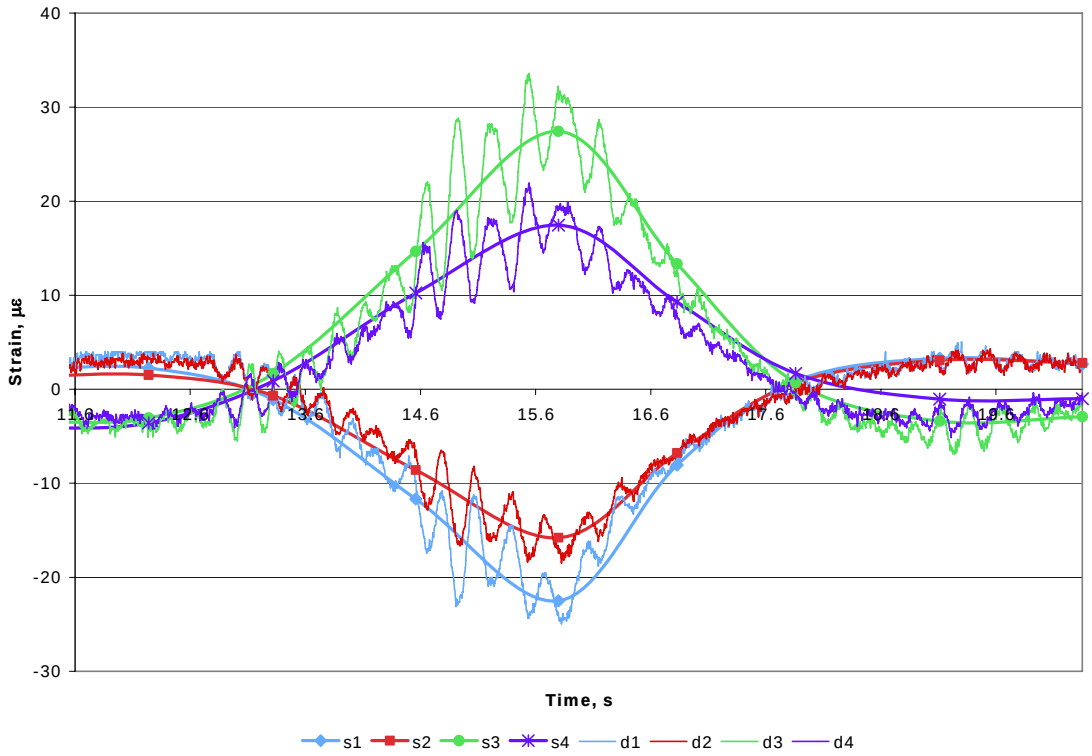

Figure 29. Static and Dynamic Strain Comparison, Outside of Girder 3, Outside Run

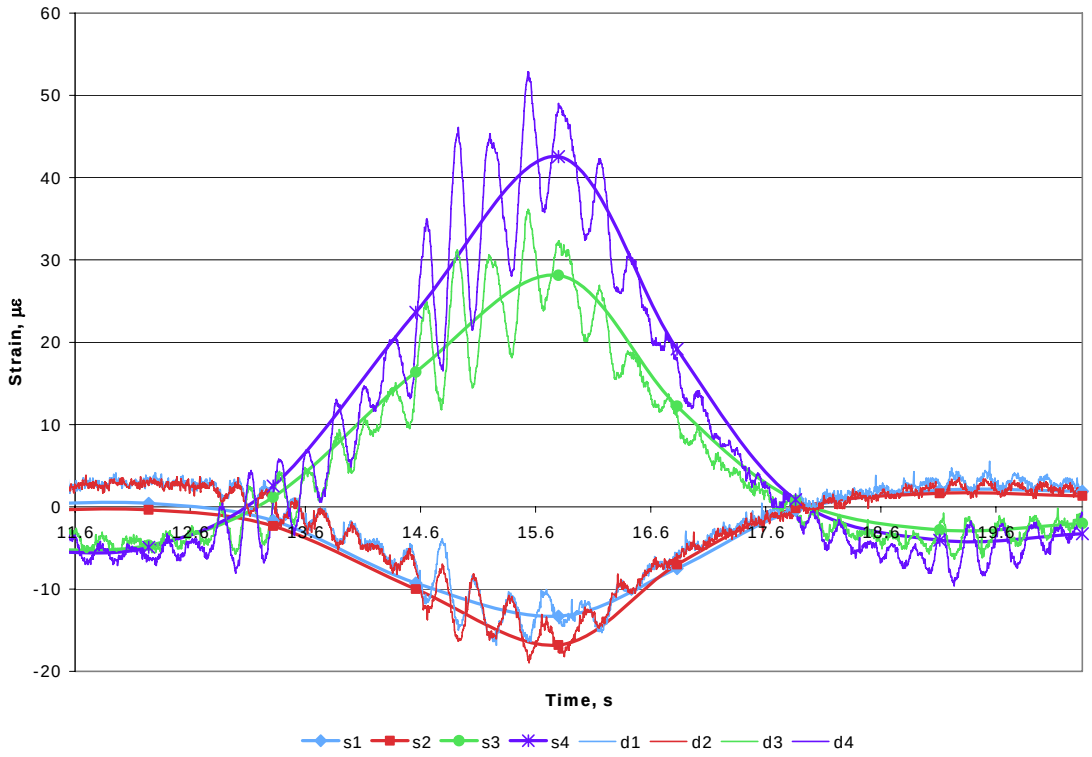

Figure 30. Static and Dynamic Strain Comparison, Inside of Girder 3, Outside Run

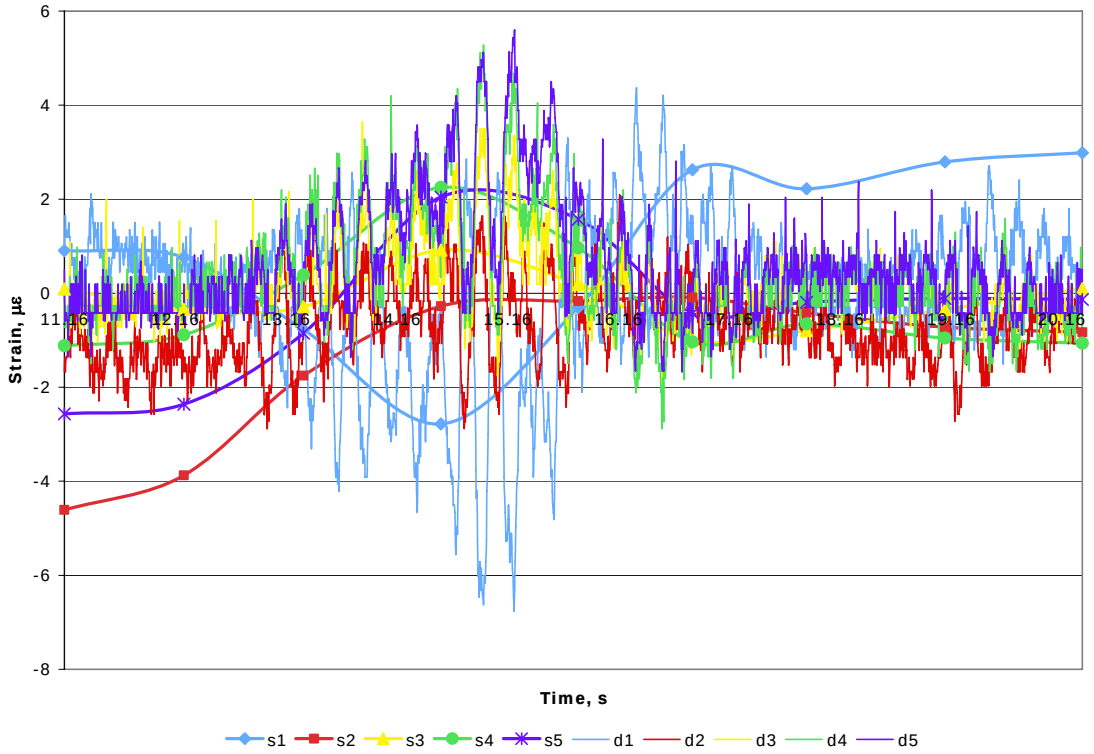

Figure 31. Static and Dynamic Strain Comparison, Diaphragm 3-4, Outside Run

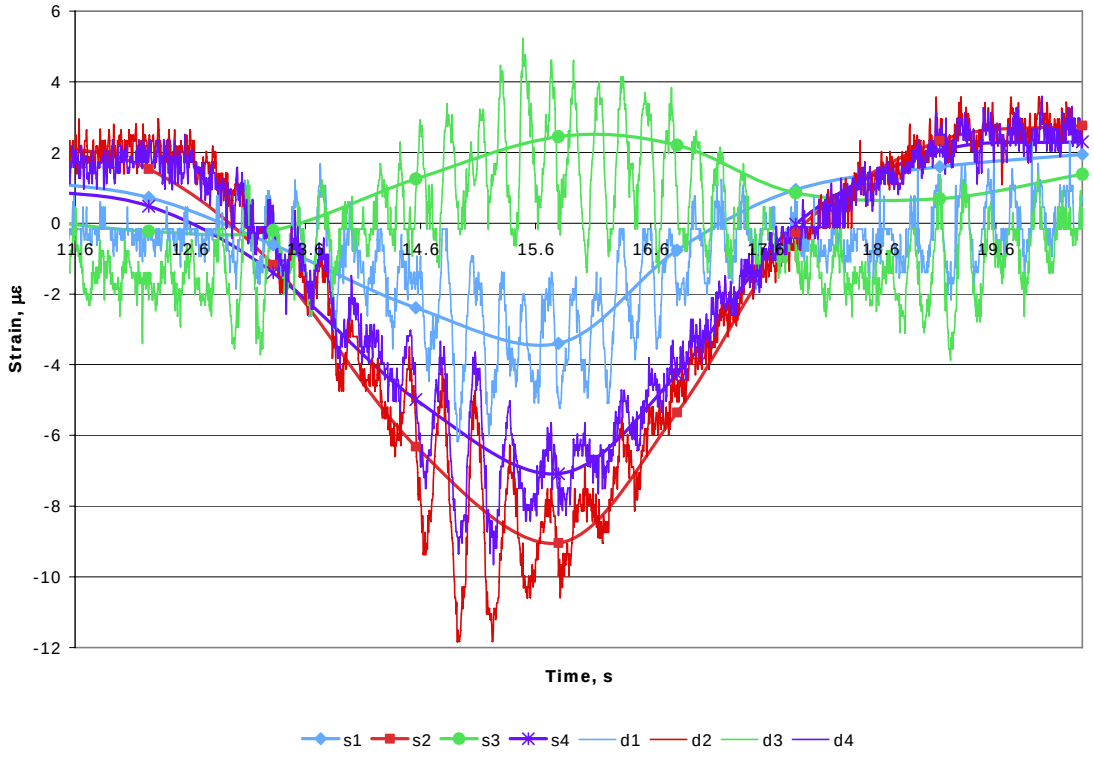

Figure 32. Static and Dynamic Strain Comparison, Outside of Girder 4, Outside Run

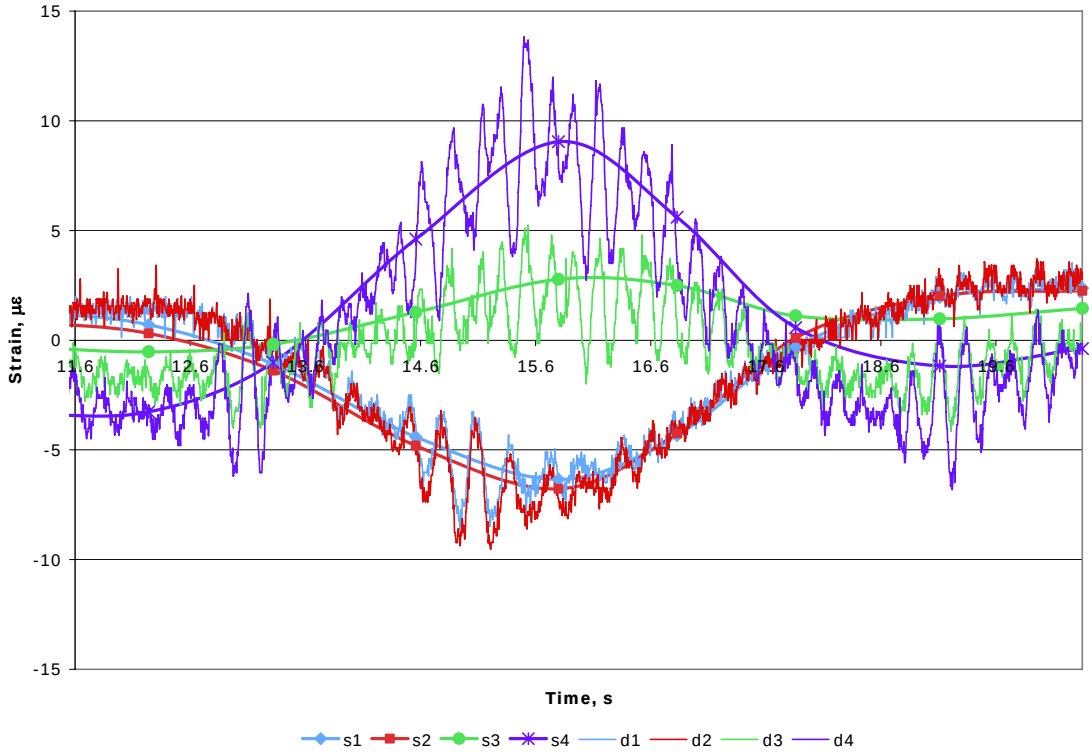

Figure 33. Static and Dynamic Strain Comparison, Inside of Girder 4, Outside Run

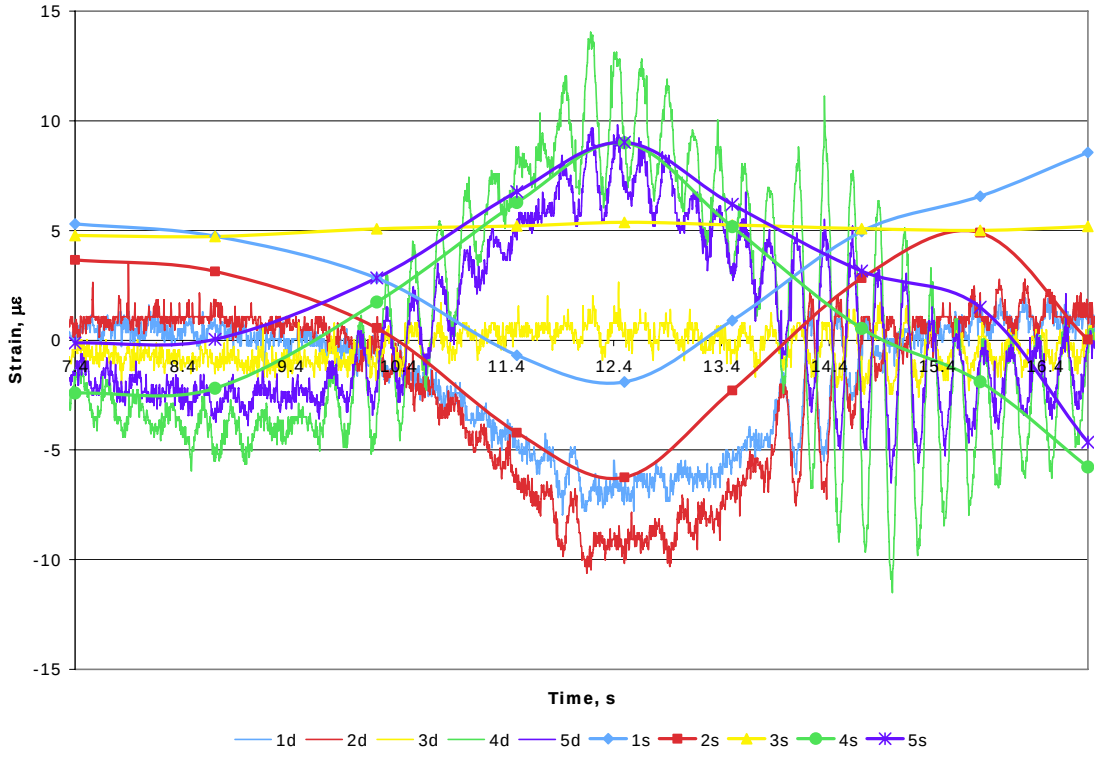

Figure 34. Static and Dynamic Strain Comparison, Outside of Girder 1, Inside Run

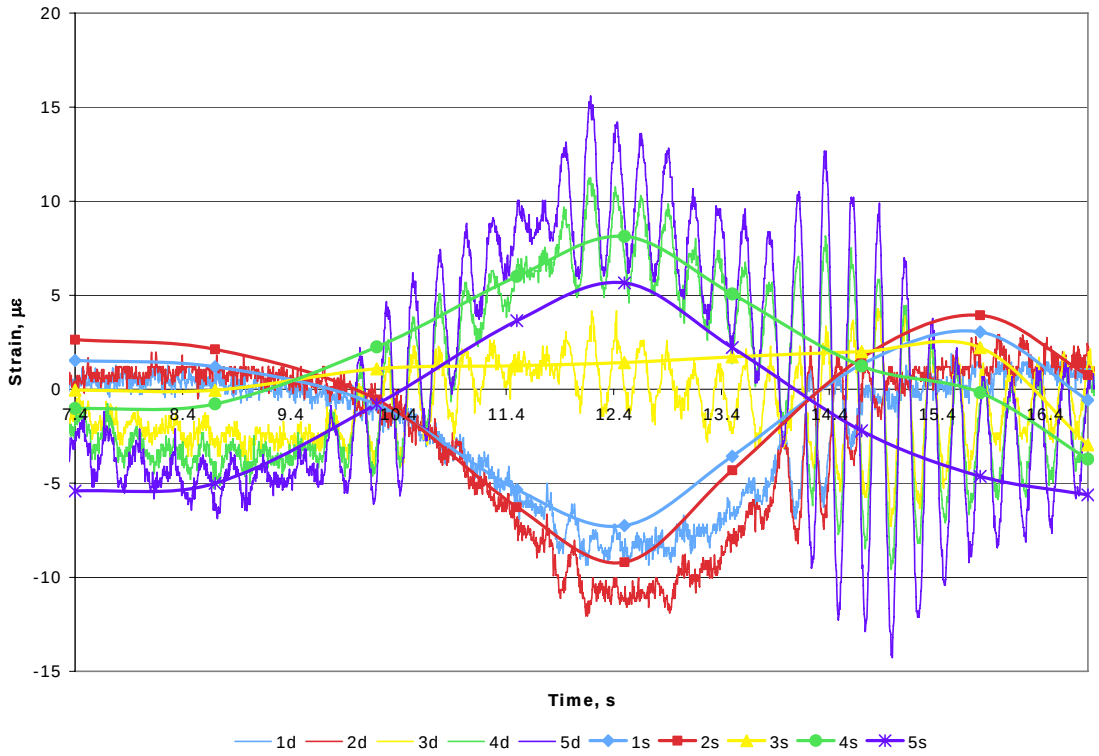

Figure 35. Static and Dynamic Strain Comparison, Inside of Girder 1, Inside Run

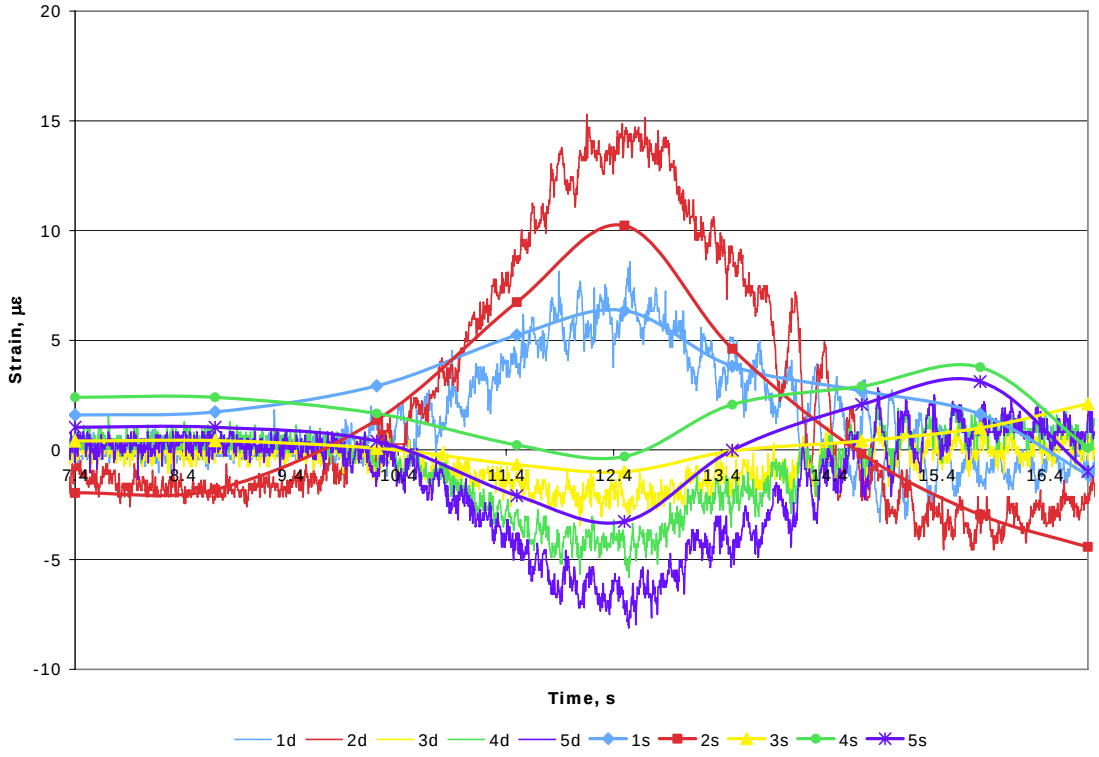

Figure 36. Static and Dynamic Strain Comparison, Diaphragm 1-2, Inside Run

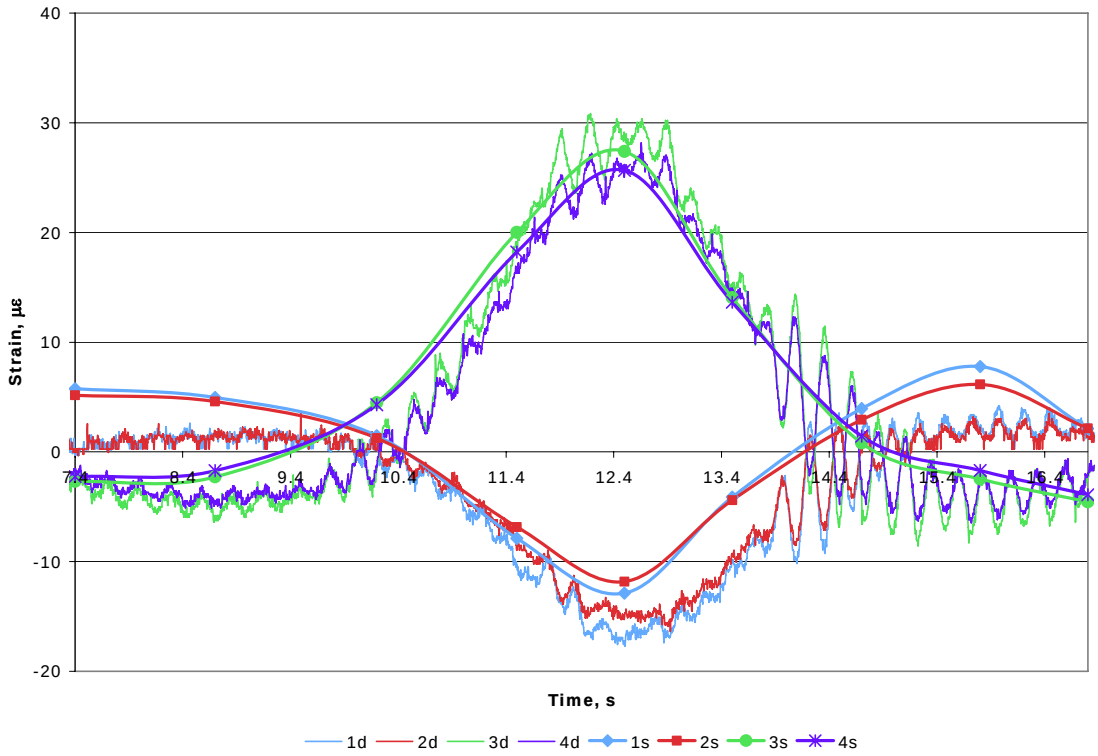

Figure 37. Static and Dynamic Strain Comparison, Outside of Girder 2, Inside Run

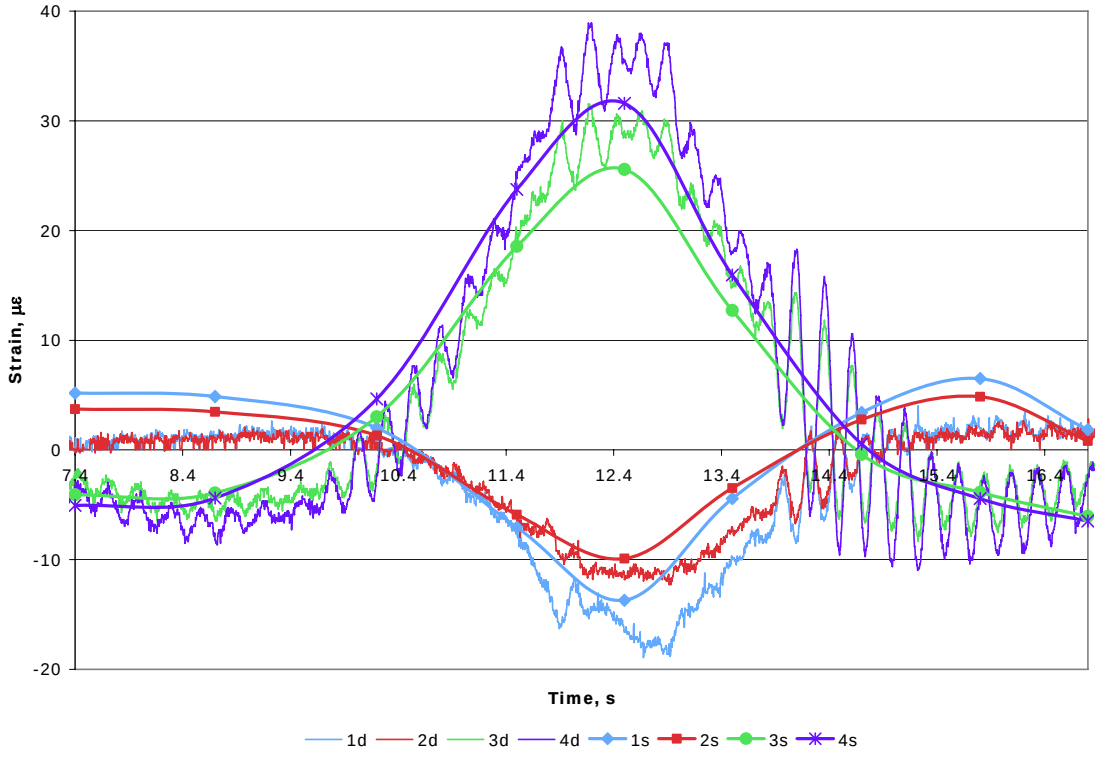

Figure 38. Static and Dynamic Strain Comparison, Inside of Girder 2, Inside Run

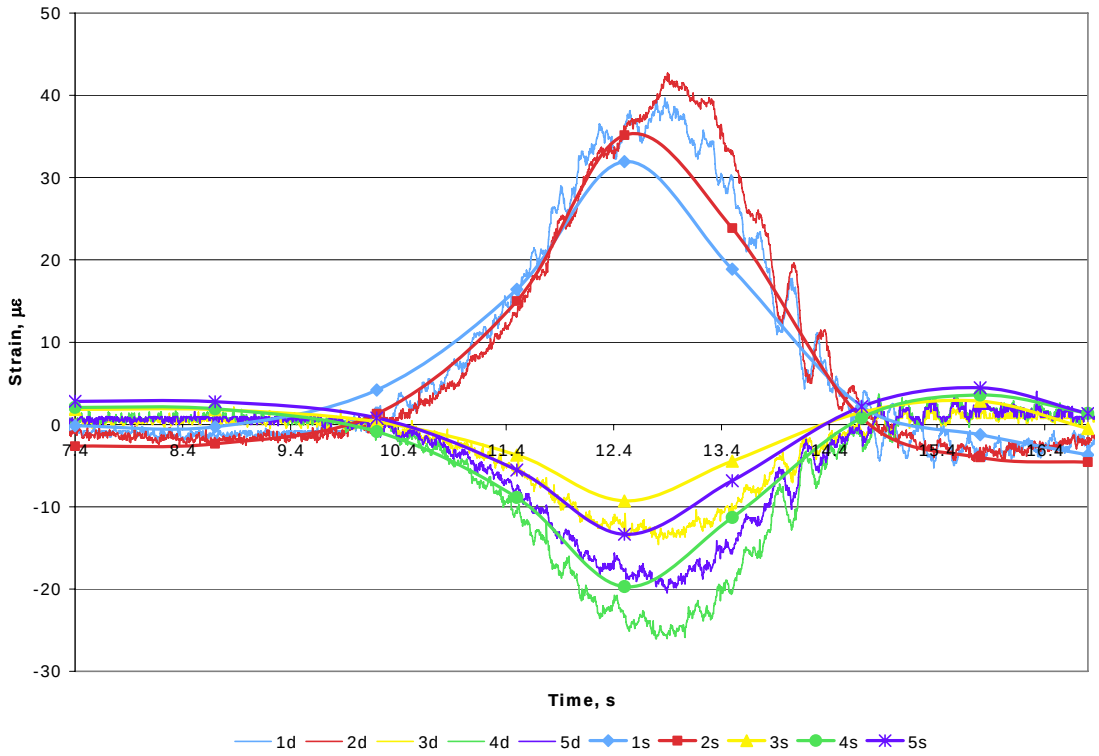

Figure 39. Static and Dynamic Strain Comparison, Diaphragm 2-3, Inside Run

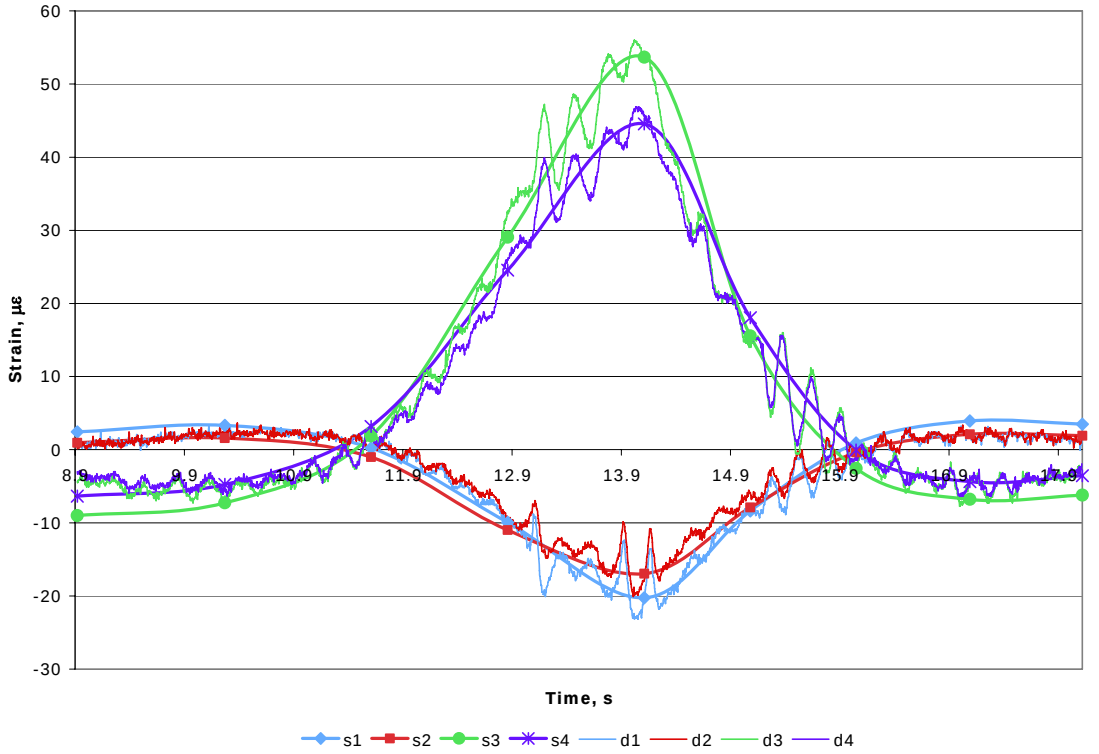

Figure 40. Static and Dynamic Strain Comparison, Outside of Girder 3, Inside Run

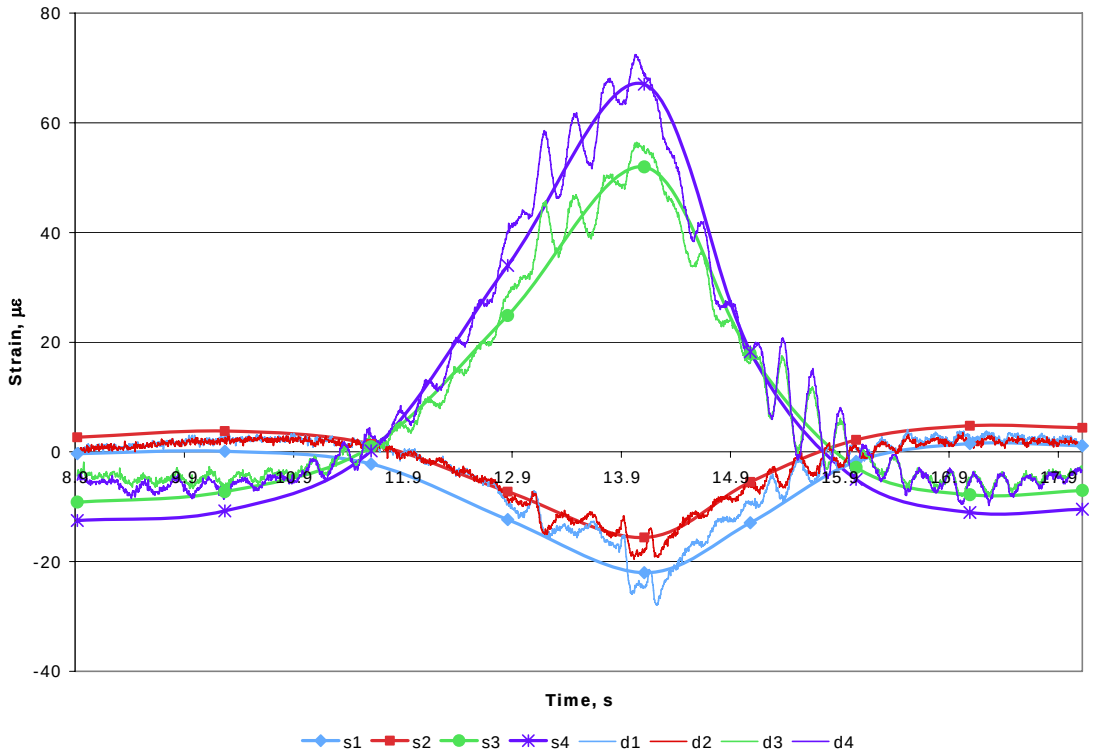

Figure 41. Static and Dynamic Strain Comparison, Inside Girder 3, Inside Run

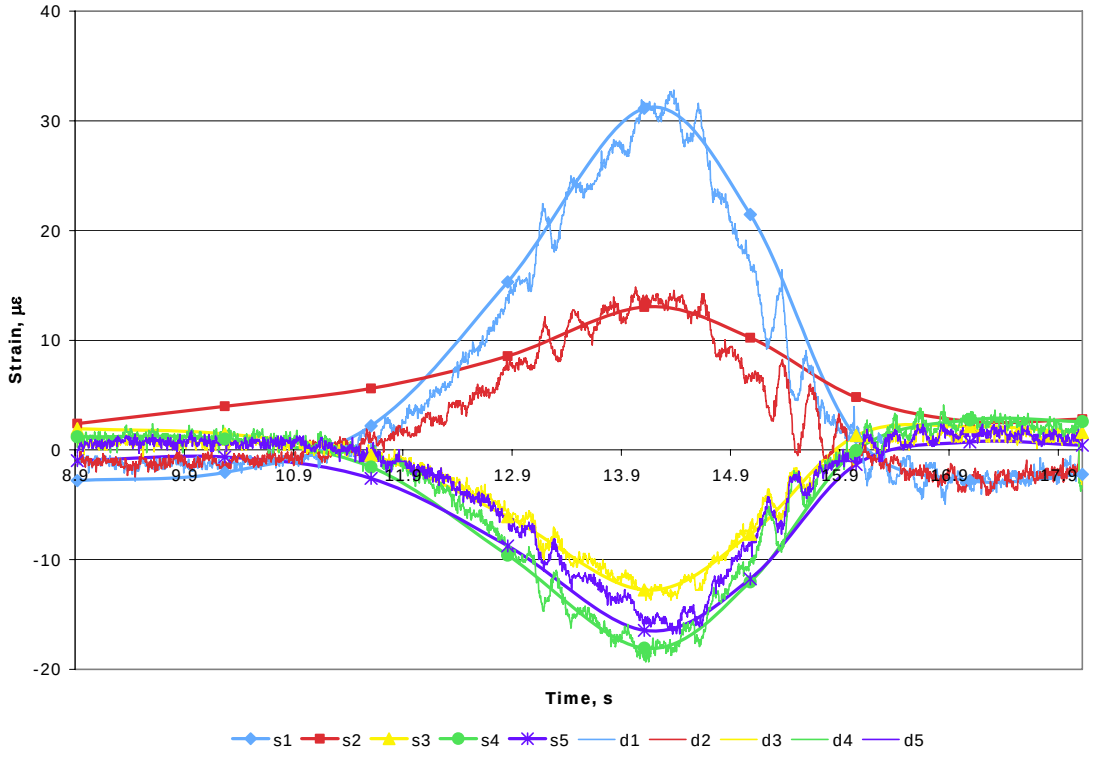

Figure 42. Static and Dynamic Strain Comparison, Diaphragm 3-4, Inside Run

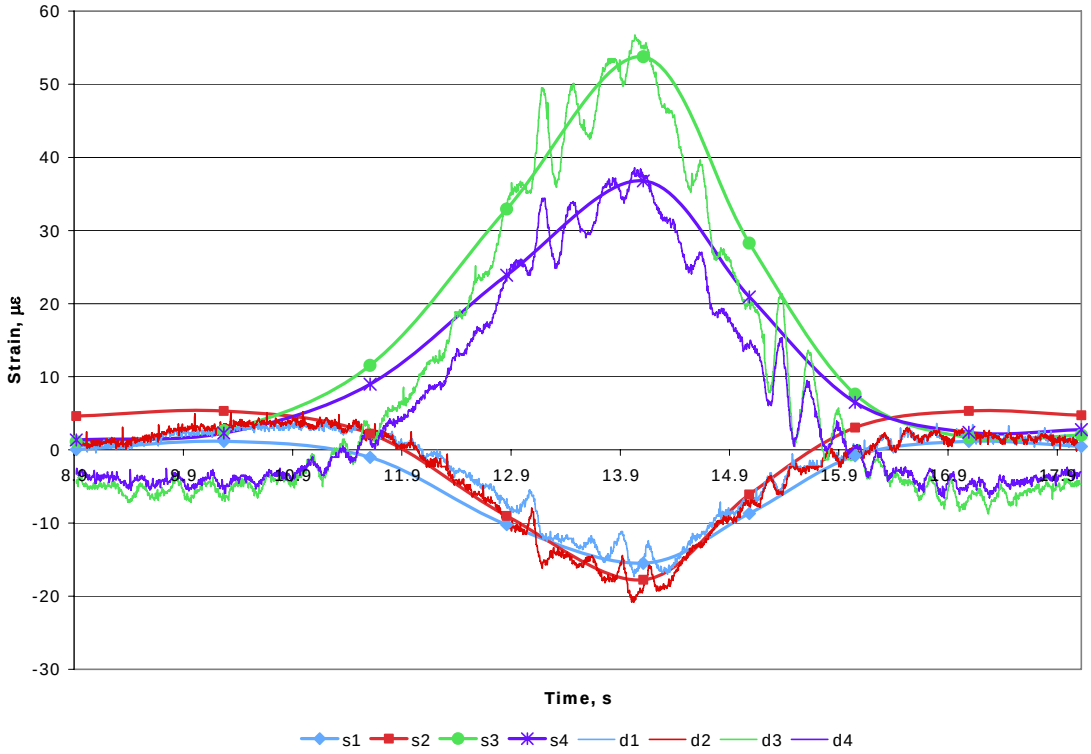

Figure 43. Static and Dynamic Strain Comparison, Outside of Girder 4, Inside Run

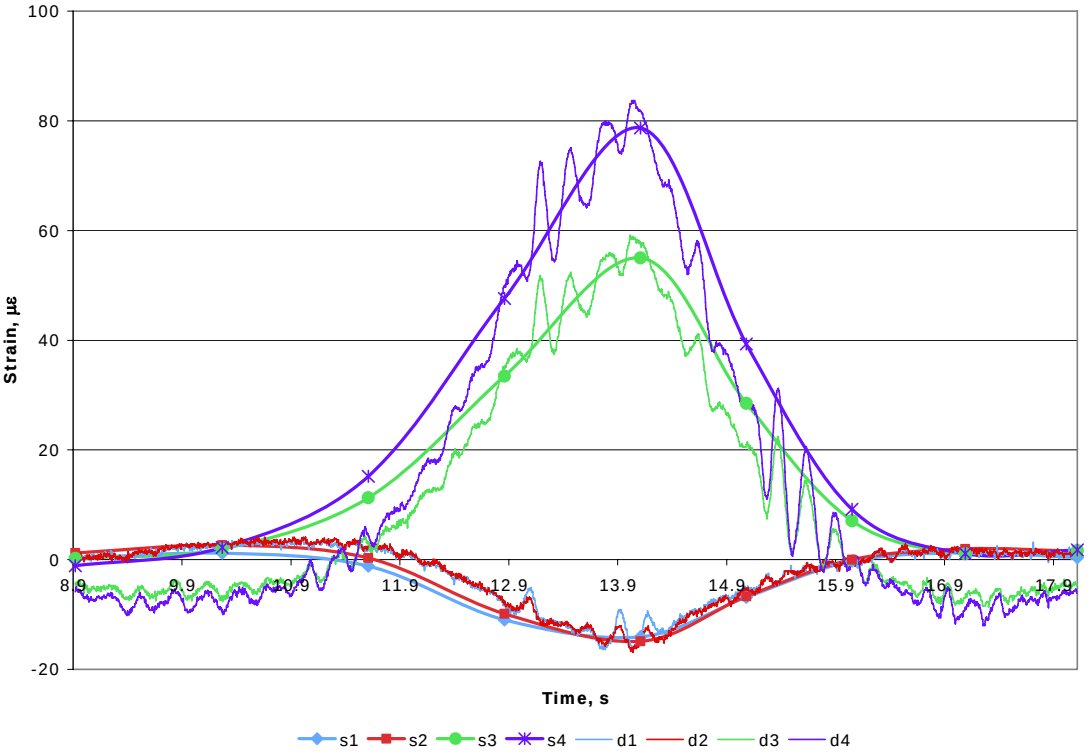

Figure 44. Static and Dynamic Strain Comparison, Inside of Girder 4, Inside Run

DISCUSSION

Measured Girder Strains

The data from the first setup yielded a high correlation between the static and dynamic strain readings in girders 1 and 2. The largest measured strains occurred on the bottom flanges of the girders directly under the loaded lane. These strains were negative when the truck loads were on the side spans, and positive when the truck was on the center span. At the top of the girders there were relatively small positive bending strains when the truck was located on the outer spans, and larger negative bending strains when located on the center span. A distinct reversal of curvature was shown to occur at roughly the time the truck crossed the piers.

When the truck was on the outside of the curve, the measured strains were largest in girders 1 and 2. The measured tensile strains on the inner edges of the bottom flanges of all girders were significantly larger than those on the outer edges, indicating the expected lateral bending of the curved girder flanges, a measure of warping torsion. The torsional strains in the inside girders 3 and 4 were of comparable magnitude to the bending strains.

Placing the truck on the inside of the curve resulted in a similar pattern; maximum bending strains occurred in girders 3 and 4, the girders under the loaded lane. By comparison, the measured strains in the outside girders showed significant torsion relative to the amount of bending. For all loading cases, both static and dynamic, a recognizable pattern of lateral flange bending consistent with warping torsion was present in all girders. This was evident from the unequal strains in the flange tips and at the web-flange interface.

Dynamic Amplification Factors

The strongest data signals for the outside and inside lanes were used to calculate the dynamic amplification factor (DAF) of the truck driving across the bridge. For the outside run, girders 1 and 2 were investigated, and girders 3 and 4 were considered for the inside run. The calculation for the DAF is simply the difference between the peak dynamic reading and the static reading at mid-span, divided by the same static reading. These results are shown in Table 1.

Table 1. Dynamic Amplification Factors

	Outside Run				Inside Run			
	OG1	IG1	OG2	IG2	OG3	IG3	OG4	IG4
Dynamic	71.2	92.9	67.2	100.0	55.5	71.5	56.4	83.1
Static	56.5	72.1	59.6	82.1	53.7	67.0	53.8	78.7
DAF	26.0%	28.8%	12.7%	21.8%	3.4%	6.7%	4.9%	5.6%

Dynamic amplification for the outside run was considerably larger than that for the inside run. However, as can be seen in Figures 33 and 34, large oscillations of the measured strains in the outer girders appeared when the truck was driven across the bridge in the inside lane as it crossed the second pier.

Only the outside girder DAFs were calculated when the load is in the outer lane, and only the inner girder DAFs were calculated when the load is in the inner lane, since much larger DAFs predicted when the load is in the lane away from the girders are not accompanied by controlling overall stress levels. Hence these much larger DAF values are not particularly relevant for design.

In some of the comparisons, such as in the outside of Girder 1 (Figure 34) and Diaphragm 1-2 (Figure 36) on the inside run, inconsistencies appear between the static and dynamic data. The static values follow the same general trends as the dynamic data, though slightly offset. Also, a drift exists in the data at the exit end of the bridge. In all of the comparisons in which significant discrepancies appear, the strains are relatively small, less than 10με. Thus, small changes within the bridge, such as thermal strains during the period required to complete the static studies, might be able to cause the small offset seen, due to drift in the static baseline. These changes are not seen in the dynamic runs, as data were only collected for about 13 seconds and was taken within seconds of the corresponding blank data. However, blank data for the static run were taken about 30 minutes apart, as the static data took much longer to collect. As a result, any warming or cooling of the bridge that occurred as the day progressed could have introduced thermal strains that subtracting the blank data would not have eliminated. It also should be reported that there was some precipitation during the static tests on the bridge, which could have caused some fairly rapid cooling, leading to some drift of the static readings.

Measured Diaphragm Strains

Generally, the measured strains in the diaphragms are relatively small. At the lower limit, strains on the order of 1 με were observed, and these values are of questionable accuracy relative to measurement error because of the small magnitudes. However, two significant trends can be observed in the diaphragm data.

In all loading cases, a sign reversal occurred between the longitudinal strains at the outer edges of the flanges and mid-height of the web on the diaphragms. The plane of load transfer between the diaphragm channel members and the girders is at the back of the channel webs. Therefore, it may be expected that a tensile loading applied in that plane would lead to a combination of tension and lateral bending, which would tend to place the flange tips in compression, consistent with the data. In addition to this behavior, several other mechanisms, including bending in the vertical plane, and some accompanying twisting are present. In a couple of cases, calculations based upon the primary mechanism of tension accompanied by horizontal plane bending provide very reasonable estimates of tension in the diaphragms, while in other cases, the other contributing mechanisms make this calculation very inaccurate.

In almost all loading cases, a larger negative compressive strain was measured at the outer edge of the top flange than at the bottom flange. It appears that this signifies a small amount of bending about a horizontal axis, but it is not possible to rule out some warping torsion in this measured strain. Given the likely dominance of transverse bending over torsion, the relatively low torsional stiffness of the connection, and the tendency of adjacent girders to

undergo similar rotations, it is likely that most of the measured difference between top and bottom flange strains is the result of a small amount of vertical bending of the diaphragms.

Using the rosette strains, the principal strains and shearing strain at mid-height of the web were calculated for each diaphragm and loading location using methods discussed by Dally and Riley (1978).

Additional channels of data, provided by additional strain gages installed at the back face of the diaphragm channel, are needed to gain a more complete understanding of the behavior of the diaphragms. Without additional shear strain data from the back of the channel, it is not possible to separate the measured strain into bending strain, and St Venant torsion strain components. Warping shear flow can be ruled out as a major contributing factor to the shear stresses at mid-height of the web because that quantity should be zero at mid-height of the channels. Moreover, because torques can only be applied at the ends of the diaphragm members, and because the flanges are free to warp at the ends, little warping restraint can develop along the members. It is believed that most of the measured shear strain is the result of bending shear, since the shear strains are fairly significant relative to the other strains, and there does not appear to be a sufficient twisting mechanism present to generate St Venant shear strains of this magnitude.

Anomalies in Strain Readings

Overall, a slight shift in some of the strains recorded was observed in some data sets when the truck was located on the final end span, as compared to when the truck was located on the first end span. As the bridge and loading cases are symmetric, the data should be relatively symmetric as well. However, this "drift" only becomes apparent on girders undergoing small static strains, on the order of 10 με or less, indicating a weak signal. Also, the drift appeared to be present primarily on a few of the static strain channels, which were recorded over a longer period of time than the dynamic data. It is likely that at least some of the drift may be accounted for by thermal strains that occurred during this interval. The observed drift appeared to be negligible when the strain readings were larger than roughly 10 με.

With the exception of a few individual channels where significant drift of the static strains made direct comparison of static and dynamic data problematic, the static strain data obtained from the bridge and the dynamic strain data obtained from the same gages appeared to correlate well.

Dynamic Oscillations

Though the dynamic strain data consistently showed oscillations, particularly strong oscillatory results relative to the static strains appeared on the girders when the truck crossed the bridge on the inside lane. The oscillations were strongest as the truck approached Pier B, and dissipated as it crossed the southern end span. For all four girders, with data gathered from both first and second run setup runs, the amplitude of the oscillations were on the order of 10-20με. This is particularly noticeable on girder G1, where the static response is relatively small, as shown in Figures 34 and 35. Some girder strains continued to show the oscillations until the

truck exited the bridge, but the majority vanished by this time. These oscillations were especially evident in the data from the first setup, where they were greater in amplitude than the rest of the span, but can also be seen in the second setup results.

There are a few explanations that can be offered as to why these oscillations would occur. It is possible that the truck could have encountered a bump that would have excited the bridge in this manner, though no obvious surface irregularities were immediately evident. The specific path the truck took as it crossed the bridge could also have contributed to the oscillations. It should be noted that these large oscillations occurred in the absence of a sizeable static strain which would not control the design of the structure, so it is not particularly meaningful to calculate dynamic amplification factors for these cases.

Finite Element Model and Field Data Comparison

Girder Analysis

A major objective of the current study is to critically evaluate the accuracy of the FE model previously developed by Lydzinski (2006) using the field strain measurements. In particular, Turnage (2007) noted that the natural frequencies and mode shapes suggest boundary conditions at the ends of the bridge that are not modeled well with ideal rollers. Therefore, as part of the study, it was considered important to compare the measured strains with the strains calculated from an FE model under comparable loading.

The strains predicted by the FE model and the data collected in the field revealed generally similar behavior in the girders, but there were some noticeable differences. Figure 45 shows a direct comparison of the measured and calculated longitudinal strains on the girders, when the loading vehicle is at the middle of the center span. Generally these measured strains are the largest on the girders under the load. Strains in the bottom flanges of all girders follow similar patterns and correlate fairly well with one another. The strains measured on the girders away from the loaded lane are relatively small, so the precision of the measured values at those locations may not be that high.

In comparing the measured and predicted strains of the bottom flange of each girder, distinct trends emerge. Vertical bending strain, taken as the average of the bottom flange tip strains, and the corresponding distribution factors (DF), estimated by dividing each vertical bending strain by the sum of the averages, were calculated for each girder. The difference between the outside and inside flange tips represents the amount of twist present in each girder. These values are reported in Table 2.

During an outside run, the FE model predicted higher bending strains in Girder 1 than were measured in the field, and lower strains in the remaining girders. Similarly, during an inside run, somewhat higher bending strains were predicted in the outside of the bridge than shown in the field with less predicted in the inside girders. Distribution factors calculated for an outside run using field measured strains increased from Girder 1 to Girder 2, then decreased through the inner girders. In the FE model, however, the DFs steadily decreased from the

outermost girder to the innermost. Field measured strains and FE model calculations for an inside run were relatively consistent, though the FE model generally predicted higher DFs for the outer three girders than were measured in the field.

Overall, slightly less torsion was predicted by the FE models than appeared in the field data during an outside run, as indicated by the strain difference between the inner and outer flange tips. During an inside run, greater torsion was predicted by the FE model than was measured in the three outer girders, and less torsion was predicted than measured for Girder 4.

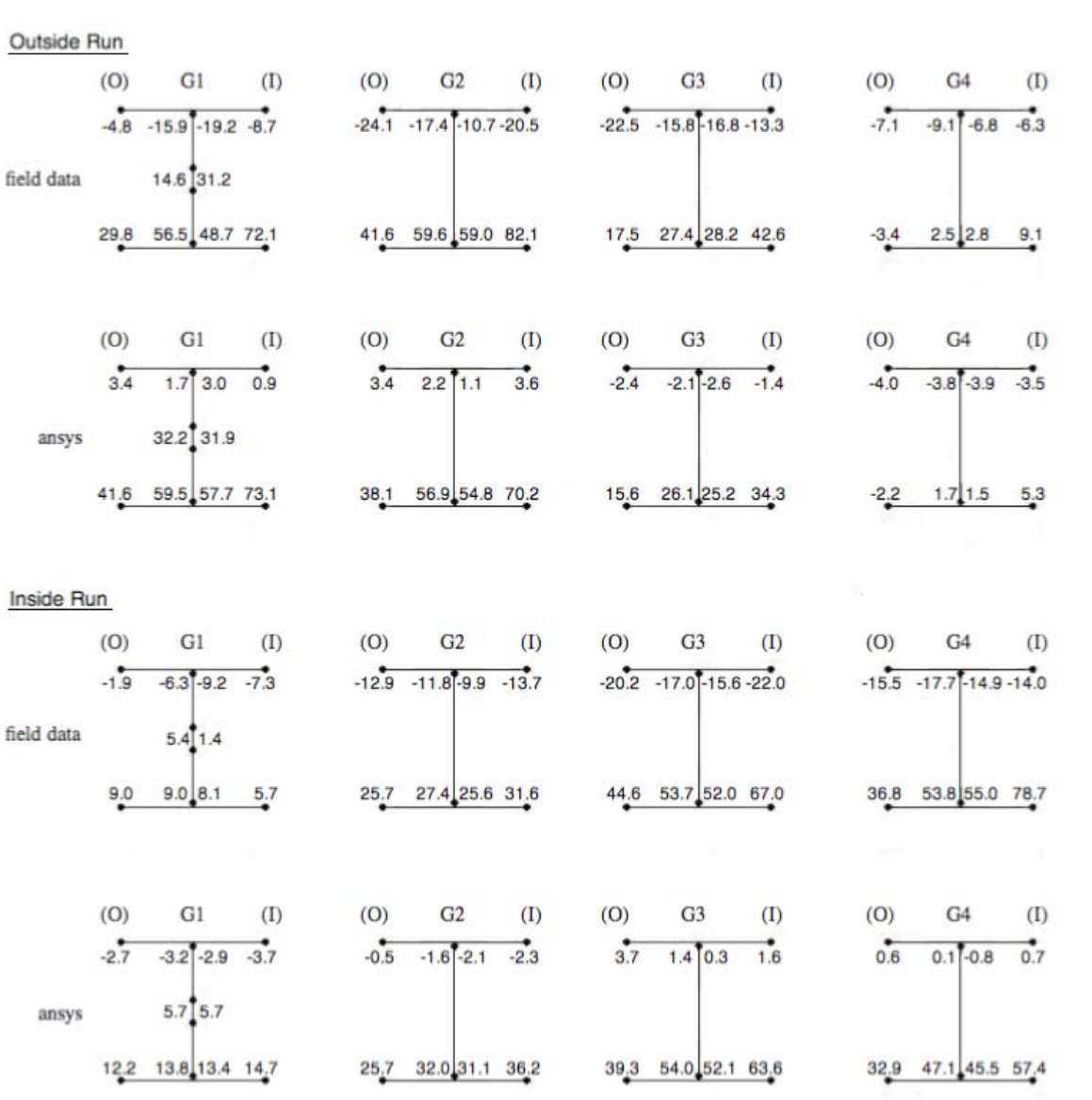

Figure 45. FE Model – Field Girder Comparisons with Load at Mid-span

Table 2. Bottom Flange Strain Comparisons

		Field			*ANSYS*		
		Average (με)	D.F.	Difference (με)	Average (με)	D.F.	Difference (με)
Outside Run	Girder 1	50.9	0.350	-42.3	57.4	0.416	-31.5
	Girder 2	61.8	0.424	-40.5	54.2	0.393	-32.1
	Girder 3	30.1	0.206	-25.1	24.9	0.180	-18.7
	Girder 4	2.9	0.020	-12.5	1.6	0.011	-7.5
Inside Run	Girder 1	7.4	0.049	+3.3	13.5	0.095	-2.5
	Girder 2	28.7	0.192	-5.9	31.0	0.220	-10.5
	Girder 3	55.8	0.373	-22.4	51.5	0.365	-24.3
	Girder 4	57.8	0.386	-41.9	45.2	0.320	-24.5

These patterns suggest that the FE model systematically predicts slightly more load transfer to the outside of the bridge than is being transferred in the field. One reason for this could be an overestimate in the diaphragm-girder connection stiffness in the FE model. Another explanation could be that the actual slab is not as stiff as predicted by the FE model either because of the level of discretization or because the SHELL63 element does not incorporate shear deformation, which might be significant in the relatively short spans between girders. Thus it is possible that a higher level of discretization may be needed to accurately predict load transfer. This possibility is considered further during the discussion of the neutral axis location.

Inconsistencies appear in the top flanges of the girders. The FE model predicts small tensile strains, whereas the field data indicate that significant compressive strains occur. Thus, the neutral axis anticipated by the FE model is above the web/top flange junction, while the field data show it to be in the web roughly 7 inches below the bottom of the top flange. This is a substantial difference and implies the presence of significant differences between modeled and observed behavior.

Finite Element Model Parameter Studies

A number of hypotheses were explored in an attempt to explain the disagreement between the neutral axis locations of the model and the field results. These hypotheses include

- Overestimated slab thickness in the FE model
- Overestimated elastic modulus of concrete in the FE model
- Boundary/support conditions effects
- Stiffness of guardrails overestimated
- Overestimated haunch stiffness
- Shear stud slippage in the field.

In order to explore the hypotheses, modified FE models were constructed with a property in question varied, and the results were compared with the field data. The details of these numerical studies can be found in Appendix A and are discussed below.

Slab Thickness

The original FE model had a slab thickness t_{slab} of 8.5 inches. However, the construction plans specify a thickness of "8.5-inch typical" and "8-inch minimum." It was hypothesized that a t_{slab} of 8 inches might be a more appropriate value of the as-built dimension for comparison with the field data, and this value was used for the remainder of the analysis.

Adjusting this depth resulted in no major changes in the overall behavior of the girders, retaining evidence of lateral bending, torsion in girders opposite of the load placement, etc. The FE model's neutral axis location was lowered slightly but remained above the web/top flange junction. Therefore, the influence of the FE model's slab thickness appears minor.

Varying E_c

It was hypothesized that the value of E_c used in the original FE model, which was based upon the ACI formula for the given concrete, might be too large. In reality, E_c may vary considerably with different parameters of concrete, such as strength, aggregate properties, unit weight of hardened concrete, and rate of loading or strain. Differences in the shapes of stress-strain curves of concrete with similar properties, even for the same concrete under different loading conditions, have been observed (Nilson et al., 2004). Furthermore, the value of E_c can be overestimated by the ACI code equations by as much as 20% in some cases (Nilson et al, 2004).

Thus variations in E_c of 10% and 20%, 3244.5 ksi and 2884 ksi respectively, were input into the curved girder FE model to explore the influence of a lower as-built property upon the neutral axis location. A decrease in tension in the top flanges was noted, but even with a reduction of 20% the neutral axis remained above the web, as shown in Appendix C. Tension in the bottom flanges increased with decreasing E_c, though not significantly. Therefore the possibility that a lower E_c than used in the model exists in the field cannot be ruled out, and if so, this could be one factor contributing to the lower neutral axis found in the field.

End Guardrails

In the original FE model, metal barrier railings at each end of the bridge were modeled as additional longitudinal and rotational restraints. As shown in Figure 46, the guardrails are secured with a number of bolts. The guardrail is of lighter gage than the structural steel that comprises the remainder of the bridge, so the bolts may provide axial restraint as shown in the model. However, the assumption of rotational restraint may be an overestimate.

Figure 46. Guardrail Fixity

When the θ-direction fixity was removed at these nodes in the FE model, tension increased in the top flange. This indicated that the neutral axis moved further into the slab in the absence of end restraints. Therefore, although the assumption of significant rotational restraint may not be correct, releasing the restraint does not improve the neutral axis location in the model.

Concrete Railing Stiffness

Figures 47 and 48 show the properties of the concrete railing along both the inside and outside of the bridge. As can be seen in Figure 47, each section of the railing is not connected directly to the next section, and no reinforcement spans the connection along the top, although the railing sections do achieve a significant degree of continuity through the railing posts. The connection of the railing sections at the abutment includes no rebar, and a space exists between the adjacent sections of railing above the piers that extends down nearly the entire height of the railing. Upon closer inspection of the FE model, the dimensions and material properties of the railing are duly replicated but the separations between the sections of railing are not included. These details could significantly reduce the contribution of the railing to bridge stiffness, lowering the neutral axis since they are present at each section of the railing.

To account for this potential reduction in stiffness as accurately as possible, it would be necessary to add nodes to the model and attempt to replicate the spaces between railing sections. However, the shell elements as built in the FE model span across the locations where separations need to be inserted. Thus these elements would need to be completely reconstructed for each segment of the railing. This modification of the model was not attempted in the current work.

To explore the influence of the railing stiffness on the neutral axis location, a reduced railing with very low stiffness was introduced into the FE model. Instead of modifying the mesh in the FE model, the thickness of the railing was reduced to 0.01 inches. This effectively negated any influence the railing could have on the stiffness of the bridge. When the railing was effectively removed, the neutral axis moved about 1.5 inches into the web, which was still relatively far from the field measured neutral axis location of 7 inches. While the overall behavior of the girders remained the same in this study, tensions in the bottom flanges increased significantly and were no longer consistent with the field results. Thus an error in modeling the

correct stiffness of the railings is probably not the main cause of the low neutral axis found in the field, though it may be a contributing factor.

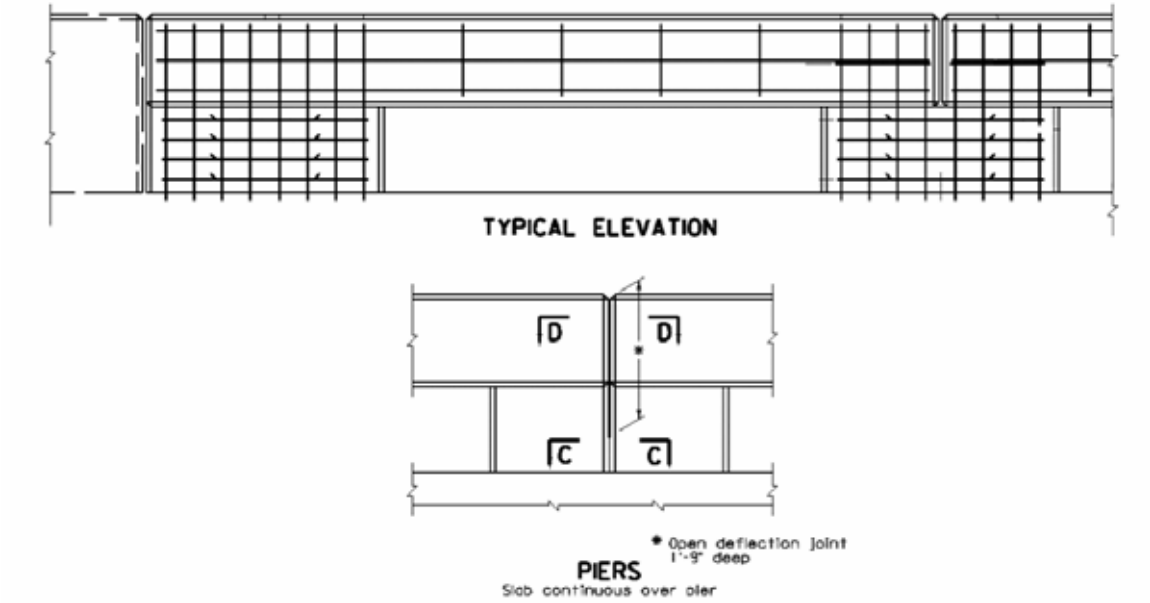

Figure 47. Railing Specifications

Figure 48. Railing Sections in the Field

Stiffness of Haunches

To determine whether the stiffness of the girder-concrete interface has an affect on the neutral axis, the thicknesses of the elements used for the concrete haunch above the girders were reduced to 50% and then 25% of their original values in the FE model. This effectively reduced E_c a similar amount, and allows for increased shear to occur. This experiment reduced tensions in the top flanges slightly, but did not bring the neutral axis into the web. Tensions in the bottom flanges varied only slightly, remaining relatively consistent with the field results, suggesting that transfer of shear across the interface may be a source of the neutral axis discrepancy.

Abutment Restraint

The strains found in the field could indicate the presence of a compressive thrust, which could have possibly been provided by the abutments. Additional restraints were added in the θ direction at the nodes already restrained in the z and r directions to test this theory. A slight increase in tension in the top flanges resulted, along with a slight decrease in tension in the bottom flanges; all changes in strain were less than 1 με. Thus the abutments cannot provide the reactive thrust to replicate the field results.

Shear Stud Slippage

A number of hypotheses as to the cause of the discrepancy between the neutral axis locations in the FE model and the field were explored, and it was concluded that none of these effects could lower the neutral axis to the level observed in the field. One additional hypothesis may be stated: a partial loss of composite action would allow some rotation of the beam relative to the haunch, and lead to a lower neutral axis than was obtained in the current FE models. Slippage of this type can be challenging to replicate in FE analysis, unless additional components such as shear studs are explicitly built in. The hypothesis is that some composite action may be lost as the result of slippage between the girders and concrete haunches, even in the presence of mechanical shear studs.

The Wolf Creek Bridge was designed to be fully composite, so theoretically, little or no slippage should occur. See Figure 49. However, a significant amount of research has shown that slippage occurs even under these circumstances. Slippage between the concrete-steel interface has been shown to occur in full and small scale T-beam tests since 1943 (Seracino et al., 2001). Though current (2000) design standards use full-interaction theory, which assumes no slip, these standards are only applicable at the limit state rather than at service loads such as the truck used in this experiment.

Figure 49. Shear Studs in the Field

Seracino et al. (2001) reported: “Slip occurs because mechanical shear connectors have a finite stiffness. Hence, the connectors must deform before they can begin to carry load.” This is defined as a partial-interaction. Unfortunately, numerical and field research conducted on shear stud slip has been mostly performed on straight spans. Much of this research explicitly uses straight girder theory and assumptions that may not be valid for curved girder analysis.

However, information gathered from this research can be useful in attempting to quantify this effect.

To obtain an approximation for the amount of slippage occurring in a specific bridge or other structure, a "push-off test" must be performed. A steel beam is connected to a concrete slab with a representative number of shear studs on each flange, and then loaded axially. A "load-slip curve" is constructed from measurements taken at certain increments, in load or displacement (Lam et al.., 2005).

Variation in slippage has been shown to be considerable and is affected by several factors, such as stud spacing and the change in shear force distribution due to the relative stiffness of members in the structure (Fang et al., 2000). Deeper slabs cause resultant forces on the shear studs to be located a distance above the base, which produces a moment arm acting on the shear stud (Rambo-Rodenberry, 2002). In some cases this can cause the maximum compressive stresses near the concrete-steel interface to triple in magnitude (Seracino et al., 2001).

Recent attempts have been made to explicitly include headed shear studs in FE models. Fang et al. (2000) reported: "whilst the finite element model is accurate, the assumed boundary and loading conditions may make the results of the analysis uncertain." Other factors may also affect the results of the analysis, such as slip resistance at the steel-concrete interface, and may require judgment on the part of the engineer (Fang et al., 2000).

The current FE model does not contain an explicit shear stud modeling capability that permits explicit slip between the slab and girder to be modeled, so it is difficult to evaluate this hypothesis explicitly. However, as the discussion below indicates, it does appear reasonable that at least some slip is occurring. This observation should be taken as a starting point for the construction of future FE models, especially if model calibration to field data is to be undertaken.

Critical Evaluation of Finite Element Model

Since none of the parameter variations introduced above could account for the significant difference in predicted neutral axis location between the FE model and the field data, it was decided to undertake a critical evaluation of the FE model representation. In his original model development Lydzinski (2006) conducted convergence studies based upon overall model stiffness. However, Lydzinski's studies did have a couple of limitations:

- The convergence criterion was displacement based, not strain based. This has the potential of providing a model that reproduces dynamic properties well, but is not suitable for predicting strains accurately.
- The convergence studies were conducted on straight beam/slab segments, because of the difficulty of modeling a single curved beam/slab segment. However, it is possible that a straight segment may have different convergence properties than a curved beam/slab.

Transformed Section Calculation

In order to provide a preliminary estimate of neutral axis location in a straight beam segment, a transformed section calculation was performed to estimate the location of the neutral axis, $\bar{y}$ for an interior girder. The calculated distance is taken from the bottom of the top flange into the web. Figure 50 shows the deck and girder dimensions used for the calculation. The calculation method is well known and is not repeated here. A $\bar{y}$ value of approximately 4.0 inches was predicted by this method. Decreasing E_c by 10% resulted in a 0.5-inch increase in $\bar{y}$, lowering the neutral axis only slightly further into the web than before. Since no test cylinder values of E_c were available for the concrete in question, the value given in the construction plans of 3605 ksi was used in the FE model.

The transformed section calculation uses straight girder theory and is only applicable to the interior girders, since the exterior composite girders do not have symmetrical slab widths to either side of the beam. The concrete railing that was included in the FE model further complicates the analysis. Thus the neutral axis calculated using this algorithm should only be viewed as a reference based upon elementary theory. The model does indicate that the measured neutral axis location should be located several inches below that predicted by the superstructure FE model, but it is also three inches above the value indicated by the field data.

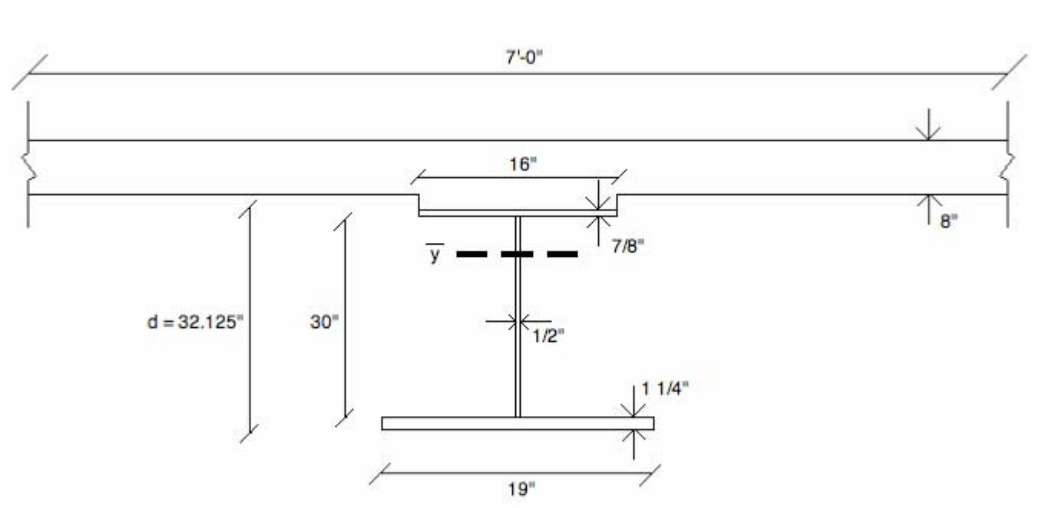

Figure 50. Transformed Section Calculation Dimensions

Straight Girder FE Model

Because of the significant difference between the neutral axis location predicted by the transformed section analysis and the Wolf Creek Bridge FE model, a comparable straight girder FE model, with similar properties, cross section and refinement as the curved girder model used in this study, was constructed to determine the neutral axis location. See Figure 51. The model consisted of a single beam with the associated slab, as opposed to reconstructing the entire bridge with diaphragms, and was restrained in a similar manner as the curved girder model. A model constructed with identical girder cross-section and slab effective width, with a similar grid to that

used in the curved girder FE model had a neutral axis location $\bar{y}$ = 4.2 inches into the web. This value is very comparable to the value obtained from the transformed section analysis discussed above.

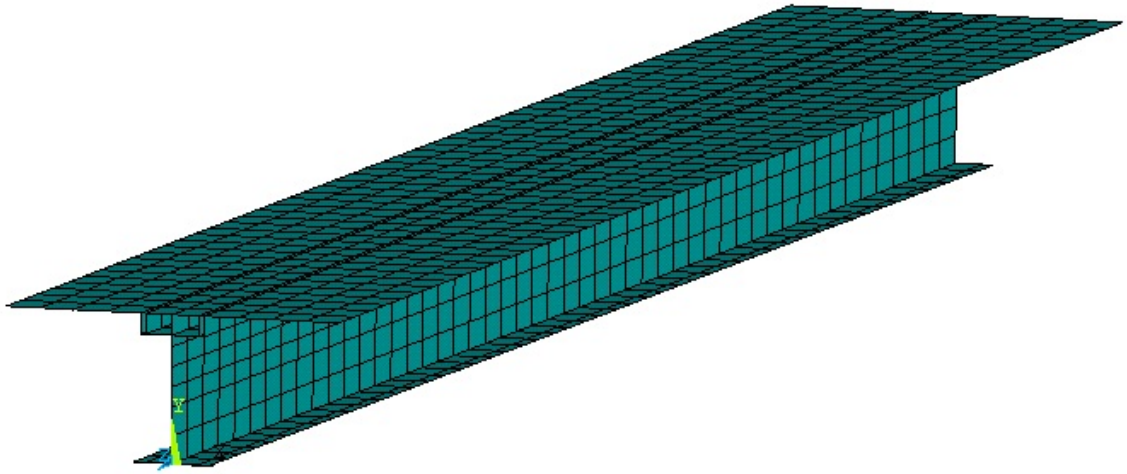

Figure 51. Straight Girder Model

A more refined straight girder model was also constructed to determine if a more refined discretization would have an effect on the neutral axis location. The neutral axis was lowered to 4.7 inches, which indicates that the level of mesh refinement could have an influence on $\bar{y}$, albeit a relatively small one. Further refinement of the FE model did not appear to be capable of lowering the neutral axis beyond this point.

The results of these studies suggest that there are significant differences between the FE analysis of a single straight girder and the curved girder bridge. The single straight girder does not include the diaphragms present in the curved girder bridge, though this is likely not the source of the discrepancy. One distinction of the curved bridge as compared to the straight girder is the concrete railing. This adds considerable stiffness to the bridge and the model used for the railing may significantly overestimate the stiffness of the actual railing. However, the presence of any railing stiffness at all in the actual structure has the potential to raise the neutral axis, so it cannot resolve the remaining difference in neutral axis location. An additional possibility is that the level of discretization appropriate for a straight girder/slab section might not be adequately refined for a comparable curved girder bridge, because of the more complex strain pattern expected to develop in the latter structure. Because of the limits already imposed on the model size, it has not been possible to evaluate this hypothesis at present.

Even if all of the discrepancies between the straight girder FE model and the curved girder FE model can be resolved, there remains a difference between the model neutral axis and the measured neutral axis of between 2.2 inches and 2.8 inches, so additional sources of possible discrepancies must be considered. The most likely remaining factor that could contribute to the lower neutral axis is possible slip between the top flange and the concrete haunch, as discussed above.

Diaphragm Analysis

Strain values obtained from the FE model and field analyses in the diaphragms correlated well when the truck was located on the outer lane of the bridge, but were not as consistent when the truck was located on the inner lane of the bridge. The measured and computed strains are shown in Figure 52, and the resolution of the rosette values into principal components and shear strains is given in Table 3. However, a pattern of sign reversal between the web and flanges, as discussed in the comparison of dynamic and static data, can also be seen in the FE model data in both outside and inside run data sets. Generally, the diaphragms attempt to transfer the moment outward.

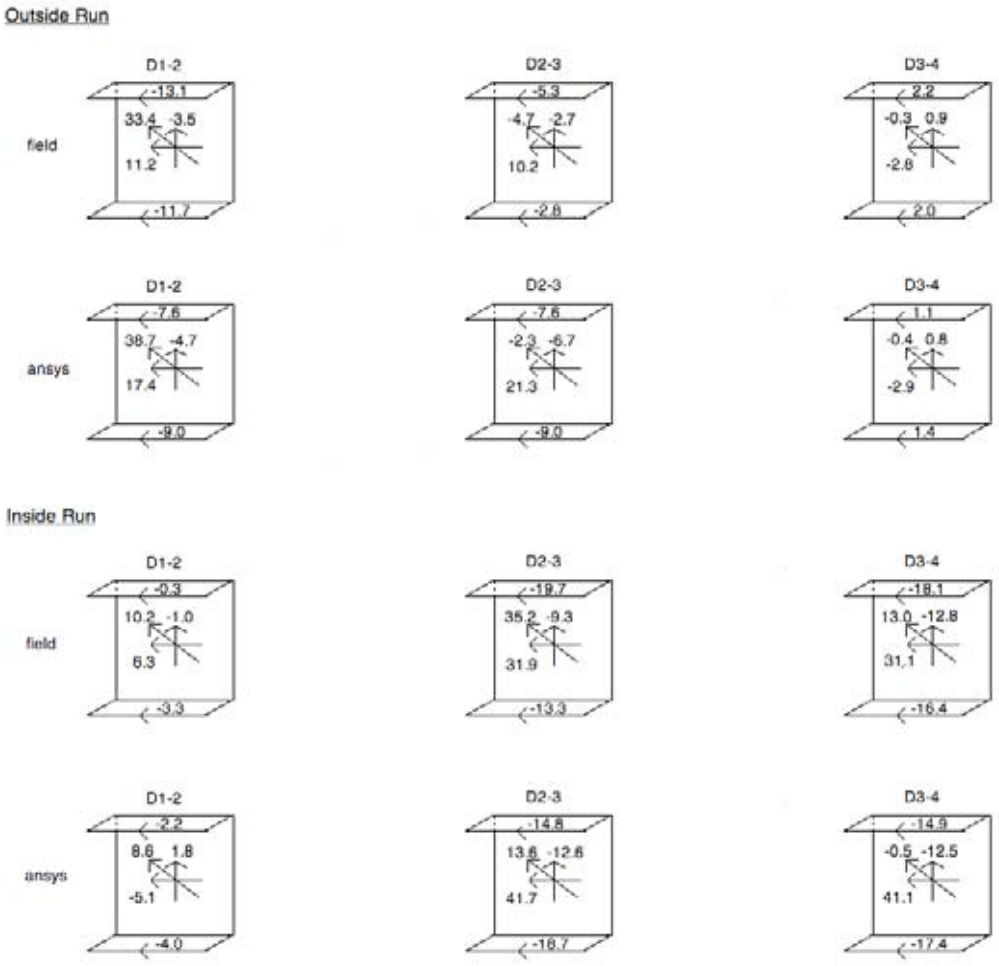

Figure 52. FE Model – Field diaphragm Comparisons with Load at Mid-span

The data from the FE model are much more informative, as strains can be extrapolated from any nodal location and can also be shown graphically, while field values can only be gained from instrumented locations. As shown in Figure 53, the FE model shows a distinct twist in the diaphragms. However, data gained in the field are not sufficient to confirm or refute this finding.

Figure 53. D1-2 and D2-3 with Load at Mid-span, Outer Run

Data from the FE model and the field data with the load located on both the inner lane and the outer lane of the bridge are relatively consistent, given the approximations used to model the diaphragm-girder connections. Many of the differences in these data sets are small enough to be explained by slight differences in loading locations, since it was difficult to place the truck in the field precisely in the radial direction. Two principal strains ε_1 and ε_2, the shearing strain γ_{xy}, and the principal angle ϕ were calculated using the three strains from the rosette: horizontal (0°), diagonal (45°), and vertical (90°). Results with the load placed at mid-span on the outside and inside of the bridge are shown in Table 3.

Table 3. Calculated Strains, Angles with Load at Mid-span

			γ_{xy} (με)	ε_1 (με)	ε_2 (με)	ϕ_1 (rad)
Outside Run	D1-2	Field	59.08	34.27	-26.62	0.663
		Ansys	64.59	40.52	-27.77	0.620
	D2-3	Field	-16.74	14.29	-6.87	-0.456
		Ansys	-19.17	24.26	-9.66	-0.300
	D3-4	Field	1.30	1.01	-2.91	-0.169
		Ansys	1.18	0.89	-2.98	-0.155
Inside Run	D1-2	Field	15.10	11.07	-5.72	0.559
		Ansys	20.55	9.21	-12.48	-0.622
	D2-3	Field	47.68	42.85	-20.19	0.429
		Ansys	-1.84	41.77	-12.63	-0.017
	D3-4	Field	7.69	31.47	-13.10	0.087
		Ansys	-29.59	44.93	-16.35	-0.252

Generally, when the load was located on the outer lane of the bridge, the strains calculated using the FE model were slightly larger than the measured field strains. When the magnitude of the principal, or axial, strains is compared to that of the shear strains, the FE model and field data are consistent in predicting greater shearing strains than axial strains in D1-2 and vice versa for D2-3. Shearing and axial strains are comparable in D3-4. These findings may imply that the diaphragms transfer load through a transverse shear mechanism rather than a bending mechanism acting though the slab, though without further instrumentation in the field this cannot be stated with certainty.

More significant differences between the FE model and field strains appear when the load is located on the inner lane of the bridge. In the instances of largest differences, more tension was measured in the field than calculated in the FE model. Substantial inconsistencies were found in the shearing strains of both D2-3 and D3-4, as well as the principal angle of all three diaphragms. Although the manual adjustment of the second run data could have introduced errors into this calculation, this would only affect D3-4 and not D2-3. Since no inconsistency was observed in the data for this particular diaphragm in the outer lane run, it is thus assumed that the error introduced by the additional adjustment of data was not significant enough to cause the conflicting data.

In comparing the magnitude of the axial and shear strains of the inner lane run, both the FE model and the field data predict larger shear strain than axial strain in D1-2. However, the shearing strains in the FE model and field data do not correlate as well for the other two diaphragms, as the field data predict much higher positive shearing strains than the FE model for D2-3 and D3-4. The principal strains for all three diaphragms with the load placed on both the inside and outside lanes compare reasonably well.

The cause of the inconsistencies is difficult to determine, since only five data points were collected on each diaphragm in the field. However, it is possible that the FE model could be overestimating the rigidity of the connections. One source could be slippage occurring in the field at the connection of the diaphragm to the girder, which is modeled as a rigid connection in the FE model. Since the distribution of strains across the bridge is not significant, this is likely not the case. Additionally, as the diaphragms and the slab act in unison as struts, it is hard to distinguish separate actions of the two.

It is also possible that the way the connections were modeled in the FE model could have an effect on the predicted behavior. In the model, the thickness of the plate was doubled at the connections as shown in Figure 54. This results in a different kind of eccentricity than is present in the field, and thus could predict a different bending and transfer than is actually occurring.

Figure 54. Difference in Field and FE Model Diaphragm-Girder Connections

CONCLUSIONS

Field Data Analysis

- The field data indicated that there is relatively little transfer of load across the bridge, with the outer two girders carrying approximately 77% of the moment when the load was in the outer lane and the inner two girders carrying nearly 76% of the moment when the load was applied in the inner lane.

- The field data indicated dynamic amplification factors on the order of 21% to 29%, well within the usual AASHTO recommendations.

- Smaller dynamic amplification factors were predicted on all girders when the load was applied on the inner lane, possibly because the vehicle approached the bridge from a paved surface in this case, while it approached from a gravel road when loading was in the outer lane.

- The field data obtained from girder 1 indicate a significant difference between measured strains on the inner and outer sides of the web, suggesting that at least some web lateral bending is present. This is most noticeable when the vehicular load is on the outer lane.

- The neutral axis estimated from the measured strain data is located approximately 7 inches below the web-flange junction, well into the web.

- Additional gages are needed at the back face of the diaphragm channels to permit calculations that can separate bending strain from St Venant torsion.

Field Data/FE Model Comparison

- The field data and FE model indicated generally similar behavior trends based upon the measured and computed strains. However there were some significant differences.

- The FE model indicated slightly more transfer of load across the bridge toward the outer edge. When the load was applied in the outer lane, nearly 81% of the load was carried by the outer two girders with the most being carried by girder 1. When the load was applied in the inner lane, the inner two girders carried about 69% of the load, with the remaining load being transferred to the outer two girders.

- The FE model and field studies predict relatively similar diaphragm shear strains when the vehicular load is on the outer lane, and the normal strains appear relatively similar for both outer lane and inner lane loadings. However the field studies predict much larger shear strains, especially in diaphragm 2-3 when the vehicular load is on the inner lane. This implies that a significant difference may exist between the load transfer mechanism of the FE model and the actual bridge.

- A distinct sign reversal between longitudinal strains in the diaphragm flanges and mid-height of the diaphragm web was both measured and calculated. A combination of tension and lateral bending, possible because the back of the channel is the plane of load transfer, explains this result.

- The FE model that most closely agreed with the field data was the model with flexible piers but without the end restraint imposed by the highway railing. This does not necessarily imply that no restraint is present, but it does suggest strongly that the particular implementation of that restraint used in earlier studies was too restrictive on bridge motion, since it prevents both translation and rotation at the end of the structure. A more realistic constraint should provide an elastic restraint on both translation and rotation, with the rotational restraint being relatively small.

- The neutral axis location estimated from the FE model strain data is above the web flange junction, more than 7 inches above the field measured value. Several contributing factors, including elastic modulus variation from nominal ACI values, overestimate of railing stiffness, variations in as-constructed slab thickness and some slip of the haunch relative to the girder flange may be contributing factors.

- A straight girder model of the same proportions as the curved girder section predicted a neutral axis location roughly 4.5 inches below the web/flange junction, much lower than the curved girder model. The neutral axis location predicted by the straight girder model appears to be at least somewhat sensitive to mesh refinement. This suggests that the more complex strain distribution present in the curved girder model may require a more refined mesh for adequate strain convergence than does a straight girder.

RECOMMENDATIONS

Design Recommendations

1. Bridge designers should consider modeling pier flexibility of curved girder bridges during the design phase because it contributes in important ways to the behavior of such bridges.

2. Channel type diaphragms such as the ones used on the current structure may not be able to adequately transfer loads between girders of a curved bridge. Bridge designers and researchers should focus on additional studies in this area.

Future Research Studies

3. A modified FE model of the Wolf Creek Bridge should be constructed with full-depth cross-frames in order to assess the effectiveness of the channel type diaphragms in lateral load transfer.

4. Additional study of the diaphragms is warranted with gages added on the back of the channels to assess the load transfer in those members. As a minimum, longitudinal gages at the top and bottom of the channel and a second rosette directly opposite the current rosette on the web are recommended.

5. A transducer capable of measuring slip between the girder top flange and the haunch should be installed as part of field studies of this type to assess the extent to which the flange/haunch connection can be assumed to be rigid.

6. An FE model of the bridge, including the results of the end railing model constructed by Fuchs (2008), should be constructed to evaluate the influence of end restraint more fully. In addition, flexible connections between haunches and flanges should be modeled to incorporate the potential effect of shear slip.

7. In view of the straight girder FE results, a more refined curved girder bridge FE model needs to be constructed to determine whether mesh refinement will lead to a neutral axis location that is more consistent with the measured field data.

BENEFITS AND IMPLEMENTATION PROSPECTS

Implications of this study could have a significant effect on future health monitoring applications as they pertain to both curved and straight girder bridges. It is essential that FE models in such long-term applications be able to reproduce the "as-built" response characteristics of a bridge. The current study raised significant issues about the ability to correctly model the behavior of curved girder bridges correctly. Thus it will be important to perform subsequent numerical research studies to develop models that will result in more precise predictions and to use these and other methods being developed in any health monitoring applications.

ACKNOWLEDGMENTS

The work reported in this study was supported by a research grant from the Virginia Transportation Research Council. That support is gratefully acknowledged.

REFERENCES

Abdel-Sayed, G. (1973). Curved webs under combined shear and normal stresses, *Journal of the Structural Division*, ASCE, 99, 3, 511-525

Armstrong, W. L. (1972) Dynamic testing of curved bridge-Hyuck stream, *Journal of the Structural Division*, ASCE, 98, 9, 2015-2030

Batoz, J.L., et al. (1980). *International Journal of Numerical Methods in Engineering*, 15, 1771-1812.

Christiano, P.P. and Culver, C.G. (1969). Horizontally curved bridges subject to moving loads, *Journal of the Structural Division*, ASCE, 95, 8, 1615-1643.

Culver, C.G. and Christiano, P.P. (1969). Static model tests of curved girder bridge, *Journal of the Structural Division*, ASCE, 95, 8, 1599-1614.

Culver, C.G. and Frampton, R.E. (1970) Local instability of horizontally curved beams, *Journal of the Structural Division*, ASCE, 96, 2, 245-265.

Culver, C.G., and Nasir, G. (1971) Inelastic flange buckling of curved plate girders, *Journal of the Structural Division*, ASCE, 97, 4, 1239-1256.

Culver, C.G., Dym, C.L., and Brogan, D.K. (1972) Bending behavior of cylindrical web panels, *Journal of the Structural Division*, ASCE, 98, 10, 2291-2308.

Dabrowski, R. (1968). *Curved thin-walled girders, theory and analysis*, Cement and Concrete Association, London (translated from German).

Dally, J.W., and Riley, W.F. (1978) *Experimental Stress Analysis*, 2nd Edition, McGraw-Hill, New York.

Davidson, J.S., Ballance, S.R., and Yoo, C.H. (1999a). Analytical Model of Curved I-Girder Web Panels subjected to Bending, *Journal of Bridge Engineering*, ASCE, 4, 3, 204-212.

Davidson, J.S., Ballance, S.R., and Yoo, C.H. (1999b). Finite Displacement Behavior of Curved I-Girder Webs subjected to Bending, *Journal of Bridge Engineering*, ASCE, 4, 3, 213-220.

Davidson, J.S., Ballance, S.R., and Yoo, C.H. (2000a). Behavior of Curved I-Girder Webs Subjected to Combined Bending and Shear, *Journal of Bridge Engineering*, ASCE, 5, 2, 165-170.

Davidson, J.S., Ballance, S.R., and Yoo, C.H.,(2000b). Effects of Longitudinal Stiffeners on Curved I-Girder Webs, *Journal of Bridge Engineering*, ASCE, 5, 2, 171-178.

Domalik, D.E., Shura, J.F., and Linzell, D.G. (2005). Design and Field Monitoring of Horizontally Curved Steel Plate Girder Bridge, *Transportation Research Record*, No. 1928, Transportation Research Board, Washington, D., 83-91.

Faella, C., Martinelli, E., and Nigro, E. (2003). Shear Connection Nonlinearity and Deflections of Steel-Concrete Composite Beams: A Simplified Method, *Journal of Structural Engineering*, 129, 1, 12-20.

Fang, L.X., Chan, S.L., and Wong, Y.L. (2000). Numerical Analysis of Composite Frames with Partial Shear-Stud Interaction By One Element per Member, *Engineering Structures*, 22, 10, 1285-1300.

Fuchs, S. (2008). *Boundary Condition Modeling of the Wolf Creek Curved Girder Bridge*, B.S. Thesis, University of Virginia, Charlottesville.

Galambos, T.V., Hajjar, J.F., Huang, W-H., Pulver, B.E., Leon, R.T., and Rudie, B.J. (2000). Comparison of Measured and Computed Stresses in a Steel Curved Girder Bridge, *Journal of Bridge Engineering*, ASCE, 5, 3, 191-199.

Hall, D.H. (1996). Curved Girders are Special, *Engineering Structures*, 18, 10, 769-777.

Hall, D.H., Grubb, M.A., and Yoo, C.H. (1999). Improved design specifications for horizontally curved steel girder highway bridges, *National Cooperative Highway Research Program Research Report No. 424*, Washington, DC.

Lam, D., and El-Lobody, E. (2005). Behavior of Headed Stud Shear Connectors in Composite Beam, *Journal of Structural Engineering*, 131, 1, 96-107.

Linzell, D.G. (1999). Studies of a full-scale horizontally curved steel I girder bridge system under self-weight, Ph.D. Dissertation, School of Civil and Environmental Engineering, Georgia Institute of Technology, Atlanta.

Linzell, D., Leon, R.T., and Zureick, A.H., (2004). Experimental and Analytical Studies of a Horizontally Curved Steel I-Girder Bridge during Erection, *Journal of Bridge Engineering*, ASCE, 9, 6, 521-530.

Linzell, D., Hall, D., and White, D. (2004). Historical Perspective on Horizontally Curved I Girder Bridge Design in the United States, *Journal of Bridge Engineering*, 9, 3, 218-229.

Linzell, D., Leon, R.T., and Zureick, A.H. (2004). Experimental and Analytical Studies of a Horizontally Curved Steel I-Girder Bridge during Erection, *Journal of Bridge Engineering*, ASCE, 9, 6, 521-530.

Lydzinski, J. (2006). Finite Element Modeling of a Multispan Horizontally Curved Girder Bridge, M.S. Thesis, Civil and Environmental Engineering Department, University of Virginia, Charlottesville.

McManus, P.F. Nasir, G.A. and Culver, C.G. (1969) Horizontally Curved Girders – State of the Art, *Journal of the Structural Division*, ASCE, 95, ST5, 853-870.

McElwain, B.A., and Laman, J.A. (2000). Experimental Verification of Horizontally Curved I-Girder Bridge Behavior, *Journal of Bridge Engineering*, ASCE, 5, 4, 284-292.

Miller, J.E. (2008). Strain Instrumentation of a Multi-Span Curved Girder Bridge, M.S. Thesis, Department of Civil and Environmental Engineering, University of Virginia, Charlottesville.

Nilson, A., Darwin, D., and Donan, C. (2004). *Design of Concrete Structures*, 13th Edition, McGraw-Hill, New York.

Oden, J.T. (1967). *Mechanics of Elastic Structures*, McGraw-Hill, New York.

Rambo-Roddenberry, M.D. (2002). Behavior and Strength of Welded Stud Shear Connectors, Ph.D. Dissertation, Department of Civil and Environmental Engineering, Virginia Polytechnic Institute and State University, Blacksburg.

Seracino, R., Oehlers, D.J., and Yeo, M.F. (2001). Partial-Interaction Flexural Stresses in Composite Steel and Concrete Bridge Beams, *Engineering Structures*, 23, 9, 1186-1193.

Simons, D.C. (2005). *AASHTO LRFD Impact upon Bridge Stiffness and Strength*, M.S. Thesis, University of Virginia, Charlottesville.

Tilley, M. (2004). *Dynamic analysis and testing of a curved girder bridge*, M. S. Thesis, Department of Civil and Environmental Engineering, University of Virginia, Charlottesville.

Turnage, R. (2007). Vibration Testing of the Wolf Creek Curved Girder Bridge, M.S. Thesis, Department of Civil and Environmental Engineering, University of Virginia, Charlottesville.

Turnage, R.S., and Baber, T.T. (2009). *Field Testing of the Wolf Creek Curved Girder Bridge: Part I: Vibration Tests.* VTRC 09-CR13. Virginia Transportation Research Council, Charlottesville.

Wang, X., Kangas, S., Padur, D., Liu, L., Swanson, J., Helmicki, A., and Hunt, V. (2005). Overview of a Modal-Based Condition Assessment Procedure, *Journal of Bridge Engineering*, 10, 4, 460-467.

Womack, K., Halling, M., and Bott, S. (2001). *Static and Dynamic Testing of a Curved Steel Girder Bridge in Salt Lake City, Utah*, Report No. UT-00.13, Utah Department of Transportation Research Division, August.

Zhang, Z.F., and Aktan, A.E. (1997). Different levels of modeling for the purpose of bridge evaluation, *Applied Acoustics*, 50, 3, 189-204.

Zureick, A., Naqib, R., and Yadlosky, J.M. (1993). Curved steel bridge research project Interim report I: Synthesis, Rep. No. FHWA-RD-93-129, Federal Highway Administration, McLean, VA.

Zureick, A. and Naqib, R. (1999). Horizontally Curved Steel I-Girders State of the Art Analysis Methods, *Journal of Bridge Engineering*, ASCE, 4, 1, 38-47.

APPENDIX A. MATLAB MODULES

CoordInput.m

```
% This m-file reads three arrays: radii, degrees, and nodes
% from their binary versions

rid = fopen('rad.bin','rb')
radii=fread(rid,48,'float')
fclose(rid)
did=fopen('deg.bin','rb')
degrees=fread(did,217,'float')
fclose(did)
nid = fopen('nodes.bin','rb')
nodes=fread(nid,[217,48],'integer*4')
fclose(nid)
```

TruckInner.m

```
% An m-file to generate the local truck data when the truck is
% in the INSIDE lane. The data consists of local
% x axis, local y axis, and point load values
txcl = [-178 -178 0 0 54 54];
tycl = [-6 78 0 72 0 72];
tpl = [-6.080 -6.080 -8.080 -8.080 -8.080 -8.080];
```

TruckOuter.m

```
% An m-file to generate the local truck data when the truck is
% in the OUTSIDE lane. The data consists of local
% x axis, local y axis, and point load values.
txcl = [178 178 0 0 -54 -54];
tycl = [-6 78 0 72 0 72];
tpl = [-6.080 -6.080 -8.080 -8.080 -8.080 -8.080];
```

CreateLoadFileInner.m

```
CoordInput
TruckInner
[WheelRadius,WheelTh]=WheelLocRadial(radwho,angwho,txcl,tycl)
[jrad,jrw,jang,jaw,wnodloc,wnodwt]=locate(WheelRadius,WheelTh,radii,degrees,n
odes)
[load1]=writeloadstoansys(wnodloc,wnodwt,tpl)
```

CreateLoadFileOuter.m

```
CoordInput
TruckOuter
[WheelRadius,WheelTh]=WheelLocRadial(radwho,angwho,txcl,tycl)
[jrad,jrw,jang,jaw,wnodloc,wnodwt]=locate(WheelRadius,WheelTh,radii,degrees,n
odes)
[load1]=writeloadstoansys(wnodloc,wnodwt,tpl)
```

WheelLocRadialE.m

```
function[WheelradiusE,WheelThE] = WheelLocRadialE(r,ang,txcl,tycl)

% Generate radial coordinates
for i = 1:6
    WheelradiusE(i)=sqrt((r+tycl(i))^2+txcl(i)^2);
    WheelThE(i)=180*atan2(txcl(i),WheelradiusE(i))/pi+ang;
end
WheelradiusE
WheelThE
```

Locate.m

```
function[jrad,jrw,jang,jaw,wnodloc,wnodwt]=...
    locate(Wheelradius,WheelTh,radii,degrees,nodes)

% m-file to construct the nodes at which the loads are to be applied.
for i=1:6 %counter on the wheels
        jrad(i,1)=1;
        jrad(i,2)=2;
    for j = 1:47 %counter on the number of radii
        if Wheelradius(i)>=radii(j)&&Wheelradius(i)<=radii(j+1)
            jrad(i,1)=j;
            jrad(i,2)=j+1;
            jrw(i,2)=(Wheelradius(i)-radii(j))/(radii(j+1)-radii(j));
            jrw(i,1)=1-jrw(i,2);
            break
        end
    end
    jang(i,1)=1;
    jang(i,2)=2;
    for k=1:216 %counter on the number of angles
        if WheelTh(i)>=degrees(k)&&WheelTh(i)<=degrees(k+1)
            jang(i,1)=k;
            jang(i,2)=k+1;
            jaw(i,2)=(WheelTh(i)-degrees(k))/(degrees(k+1)-degrees(k));
            jaw(i,1)=1-jaw(i,2);
            break
        end
    end
    ja1=jang(i,1)
    jr1=jrad(i,1)
    ja2=jang(i,2)
    jr2=jrad(i,2)
    wnodloc(i,1)=nodes(ja1,jr1);
    wnodwt(i,1)=jaw(i,1)*jrw(i,1);
    wnodloc(i,2)=nodes(ja1,jr2);
    wnodwt(i,2)=jaw(i,1)*jrw(i,2);
    wnodloc(i,3)=nodes(ja2,jr1);
    wnodwt(i,3)=jaw(i,2)*jrw(i,1);
    wnodloc(i,4)=nodes(ja2,jr2);
    wnodwt(i,4)=jaw(i,2)*jrw(i,2);
end
```

Writeloadstoansys.m

```
function[load1] = writeloadstoansys(wnodloc,wnodwt,tpl)

% mfile that writes data to an ANSYS format

fid=fopen('Loaddata.txt','w+')
for i=1:6
    load1=wnodwt(i,1)*tpl(i);
    fprintf(fid,'f,%6i,fz,%6.2d\n',wnodloc(i,1),load1);
    load1=wnodwt(i,2)*tpl(i);
    fprintf(fid,'f,%6i,fz,%6.2d\n',wnodloc(i,2),load1);
    load1=wnodwt(i,3)*tpl(i);
   fprintf(fid,'f,%6i,fz,%6.2d\n',wnodloc(i,3),load1);
    load1=wnodwt(i,4)*tpl(i);
    fprintf(fid,'f,%6i,fz,%6.2d\n',wnodloc(i,4),load1);
end
fclose(fid);
```

APPENDIX B. STATIC-ANSYS DATA COMPARISON; OUTSIDE RUN B TO A, INSIDE RUN A TO B

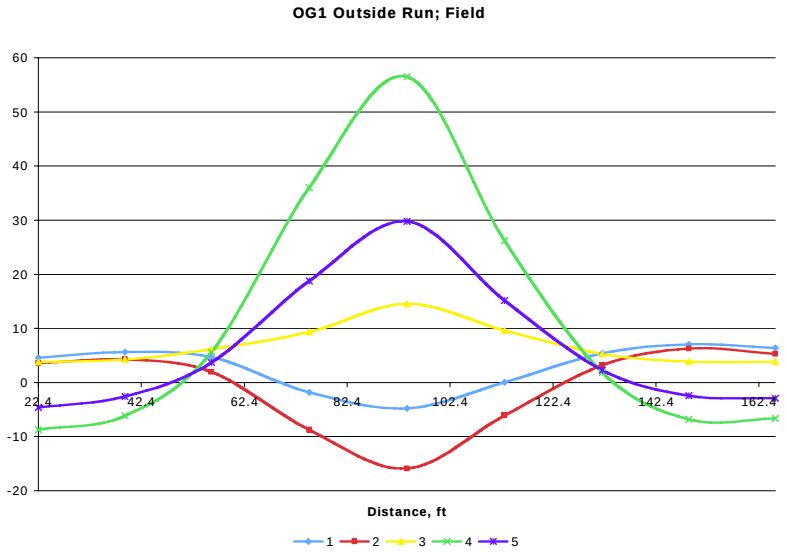

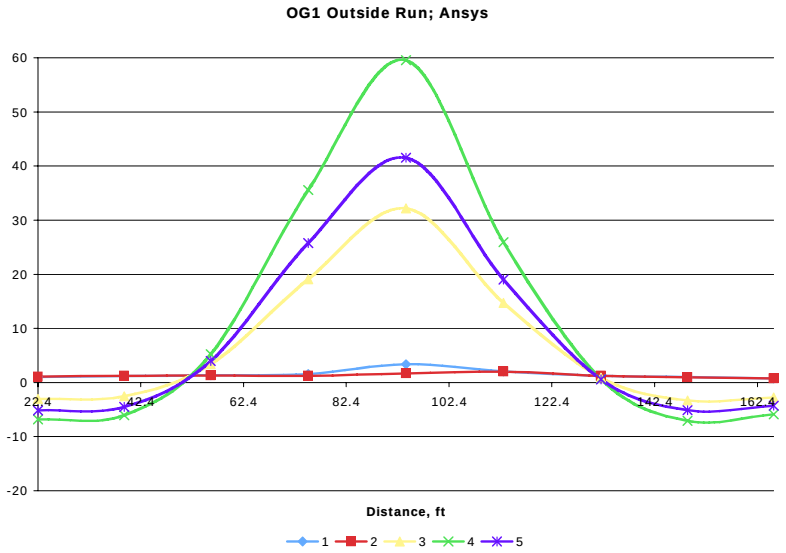

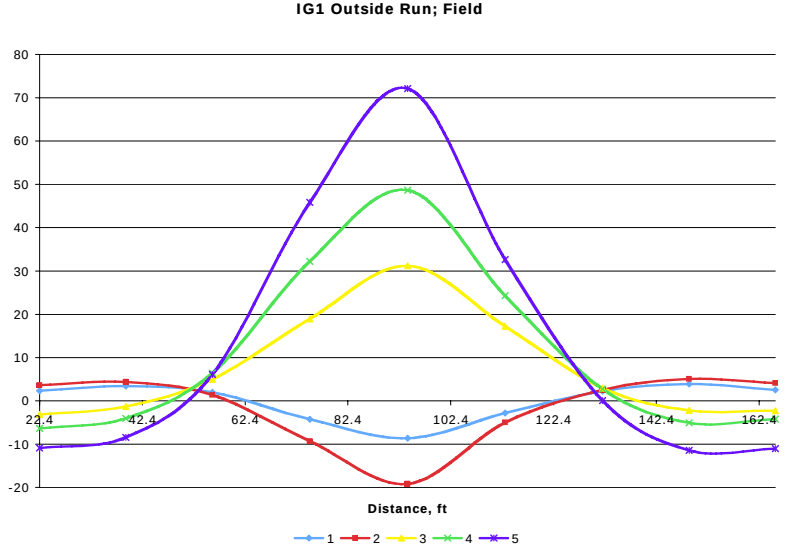

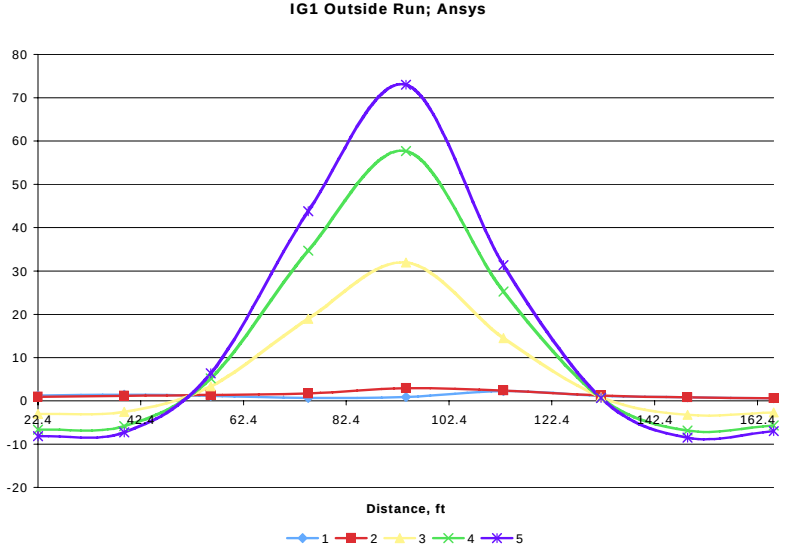

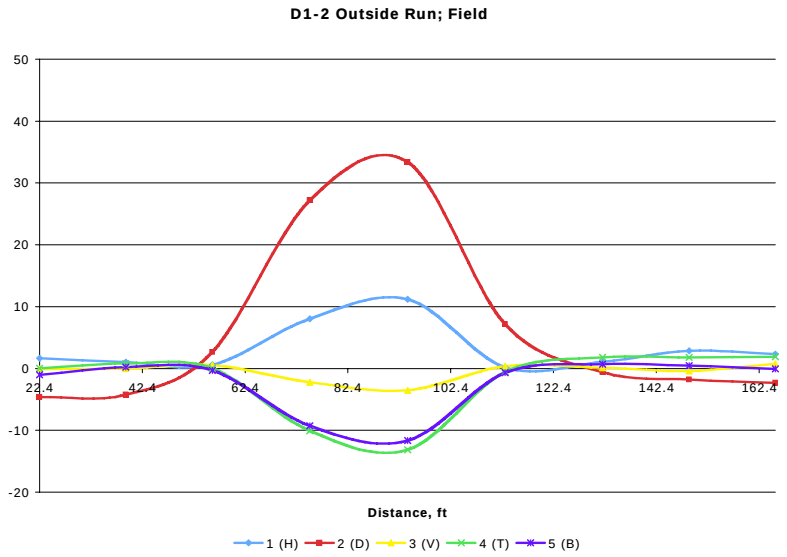
D1-2 Outside Run; Field
50
40
30
20
10
0
-10
-20
22.4
42.4
62.4
82.4
102.4
122.4
142.4
162.4
Distance, ft
1 (H)
2 (D)
3 (V)
4 (T)
5 (B)

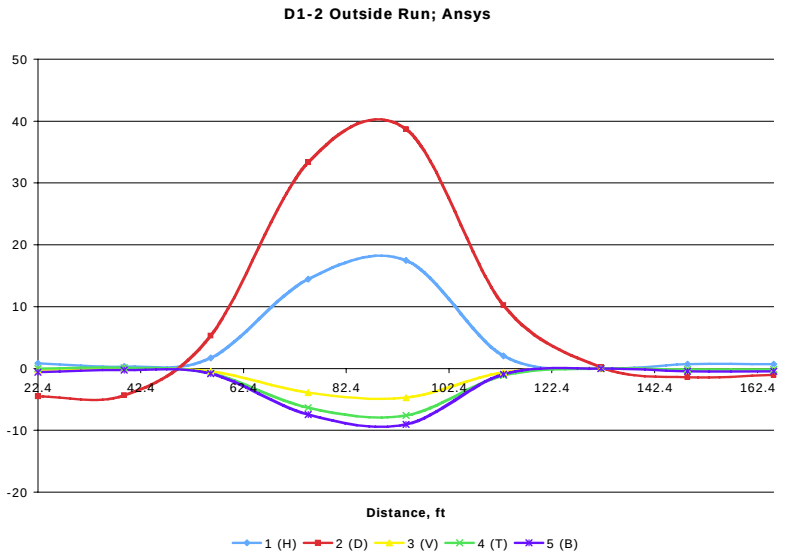
D1-2 Outside Run; Ansys
50
40
30
20
10
0
-10
-20
22.4
42.4
62.4
82.4
102.4
122.4
142.4
162.4
Distance, ft
1 (H)
2 (D)
3 (V)
4 (T)
5 (B)

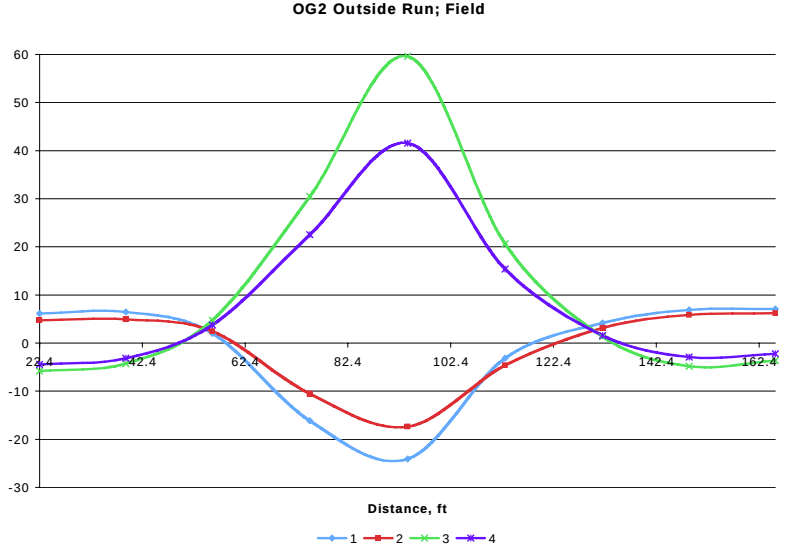
OG2 Outside Run; Field
60
50
40
30
20
10
0
-10
-20
-30
22.4
42.4
62.4
82.4
102.4
122.4
142.4
162.4
Distance, ft
1
2
3
4

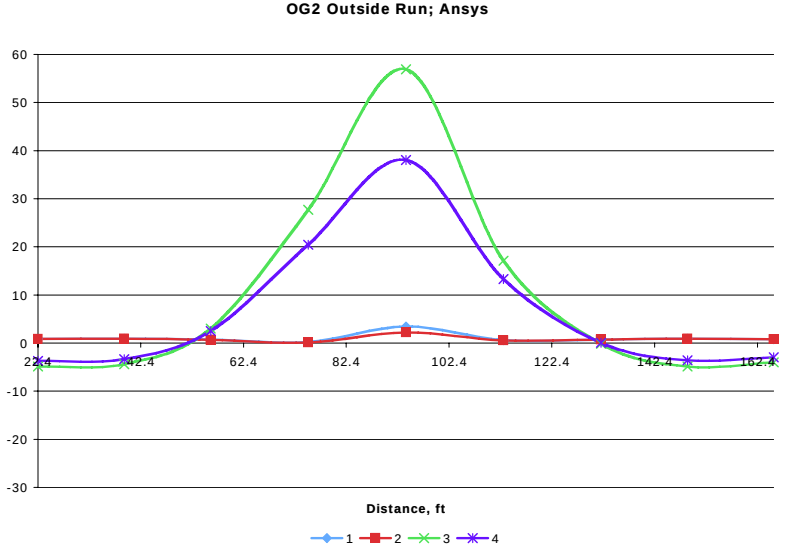
OG2 Outside Run; Ansys
60
50
40
30
20
10
0
-10
-20
-30
22.4
42.4
62.4
82.4
102.4
122.4
142.4
162.4
Distance, ft
1
2
3
4

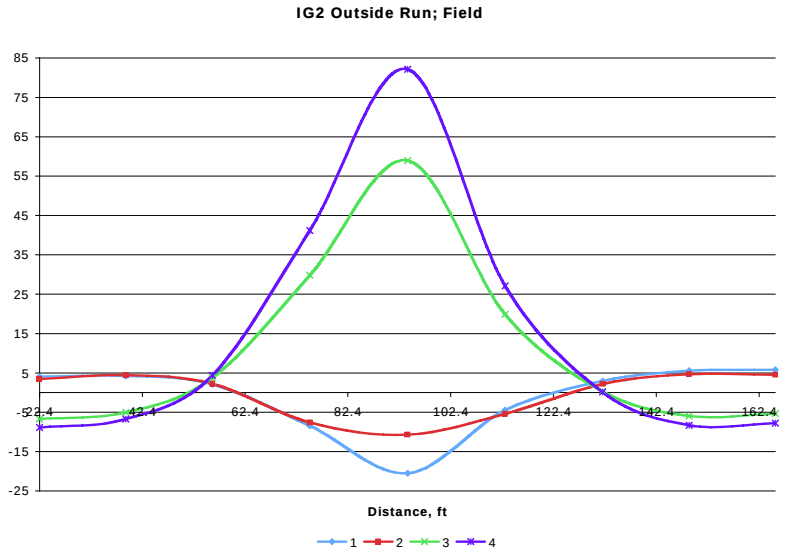
IG2 Outside Run; Field
85
75
65
55
45
35
25
15
5
-5
-15
-25
22.4
42.4
62.4
82.4
102.4
122.4
142.4
162.4
Distance, ft
1
2
3
4

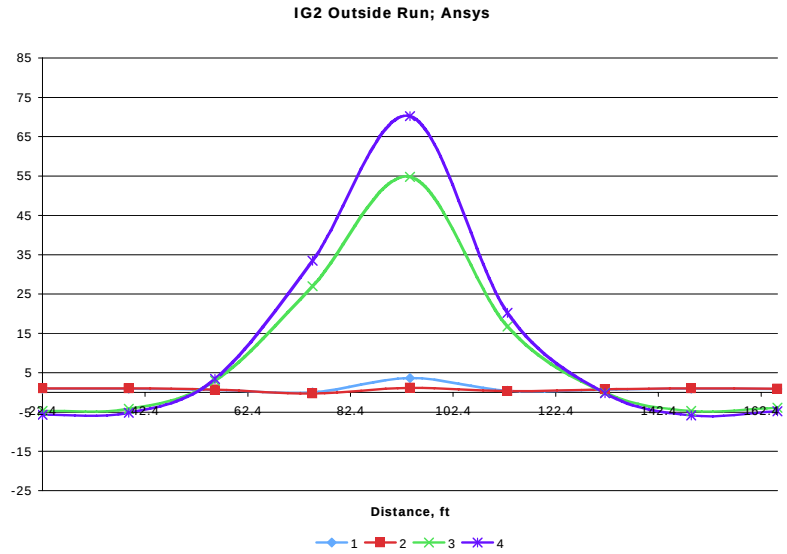
IG2 Outside Run; Ansys
85
75
65
55
45
35
25
15
5
-5
-15
-25
22.4
42.4
62.4
82.4
102.4
122.4
142.4
162.4
Distance, ft
1
2
3
4

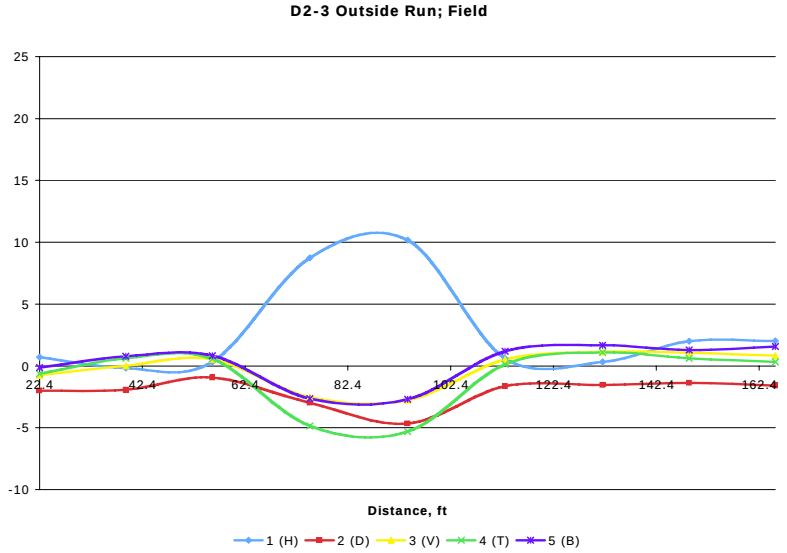
D2-3 Outside Run; Field
25
20
15
10
5
0
-5
-10
22.4
42.4
62.4
82.4
102.4
122.4
142.4
162.4
Distance, ft
1 (H)
2 (D)
3 (V)
4 (T)
5 (B)

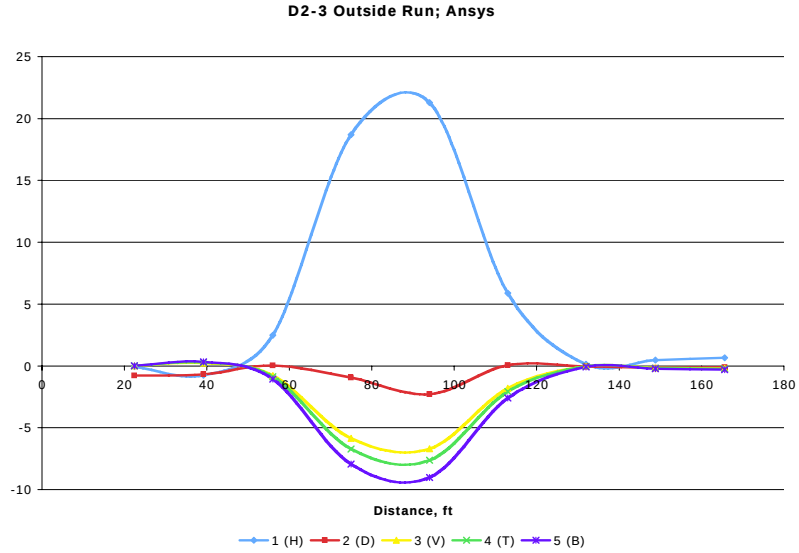
D2-3 Outside Run; Ansys
25
20
15
10
5
0
-5
-10
0
20
40
60
80
100
120
140
160
180
Distance, ft
1 (H)
2 (D)
3 (V)
4 (T)
5 (B)

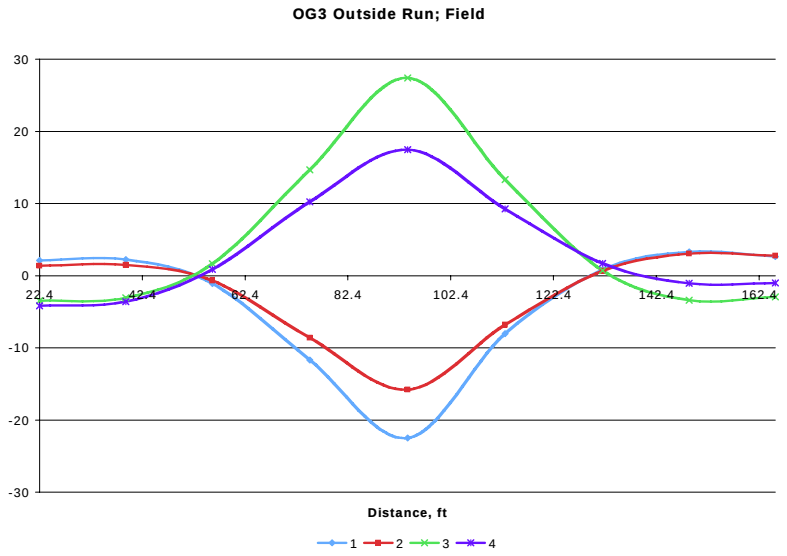
OG3 Outside Run; Field
30
20
10
0
-10
-20
-30
22.4
42.4
62.4
82.4
102.4
122.4
142.4
162.4
Distance, ft
1
2
3
4

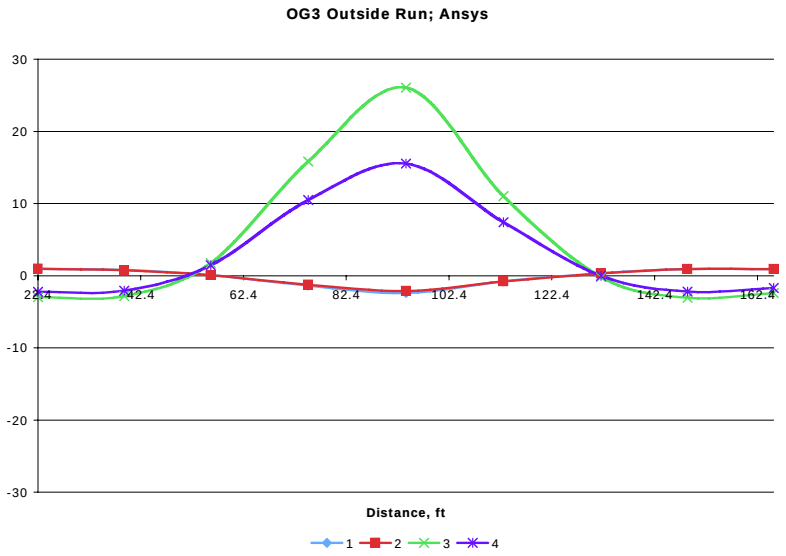
OG3 Outside Run; Ansys
30
20
10
0
-10
-20
-30
22.4
42.4
62.4
82.4
102.4
122.4
142.4
162.4
Distance, ft
1
2
3
4

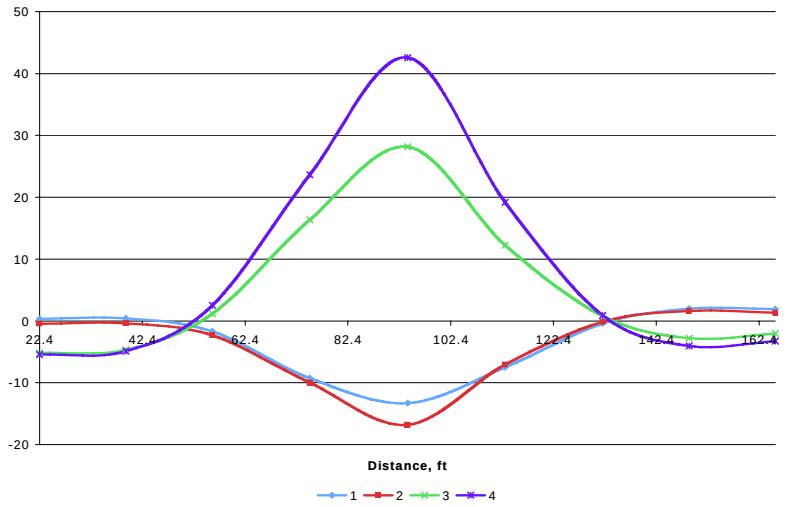
IG3 Outside Run; Field
50
40
30
20
10
0
-10
-20
22.4
42.4
62.4
82.4
102.4
122.4
142.4
162.4
Distance, ft
1
2
3
4

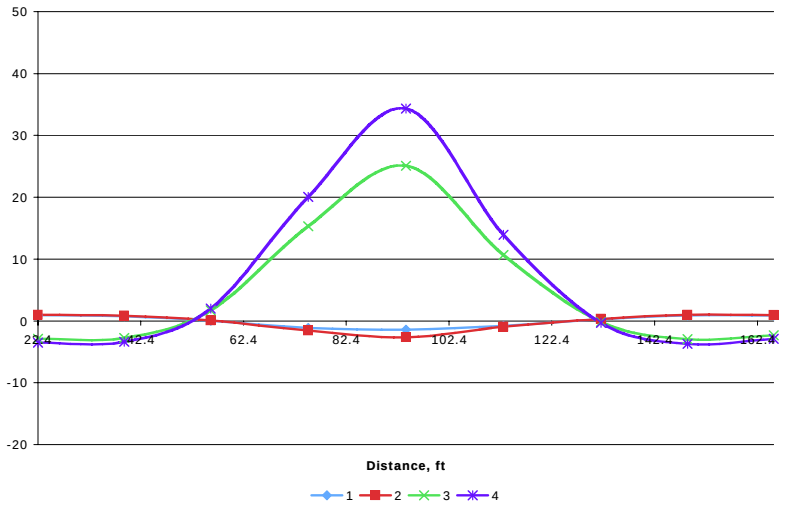
IG3 Outside Run; Ansys
50
40
30
20
10
0
-10
-20
22.4
42.4
62.4
82.4
102.4
122.4
142.4
162.4
Distance, ft
1
2
3
4

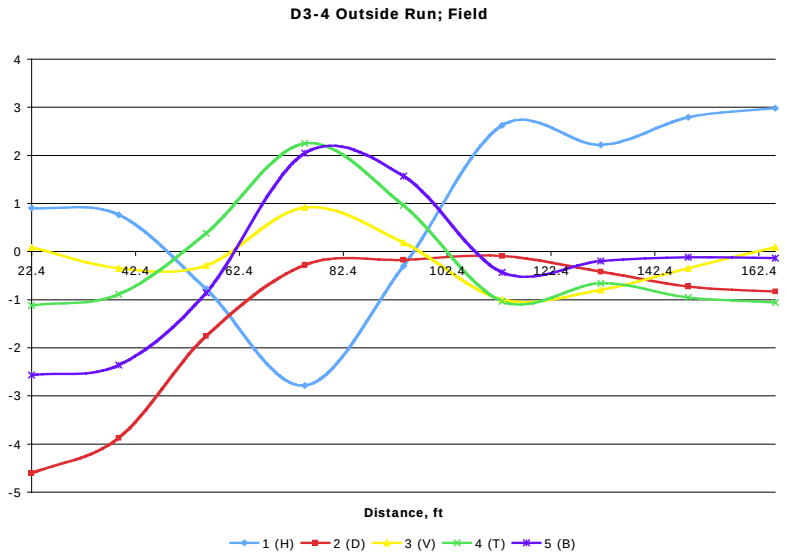
D3-4 Outside Run; Field
4
3
2
1
0
-1
-2
-3
-4
-5
22.4
42.4
62.4
82.4
102.4
122.4
142.4
162.4
Distance, ft
1 (H)
2 (D)
3 (V)
4 (T)
5 (B)

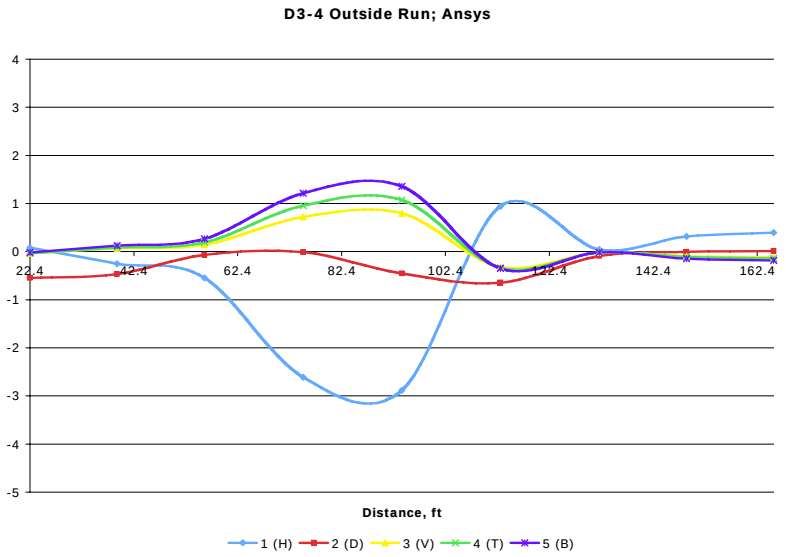
D3-4 Outside Run; Ansys
4
3
2
1
0
-1
-2
-3
-4
-5
22.4
42.4
62.4
82.4
102.4
122.4
142.4
162.4
Distance, ft
1 (H)
2 (D)
3 (V)
4 (T)
5 (B)

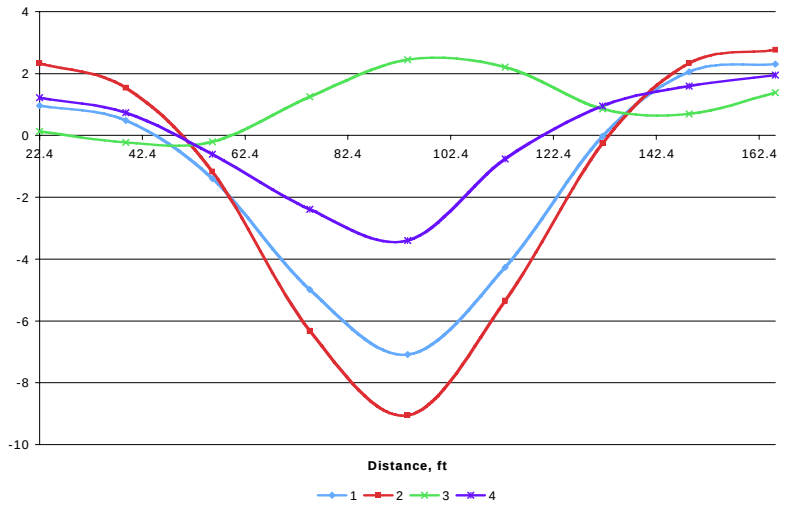
OG4 Outside Run; Field
4
2
0
-2
-4
-6
-8
-10
22.4
42.4
62.4
82.4
102.4
122.4
142.4
162.4
Distance, ft
1
2
3
4

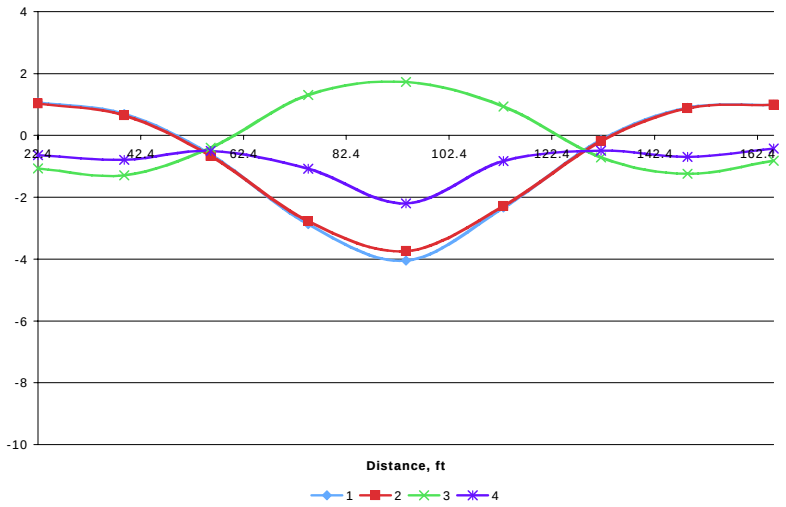
OG4 Outside Run; Ansys
4
2
0
-2
-4
-6
-8
-10
22.4
42.4
62.4
82.4
102.4
122.4
142.4
162.4
Distance, ft
1
2
3
4

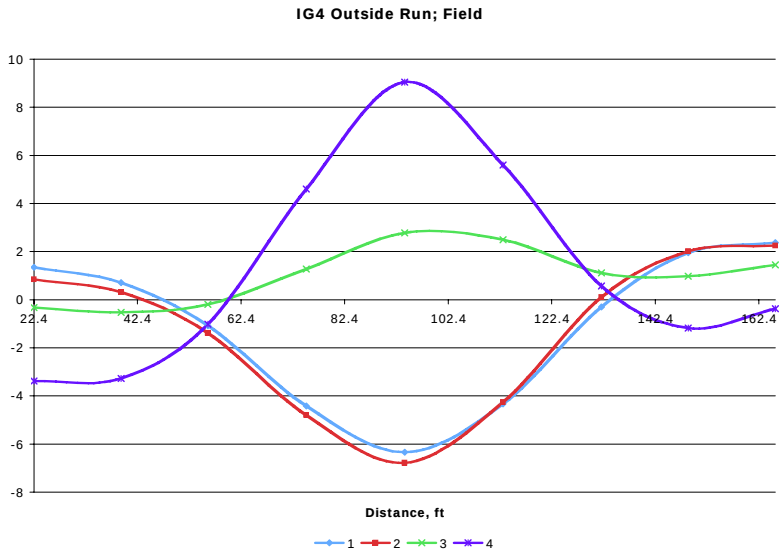
IG4 Outside Run; Field
10
8
6
4
2
0
-2
-4
-6
-8
22.4
42.4
62.4
82.4
102.4
122.4
142.4
162.4
Distance, ft
1
2
3
4

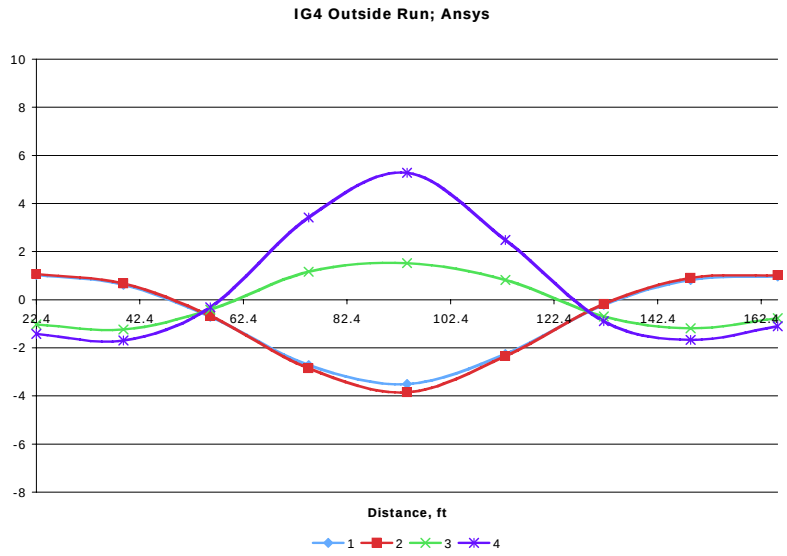
IG4 Outside Run; Ansys
10
8
6
4
2
0
-2
-4
-6
-8
22.4
42.4
62.4
82.4
102.4
122.4
142.4
162.4
Distance, ft
1
2
3
4

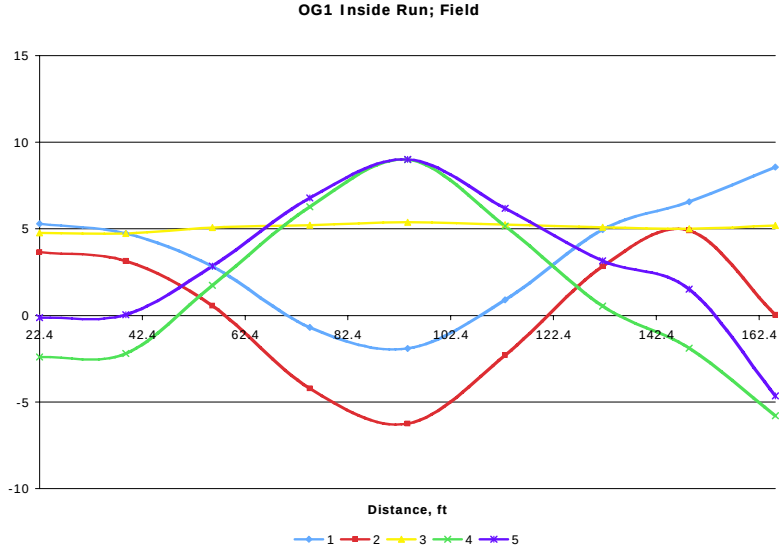
OG1 Inside Run; Field
15
10
5
0
-5
-10
22.4
42.4
62.4
82.4
102.4
122.4
142.4
162.4
Distance, ft
1
2
3
4
5

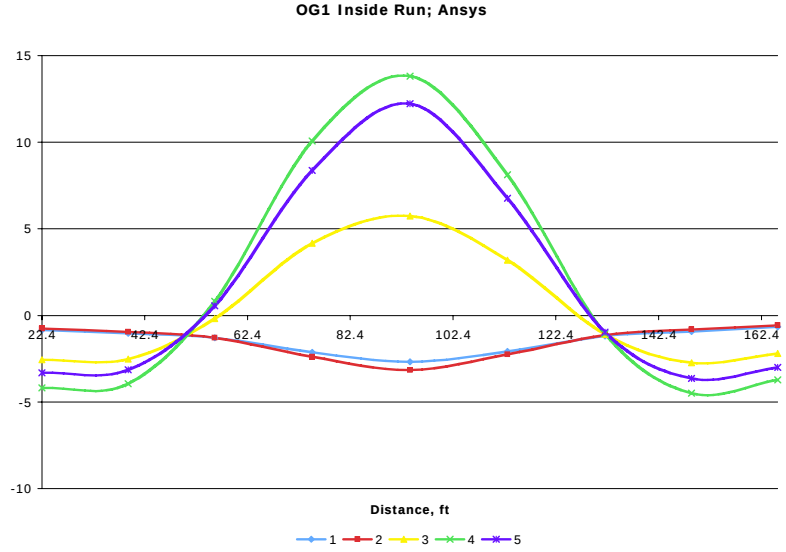
OG1 Inside Run; Ansys
15
10
5
0
-5
-10
22.4
42.4
62.4
82.4
102.4
122.4
142.4
162.4
Distance, ft
1
2
3
4
5

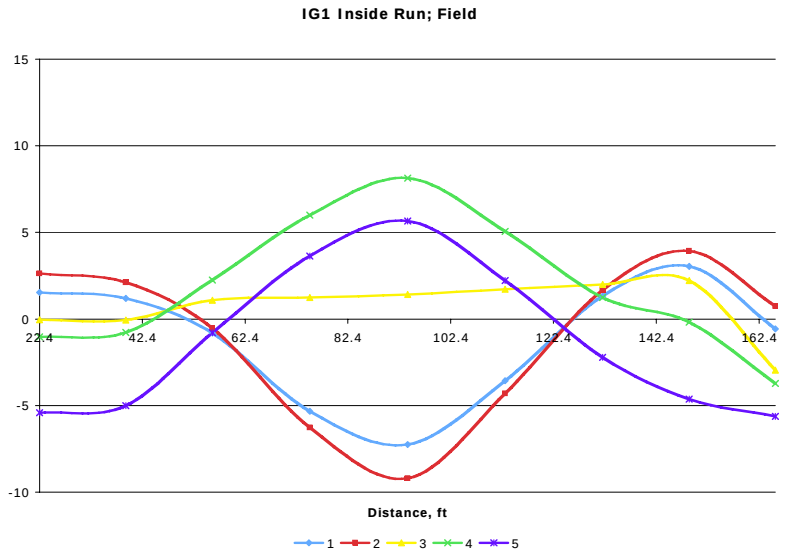
IG1 Inside Run; Field
15
10
5
0
-5
-10
22.4
42.4
62.4
82.4
102.4
122.4
142.4
162.4
Distance, ft
1
2
3
4
5

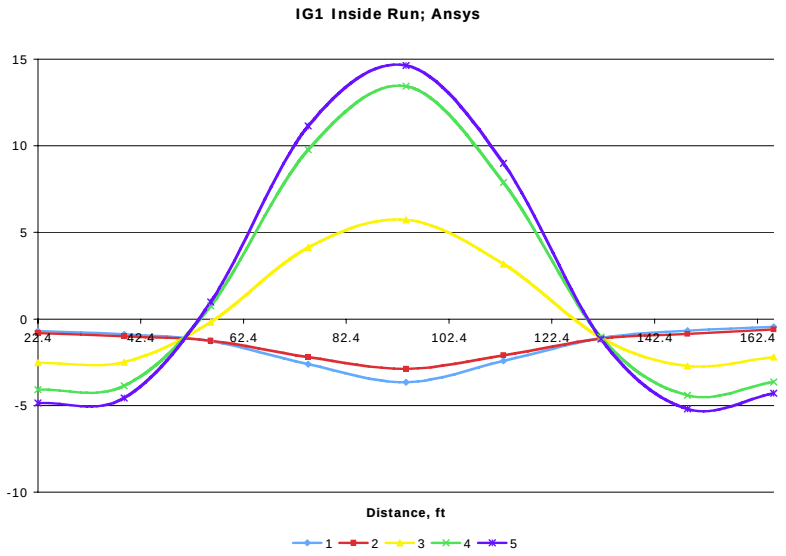
IG1 Inside Run; Ansys
15
10
5
0
-5
-10
22.4
42.4
62.4
82.4
102.4
122.4
142.4
162.4
Distance, ft
1
2
3
4
5

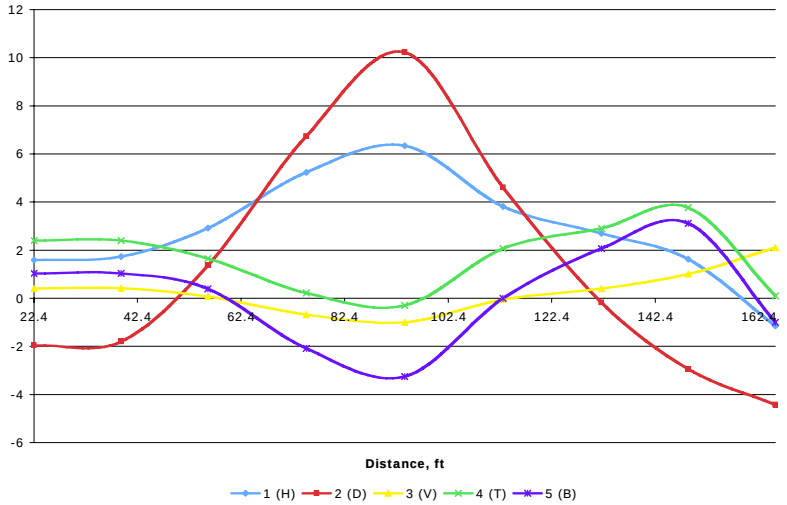
D1-2 Inside Run; Field
12
10
8
6
4
2
0
-2
-4
-6
22.4
42.4
62.4
82.4
102.4
122.4
142.4
162.4
Distance, ft
1 (H)
2 (D)
3 (V)
4 (T)
5 (B)

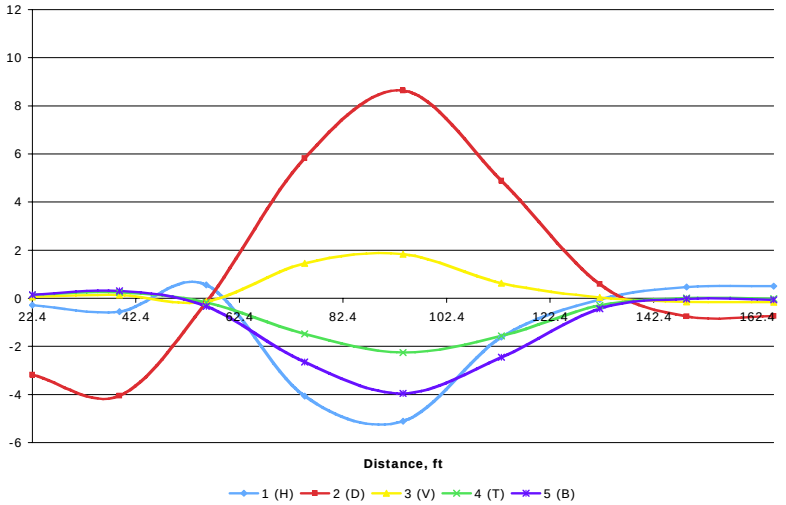
D1-2 Inside Run; Ansys
12
10
8
6
4
2
0
-2
-4
-6
22.4
42.4
62.4
82.4
102.4
122.4
142.4
162.4
Distance, ft
1 (H)
2 (D)
3 (V)
4 (T)
5 (B)

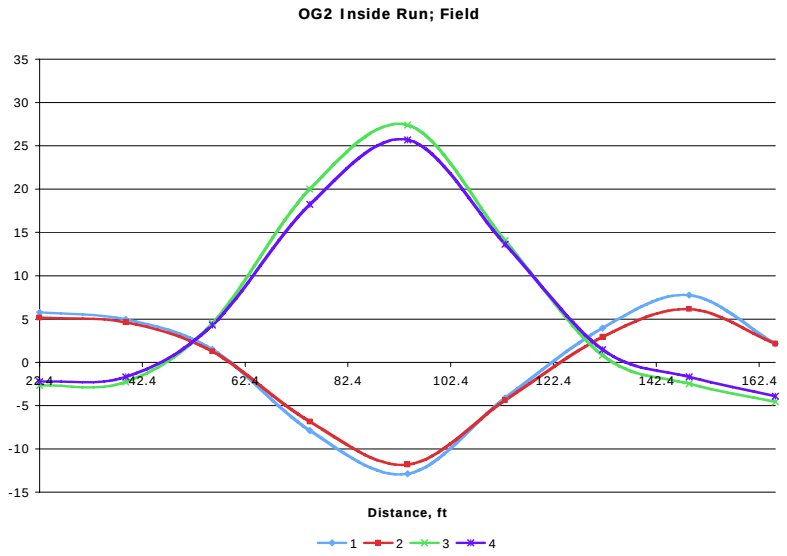
OG2 Inside Run; Field
35
30
25
20
15
10
5
0
-5
-10
-15
22.4
42.4
62.4
82.4
102.4
122.4
142.4
162.4
Distance, ft
1
2
3
4

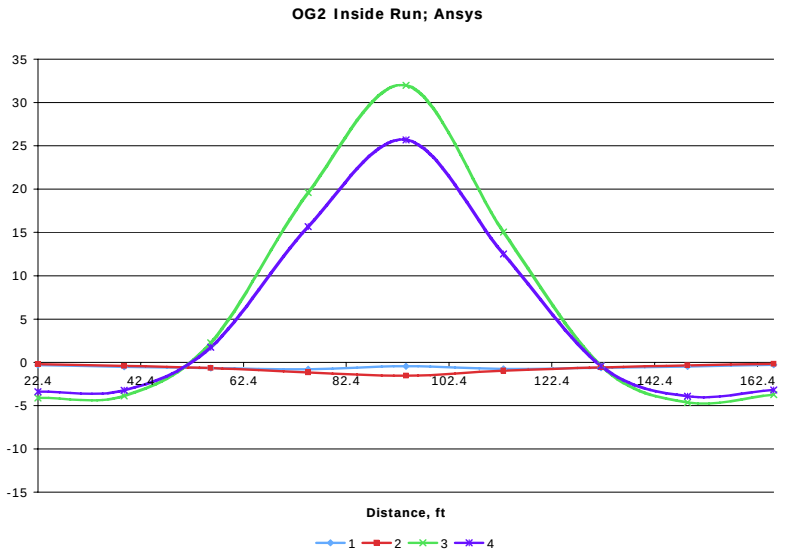
OG2 Inside Run; Ansys
35
30
25
20
15
10
5
0
-5
-10
-15
22.4
42.4
62.4
82.4
102.4
122.4
142.4
162.4
Distance, ft
1
2
3
4

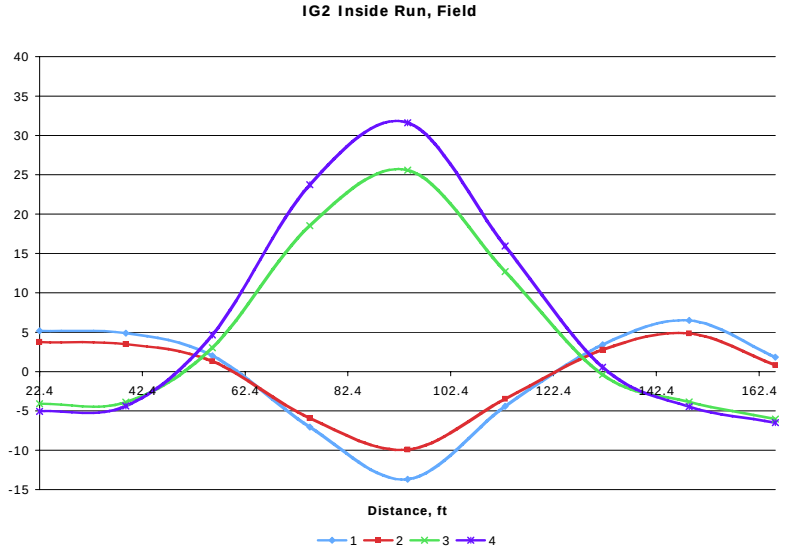
IG2 Inside Run, Field
40
35
30
25
20
15
10
5
0
-5
-10
-15
22.4
42.4
62.4
82.4
102.4
122.4
142.4
162.4
Distance, ft
1
2
3
4

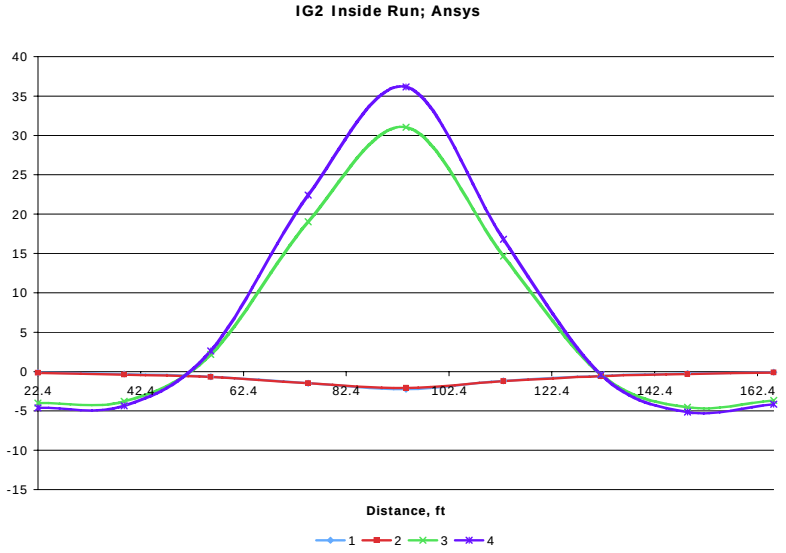
IG2 Inside Run; Ansys
40
35
30
25
20
15
10
5
0
-5
-10
-15
22.4
42.4
62.4
82.4
102.4
122.4
142.4
162.4
Distance, ft
1
2
3
4

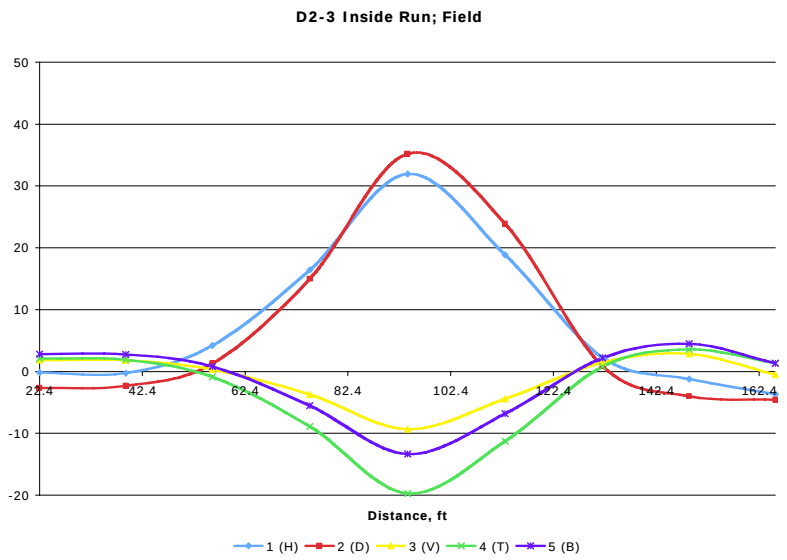
D2-3 Inside Run; Field
50
40
30
20
10
0
-10
-20
22.4
42.4
62.4
82.4
102.4
122.4
142.4
162.4
Distance, ft
1 (H)
2 (D)
3 (V)
4 (T)
5 (B)

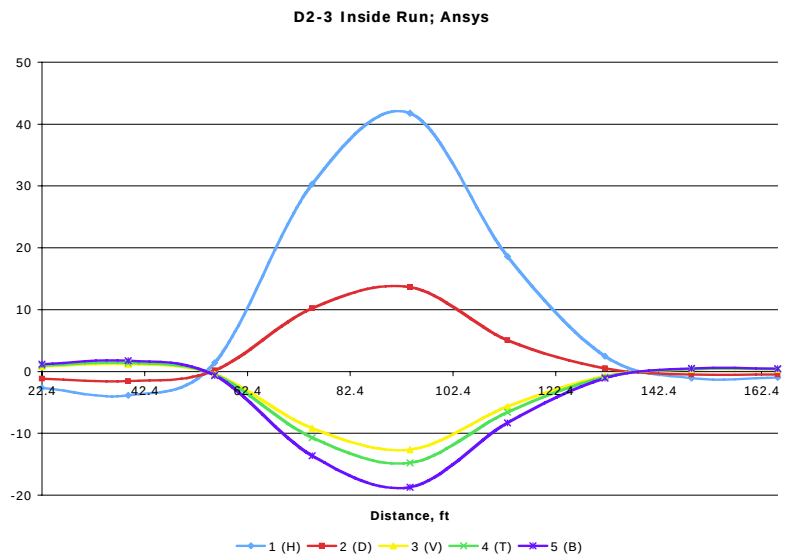
D2-3 Inside Run; Ansys
50
40
30
20
10
0
-10
-20
22.4
42.4
62.4
82.4
102.4
122.4
142.4
162.4
Distance, ft
1 (H)
2 (D)
3 (V)
4 (T)
5 (B)

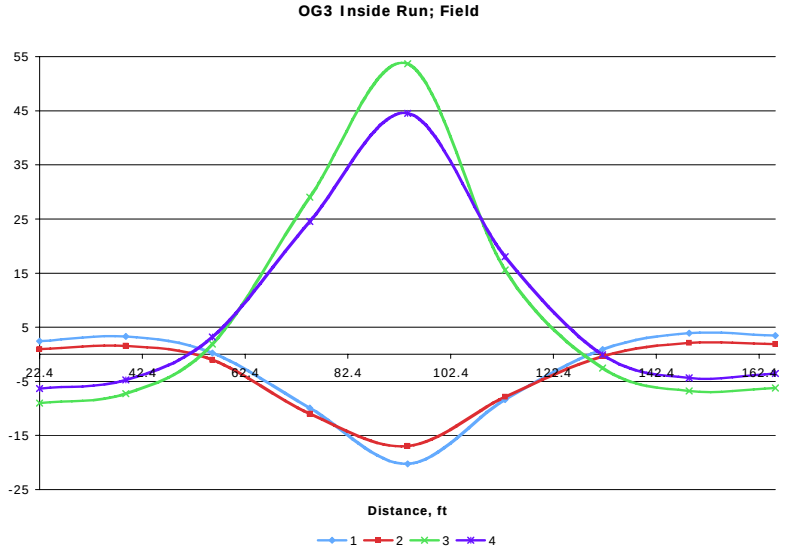
OG3 Inside Run; Field
55
45
35
25
15
5
-5
-15
-25
22.4
42.4
62.4
82.4
102.4
122.4
142.4
162.4
Distance, ft
1
2
3
4

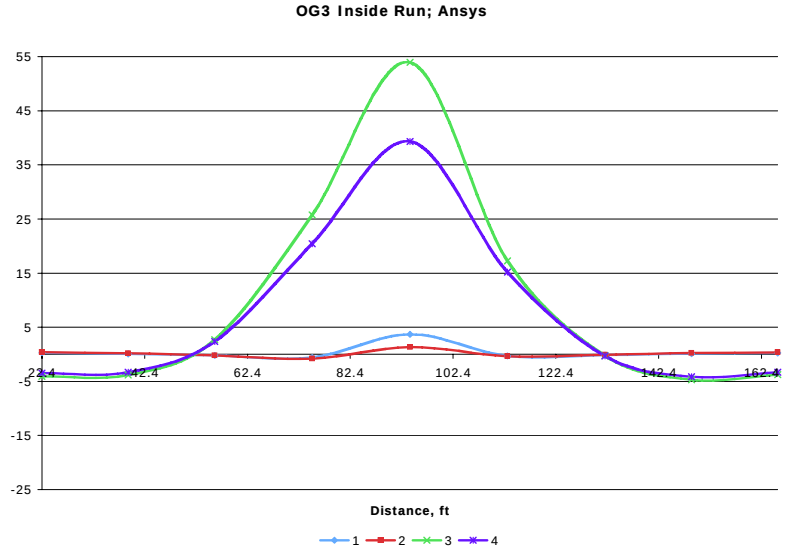
OG3 Inside Run; Ansys
55
45
35
25
15
5
-5
-15
-25
22.4
42.4
62.4
82.4
102.4
122.4
142.4
162.4
Distance, ft
1
2
3
4

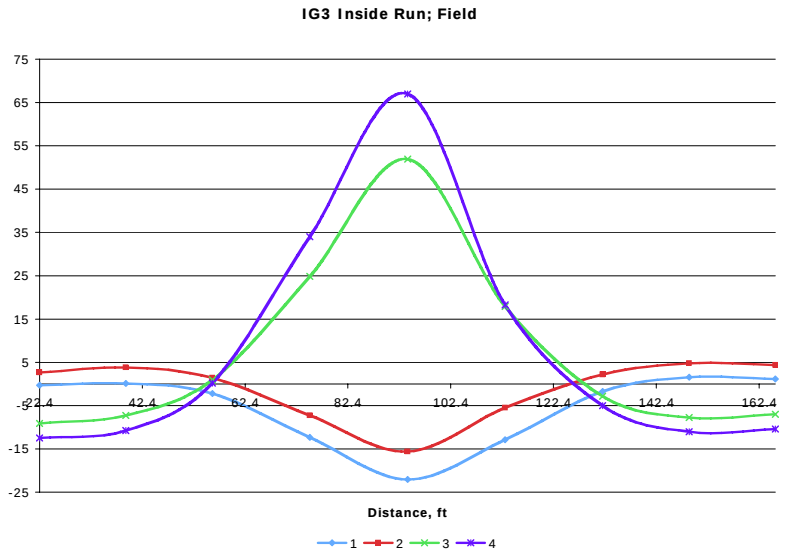
IG3 Inside Run; Field
75
65
55
45
35
25
15
5
-5
-15
-25
22.4
42.4
62.4
82.4
102.4
122.4
142.4
162.4
Distance, ft
1
2
3
4

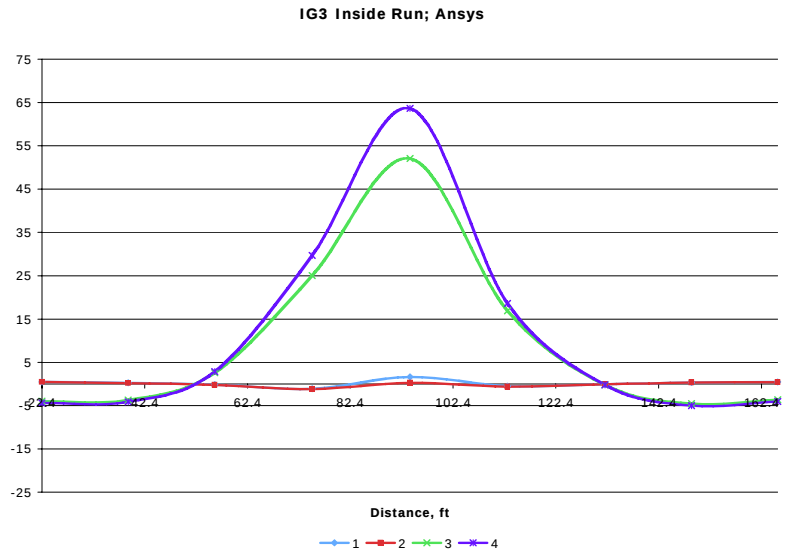
IG3 Inside Run; Ansys
75
65
55
45
35
25
15
5
-5
-15
-25
22.4
42.4
62.4
82.4
102.4
122.4
142.4
162.4
Distance, ft
1
2
3
4

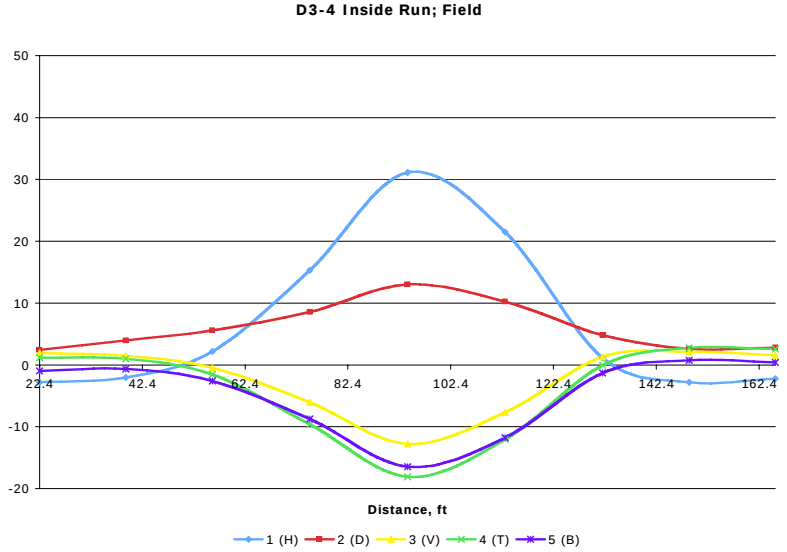
D3-4 Inside Run; Field
50
40
30
20
10
0
-10
-20
22.4
42.4
62.4
82.4
102.4
122.4
142.4
162.4
Distance, ft
1 (H)
2 (D)
3 (V)
4 (T)
5 (B)

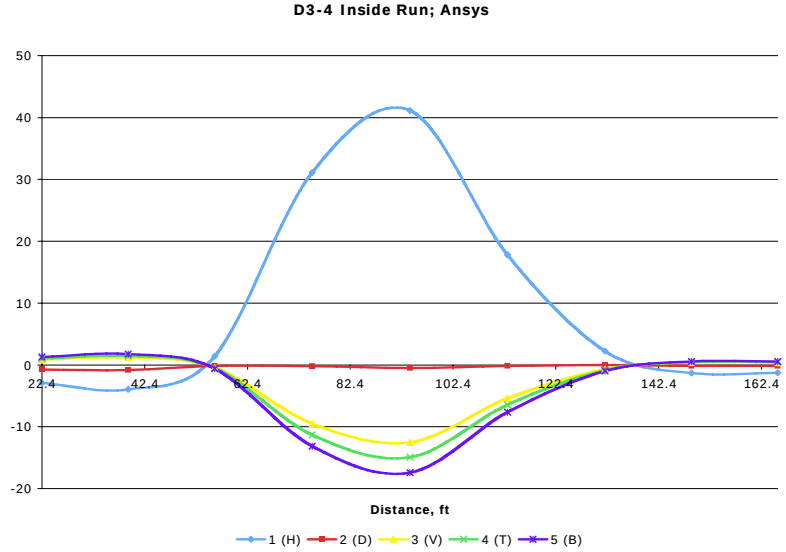
D3-4 Inside Run; Ansys
50
40
30
20
10
0
-10
-20
22.4
42.4
62.4
82.4
102.4
122.4
142.4
162.4
Distance, ft
1 (H)
2 (D)
3 (V)
4 (T)
5 (B)

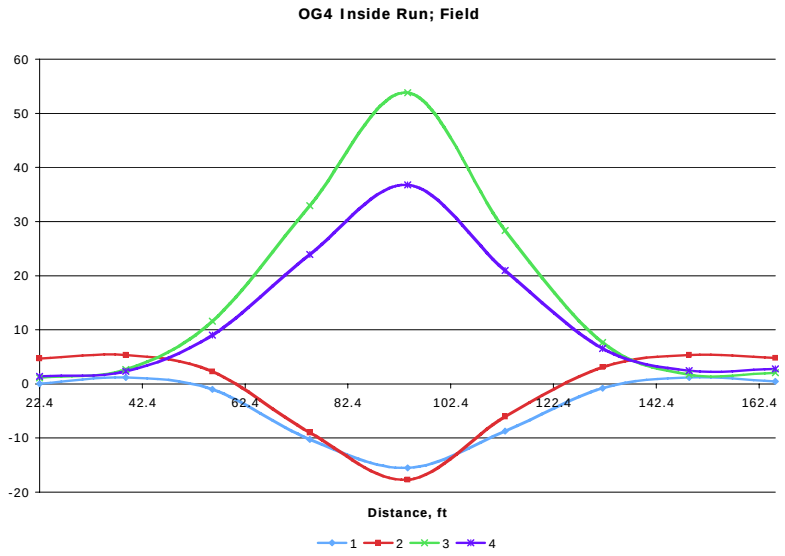
OG4 Inside Run; Field
60
50
40
30
20
10
0
-10
-20
22.4
42.4
62.4
82.4
102.4
122.4
142.4
162.4
Distance, ft
1
2
3
4

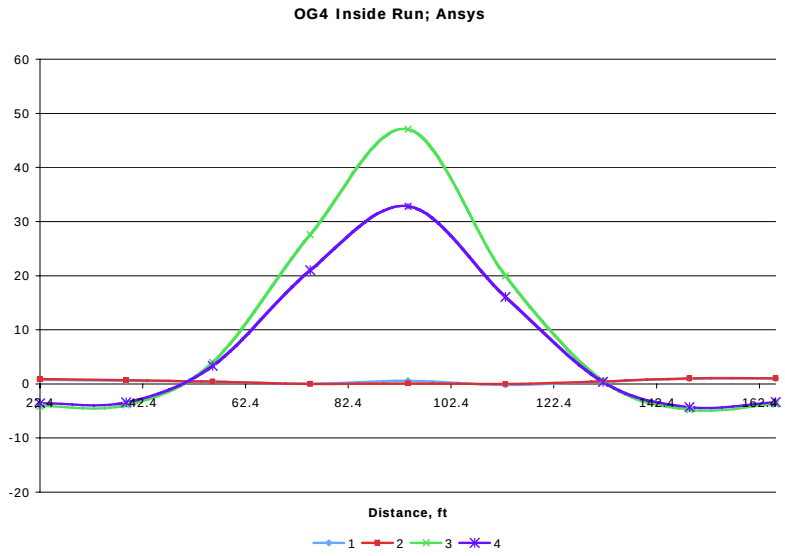
OG4 Inside Run; Ansys
60
50
40
30
20
10
0
-10
-20
22.4
42.4
62.4
82.4
102.4
122.4
142.4
162.4
Distance, ft
1
2
3
4

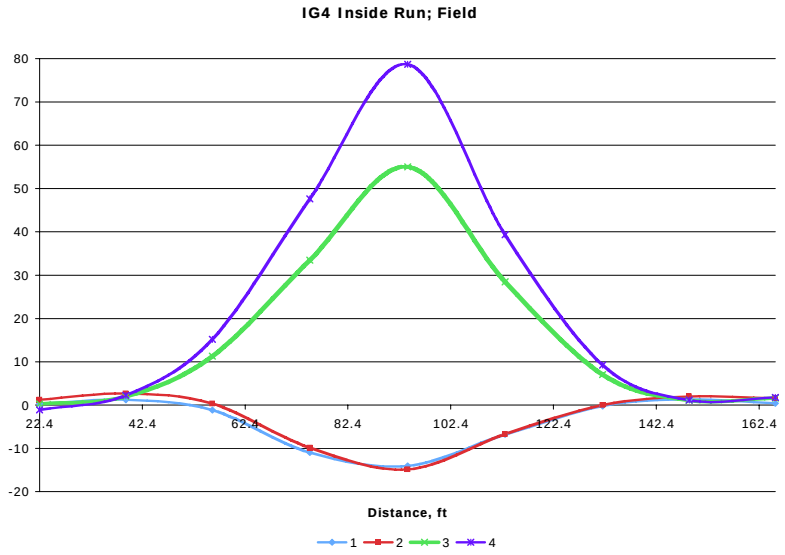
IG4 Inside Run; Field
80
70
60
50
40
30
20
10
0
-10
-20
22.4
42.4
62.4
82.4
102.4
122.4
142.4
162.4
Distance, ft
1
2
3
4

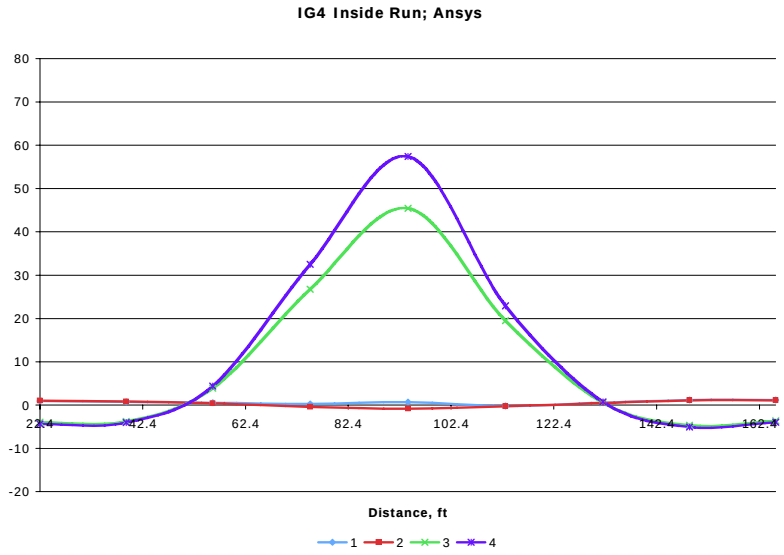
IG4 Inside Run; Ansys
80
70
60
50
40
30
20
10
0
-10
-20
22.4
42.4
62.4
82.4
102.4
122.4
142.4
162.4
Distance, ft
1
2
3
4

APPENDIX C. MODIFICATIONS TO FINITE ELEMENT MODEL

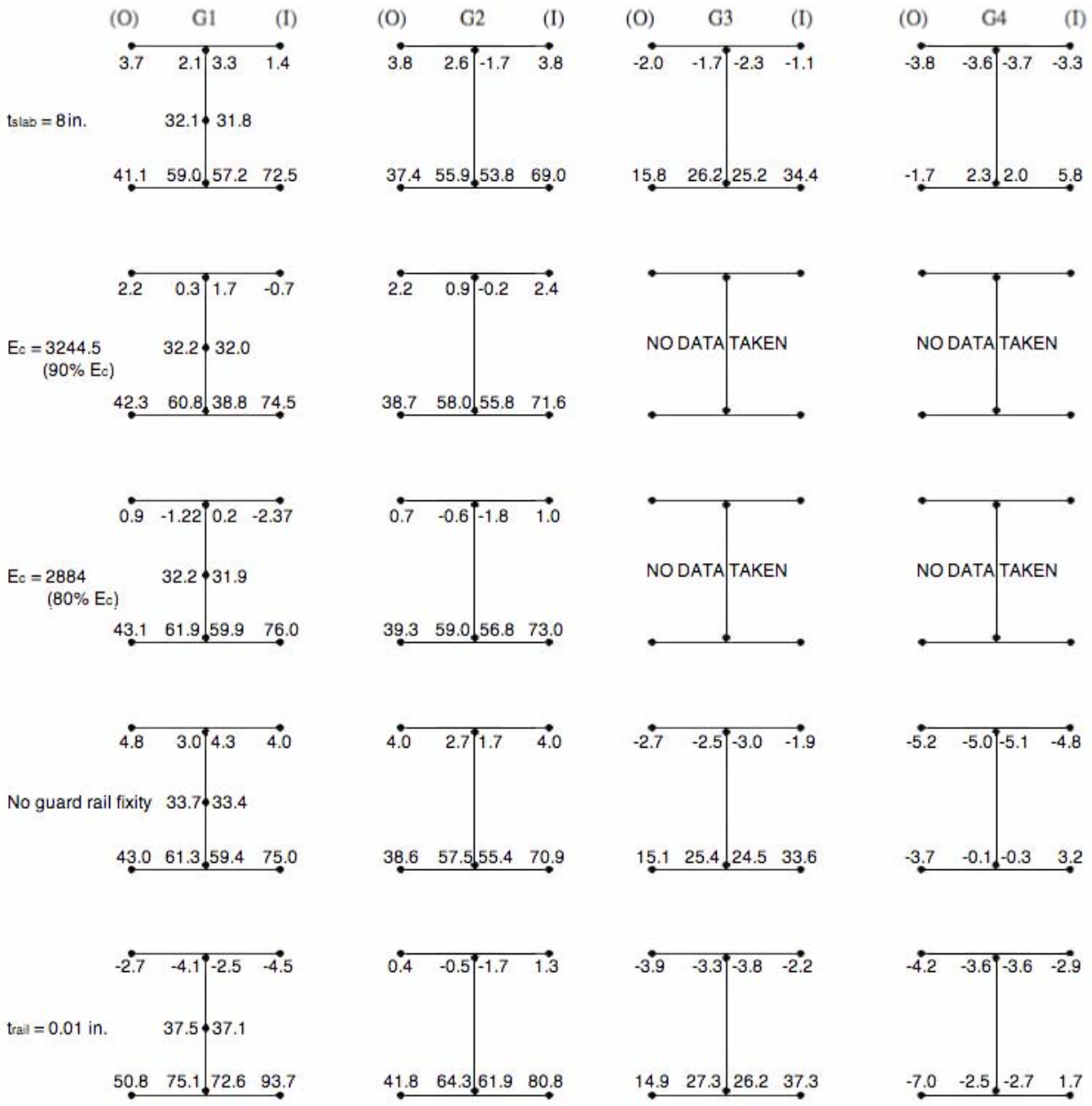

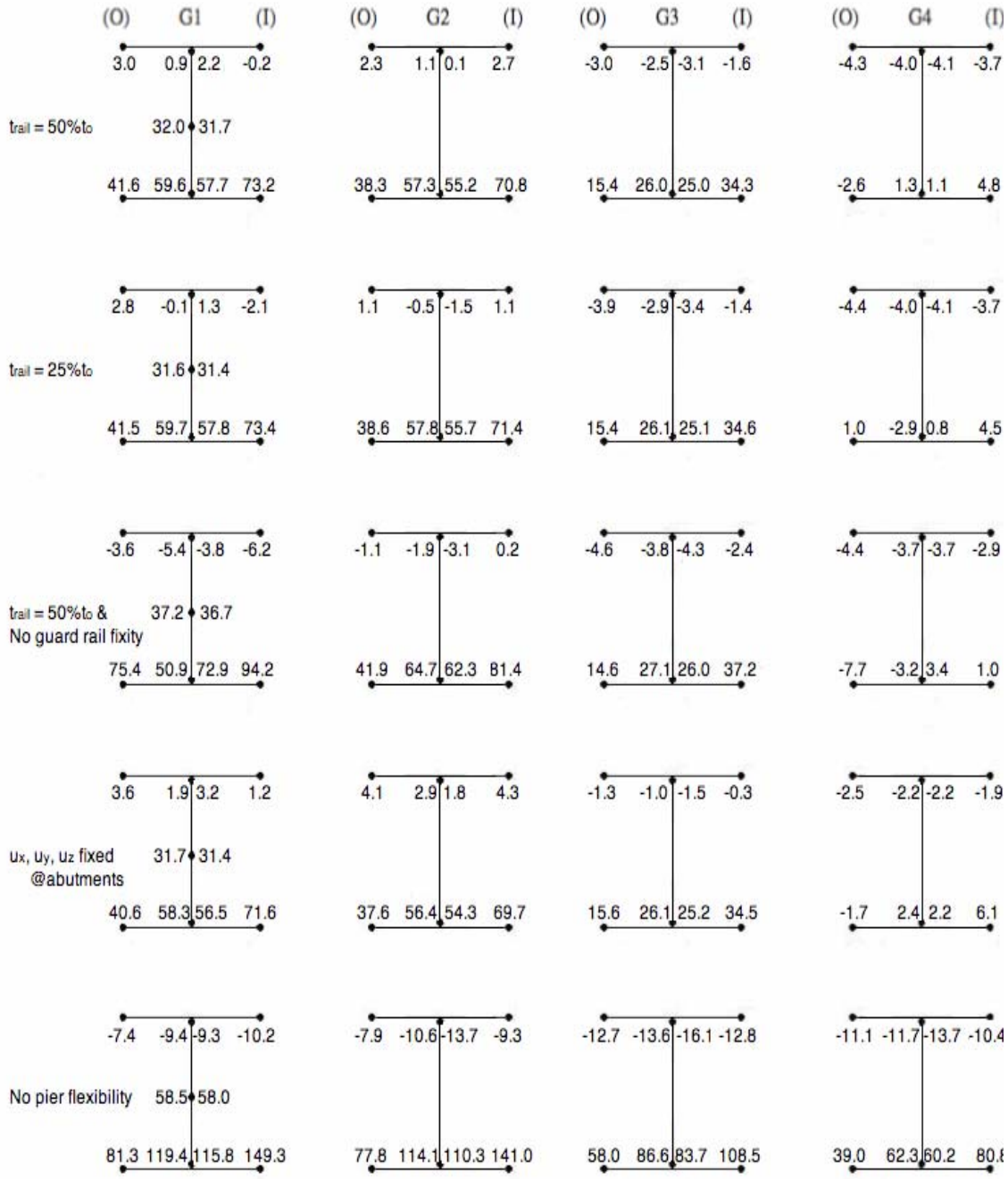
(O) G1 (I)
(O) G2 (I)
(O) G3 (I)
(O) G4 (I)
3.0 0.9 2.2 -0.2
2.3 1.1 0.1 2.7
-3.0 -2.5 -3.1 -1.6
-4.3 -4.0 -4.1 -3.7
trail = 50%to
32.0 31.7
41.6 59.6 57.7 73.2
38.3 57.3 55.2 70.8
15.4 26.0 25.0 34.3
-2.6 1.3 1.1 4.8
2.8 -0.1 1.3 -2.1
1.1 -0.5 -1.5 1.1
-3.9 -2.9 -3.4 -1.4
-4.4 -4.0 -4.1 -3.7
trail = 25%to
31.6 31.4
41.5 59.7 57.8 73.4
38.6 57.8 55.7 71.4
15.4 26.1 25.1 34.6
1.0 -2.9 0.8 4.5
-3.6 -5.4 -3.8 -6.2
-1.1 -1.9 -3.1 0.2
-4.6 -3.8 -4.3 -2.4
-4.4 -3.7 -3.7 -2.9
trail = 50%to &
No guard rail fixity
37.2 36.7
75.4 50.9 72.9 94.2
41.9 64.7 62.3 81.4
14.6 27.1 26.0 37.2
-7.7 -3.2 3.4 1.0
3.6 1.9 3.2 1.2
4.1 2.9 1.8 4.3
-1.3 -1.0 -1.5 -0.3
-2.5 -2.2 -2.2 -1.9
ux, uy, uz fixed
@abutments
31.7 31.4
40.6 58.3 56.5 71.6
37.6 56.4 54.3 69.7
15.6 26.1 25.2 34.5
-1.7 2.4 2.2 6.1
-7.4 -9.4 -9.3 -10.2
-7.9 -10.6 -13.7 -9.3
-12.7 -13.6 -16.1 -12.8
-11.1 -11.7 -13.7 -10.4
No pier flexibility
58.5 58.0
81.3 119.4 115.8 149.3
77.8 114.1 110.3 141.0
58.0 86.6 83.7 108.5
39.0 62.3 60.2 80.8